PCCP

Transmission of spin-polarization by π-orbitals: an approach to assessing its effect on NMR spin-spin coupling and EPR hyperfine structure

Journal:	*Physical Chemistry Chemical Physics*
Manuscript ID	CP-ART-07-2022-003295.R1
Article Type:	Paper
Date Submitted by the Author:	n/a
Complete List of Authors:	Malkina, Olga; Institute of Inorganic Chemistry, SAS, Theoretical Chemistry Lemken, Florian; Institute of Inorganic Chemistry, SAS, Theoretical Chemistry Asher, James; Institute of Inorganic Chemistry SAS Hierso, Jean-Cyrille; Université de Bourgogne, ICMUB-UMR CNRS 6302 Buehl, Michael; University of St Andrews, School of Chemistry Malkin, Vladimir; Institute of Inorganic Chemistry, Slovak Academy of Sciences, Theoretical chemistry

The main source of the long-range spin-polarization is $\pi - \pi^*$ excitations. Their contribution to the spin-polarization is proportional to $\pi \cdot \pi^*$, which explains the sign-alternating pattern of the FC-induced spin-polarization.

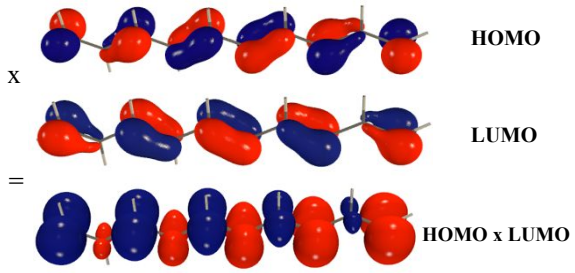

Transmission of spin-polarization by π-orbitals: an approach to assessing its effect on NMR spin-spin coupling and EPR hyperfine structure

Olga L. Malkina,*[,a] Florian Lemken[a], James R. Asher[a,b], Jean-Cyrille Hierso[c], Michael Bűhl[d], Vladimir G. Malkin*[a]

[a]*Institute of Inorganic Chemistry, Slovak Academy of Sciences, Dúbravská cesta 9, SK-84536 Bratislava, Slovakia*

[b] *Faculty of Natural Sciences, Department of Inorganic Chemistry, Comenius University, Mlynská dolina CH2, SK-84215 Bratislava, Slovakia*

[c] *Institut de Chimie Moléculaire de l'Université de Bourgogne (ICMUB, UMR CNRS 6302), Université Bourgogne–Franche-Comté (UBFC), 9 avenue Alain Savary, 21078 Dijon Cedex, France*

[d] *EaStChem School of Chemistry, University of St Andrews, St Andrews, Fife KY16 9ST, UK*

** Corresponding authors; e-mail: olga.malkin@savba.sk, vladimir.malkin@savba.sk*

Dedicated to the memory of Prof. Paul von Ragué Schleyer

A new approach to assessing the effect of the transmission of spin-polarization by π-orbitals (π-TSP) is presented. In order to switch off the π-TSP effect, we artificially average the α- and β-densities of the valence π-orbitals when calculating the exchange-correlation contribution to the Fock matrix in the unrestricted Kohn-Sham framework. The π-TSP effect is then evaluated as the difference between the results obtained with switched-on and switched-off options. This approach is applied to estimate the π-TSP effect on the Fermi-contact contribution to spin-spin couplings and EPR hyperfine structure coupling constants. The π-TSP effect on the distribution of spin-density, spin-spin coupling pathways and pathways of EPR hyperfine couplings is demonstrated for benzene, naphthalene, 1,3,5,7,9-decapentaene and 1,3,5,7,9-decapentaen-1-yl radical. The sign alternation of the spin-polarization transmitted by π-orbitals is explained in a theoretical framework based on perturbation theory. However, the delocalized nature of the π-system can interfere with the sign alternation in certain cases, two of which – cyclobutadiene dication and cyclooctatetraene dication – are examined, and an explanation for which is provided.

Introduction

The accurate description, modeling and understanding of the nature of the chemical bonds remains one of the most important issues in theoretical chemistry. Obviously, bond types are directly relevant to the stability and reactivity of the compounds, and are of primary importance concerning various molecular physical properties. For example, the impact of σ- and π-bonds on NMR shielding was studied early on by Kutzelnigg *et al*.[1] The special concept of the nucleus-independent chemical shift (NICS) was introduced to measure aromaticity by examining ring-current effects stemming from delocalized π-electrons.[2] The NICS concept generated numerous discussions, resulting in further improvements and alternative approaches.[3] The effect of the transmission of spin-polarization by π-bonds (π-TSP) on NMR indirect spin-spin coupling constants (SSCC) is more difficult to assess. For instance, when a delocalized planar system is considered, the commonly-used analyses of contributions from molecular orbitals (MO) to the Fermi Contact (FC) part of spin-spin coupling would show zero contribution from π-MOs because they have values of zero at the positions of the coupled nuclei.[4] Thus, the direct FC contribution from the π-bonds to *J*(C-C) in benzene is zero since the π-MOs have zero s-character on both coupled nuclei. However, the lack of contributions from the π-bonds is a shortcoming only of the commonly-used analyses. Indeed, the π-bonds are actively involved in the transmission of spin-polarization (π-TSP) between two carbon nuclei in benzene: the s-orbital is polarized due to Fermi-contact interaction on the first carbon, which in turn polarizes all orbitals around the carbon, including π-MOs. Then the π-MOs further transfer the polarization to the second carbon and polarize its s-orbital. Finally, the polarized s-orbital interacts with the nuclear magnetic moment of the second carbon *via* the FC mechanism. π-orbitals are delocalized and easily polarized, and they can transmit spin-polarization more efficiently and farther than sigma-orbitals. This kind of dynamic spin-polarization has also been invoked to explain the occurrence of nonzero hyperfine coupling constants on the H atoms in the planar methyl radical, and to advocate the use of the spin-unrestricted formalism in Kohn-Sham DFT.[5] The assessment of this intricate spin transmission phenomenon, however, requires a more advanced analysis.

Different ways to estimate its effect have been used in the past. In 1957 McConnell used empirical data on hyperfine splitting in aromatic free radicals to estimate the contribution of π-electrons to *J*(H-H) in aromatic molecules based on the effective "π-electron spin - proton spin interaction Hamiltonian".[6] Later he used valence bond (VB) theory to predict the negative contribution from π-electrons to *J*(H-H)

through an even number of bonds.[7] VB was also used by Barfield [8] to study the π-TSP effect on long-range proton-proton coupling. A thorough review of early works on π-TSP is available. [9]

The appearance of semi-empirical methods attracted new interest to π-TSP. Fukui, Tsuji, and Miura[10] used the SOS2-INDO expression (sum-over-states including single and double excitations at the INDO level) for the calculation of *J*-coupling. The separation of excitations into three categories (from σ to σ* orbitals, from π to π* orbitals and mixed π-σ* and σ-π* transitions) allowed them to obtain the π-contribution to spin-spin coupling constants. Engelmann, Scuseria and Contreras based their analysis on the SCPT-INDO expression.[11] The unperturbed MOs were separated into π- and σ- subspaces. SCPT (self-consistent perturbation theory) part was applied either to all MOs or only to the σ-subspace. The difference in the results showed the effect of π-orbitals on SSCC. Despite the limited accuracy of semi-empirical methods, these early works provided consistent qualitative conclusions: 1) π-TSP decayed more slowly than the spin-polarization transmitted by σ-orbitals, and 2) the contribution of π-orbitals to *J*-couplings was positive through an odd number of bonds and negative otherwise, though no satisfactory explanation of this phenomenon was given.

Interest in the π-TSP effect on SSCC was renewed with the development of DFT-based methods for calculating *J*-coupling.[12] Gräfenstein, Tuttle and Cremer followed the ideas of Fukui *et al*.[10] using the CP-DFT (coupled perturbed density functional) equations written in terms of localized molecular orbitals (LMOs).[13] Excluding different combinations of LMOs from the equations, they were able to estimate the effect of the π-mechanism on long-range C–C, C–H and H–H SSCC in polyenes. The practical applications of this promising approach were somewhat hindered by the necessity of hand-picking the relevant combinations of LMOs, and it was difficult to extend this approach to the analysis of other properties. However, the authors reached many interesting conclusions, which overall agreed with previous findings made at the semi-empirical level. The sign alternation of the contribution of π-orbitals to J^{FC}-couplings with an increasing number of bonds separating the coupled nuclei was linked to the Dirac vector model for long-range spin-spin couplings, albeit without explanation. Therefore, it remains unclear how the Dirac vector model proposed for explaining the sign alternation of long-range J^{FC}-couplings in a chain of σ-bonds can be applied to the π-mechanism.

Our motivation for addressing the topic of π-TSP is as follows: a) though the π-TSP effect on the EPR hyperfine coupling constants (HFCCs) was discussed long ago,[4,6] its detailed analysis has received much less attention than the influence of π-TSP on NMR spin-spin coupling; b) deeper insight into π-TSP can

be gained by the methods of visualization of pathways of NMR spin-spin couplings and EPR hyperfine couplings that are now available;[14] c) to the best of our knowledge, a consistent explanation for the sign alternation of the π-TSP effect along the bonds on SSCCs and HFCCs is still lacking; d) deeper understanding of π-TSP may be beneficial for further analyzing spin-spin transmission pathways in transition metal complexes that include aromatic moieties in their ancillary ligands (phenyl, naphthyl, *etc.*)[15] or that possess benzene and olefins as ligands themselves (metallocenes, *etc.*).[16]

The aim of this work is to present an approach that allows one to switch the π-TSP effect off and on easily, and which is applicable to the analysis of molecular properties that depend on the effects of spin-polarization (SSCC, HFCC). We apply this approach to show the π-TSP effect on different aspects of NMR spin-spin couplings and EPR hyperfine coupling constants. We consider the following systems: benzene, naphthalene, 1,3,5,7,9-decapentaene, and a 1,3,5,7,9-decapentaene-1-yl radical, which is obtained by removing one of the hydrogens from 1,3,5,7,9-decapentaene. We also explain the sign alternation of the contribution of π-orbitals to J^{FC}-couplings with increasing number of bonds and its relation to the Dirac vector model.[17] We furthermore identify two exceptions to the rule – cyclobutadiene dication and cyclooctatetraene dication – and discuss the reasons for this.

Computational methods

We analyzed the π-TSP effect on the FC contribution to the NMR spin-spin coupling and on the EPR hyperfine coupling constant. The FC contribution to SSCC is calculated using single finite perturbation theory (FPT) as described previously.[12] The isotropic HFCC of a particular nucleus is obtained from an unperturbed SCF calculation as the value of the spin-density at the position of the nucleus multiplied by a well-defined constant.[18]

For visualization of spin-spin coupling pathways, we used an approach based on double finite perturbation theory.[19] In this approach, the nuclear magnetic moments of the two interacting nuclei are included as finite perturbations. We perform two SCF calculations, with parallel and antiparallel orientation of the nuclear magnetic moments, as a simulation of experimental NMR measurement. Due to the FC interactions caused by the nuclear magnetic moments, the electron density distribution depends on their relative orientation. The difference between the electron densities obtained from these two calculations, called the Coupling Deformation Density (CDD), shows which parts of the electronic structure are involved in the magnetic interaction of the two nuclei. Mathematically, CDD is

the bilinear response of the total electron density to the nuclear magnetic moments, and it is expressed as follows:

$$\rho_{MN}(r) = \frac{\rho^{\uparrow\uparrow}(r) - \rho^{\uparrow\downarrow}(r)}{\lambda_1 \lambda_2} \quad (1)$$

where λ_1 and λ_2 are the perturbation parameters used in double finite perturbation theory (DFPT), and $\rho^{\uparrow\uparrow}(r)$ and $\rho^{\uparrow\downarrow}(r)$ are doubly-perturbed electron densities (*i.e*. the densities corresponding to the parallel and antiparallel orientation of the nuclear magnetic moments involved in the spin-spin coupling). From the physical point of view, CDD, being the difference between two electron densities, is an observable.

Analogously to the visualization of spin-spin coupling pathways, we have also developed an approach for the visualization of hyperfine coupling pathways.[14] The magnetic moment of a nucleus of interest is there included as a finite perturbation. The difference between the spin-densities for the two opposite orientations of the nuclear magnetic moment (Hyperfine Deformation Density, HFDD) shows the hyperfine coupling pathway. Again, from the physical point of view, HFDD is an observable.

In order to assess the π-TSP effect on the properties described above, we have to be able to switch it on and off, preferably in the same manner for both unperturbed and perturbed calculations: that is, without relying on the explicit expressions for particular properties, as was done in previous works.[11,13] Orbitals transmit spin-polarization *via* their exchange-correlation interaction with other orbitals.[20] In the DFT framework, this means through the contribution of the spin-density of the polarized orbitals to the exchange-correlation potential. In order to switch off the π-TSP effect, we artificially average the α- and β-densities of the valence π-orbitals for calculating the exchange-correlation potential. In this approach, the π-orbitals are still polarized by core and σ-orbitals but they cannot contribute to further transmission of the spin-polarization. In this case, the contribution to SSCC or HFCC due to the π-TSP effect vanishes. Herein, we consider planar systems where the π-orbitals are easily identifiable even in their canonical form. For more complex systems, localized molecular orbitals can be used. The difference between the results obtained using the switch on and switch off options is considered to be the π-TSP effect.

Computational details

All calculations have been carried out using density functional theory. The structures of 1,3,5,7,9-decapentaene, benzene, naphthalene, and the planar forms of cyclobutadienyl and cyclooctatetranyl dications were optimized at the RI-BP86-D3/6-31G* level using the G03 package [21]. We are aware that the planar form of cyclobutadienyl dication is a saddle point. It is well known that the puckered minimum is significantly more stable (by 9.6 kcal/mol at RI-BP86-D3 level, according to our calculations; this is similar to ab initio results reported earlier[22]). However, the planar form is interesting as the simplest model for a Hückel aromatic system where the sign alternation can be studied. The cartesian coordinates of the optimized structures are given in ESI. For better comparison of NMR spin-spin coupling and hyperfine coupling pathways, the structure of a 1,3,5,7,9-decapentaene radical was obtained by removing H19 from 1,3,5,7,9-decapentaene (see Fig. 1) without relaxation of the structure. The property calculations were done with a local modified version of the deMon-KS code.[23,24] In these calculations we employed the Perdew86 exchange-correlation functional in its spin-unrestricted formalism,[25, 26, 27, 28] and the IGLO-II basis set.[1] The grid for numerical integration contained about 3000 points per atom during the main SCF procedure. After reaching the SCF convergence, however, an extra iteration with about 10500 points per atom was performed in order to increase the accuracy of the molecular orbital coefficients. Visualization has been done with AVOGADRO 1.1.1.[29] On the isosurface plots, blue and red colors correspond to positive and negative values, respectively.

Results and discussion

To investigate the π-TSP effect we selected three systems, a long-chain linear olefin, a simple aromatic, and a fused-ring extended π-aromatic: 1,3,5,7,9-decapentaene, benzene and naphthalene, respectively. Their atom numbering is shown in Figure 1. We first analyzed the π-TSP effect on the FC contribution to J(C-C) in these systems. Then we considered and compared how the transmission of spin-polarization by π-orbitals affects the spin-density (induced by the FC operator on one of the carbon atoms), again in all three systems. Additionally, we examined the π-TSP effect on the induced spin density for the cyclobutadiene dication, an example with a noticeable deviation from the sign alternation pattern. We

subsequently addressed the π-TSP effect on the general NMR spin-spin coupling pathways. Finally, we analyzed the π-TSP effect on different aspects of the ^{13}C hyperfine couplings.

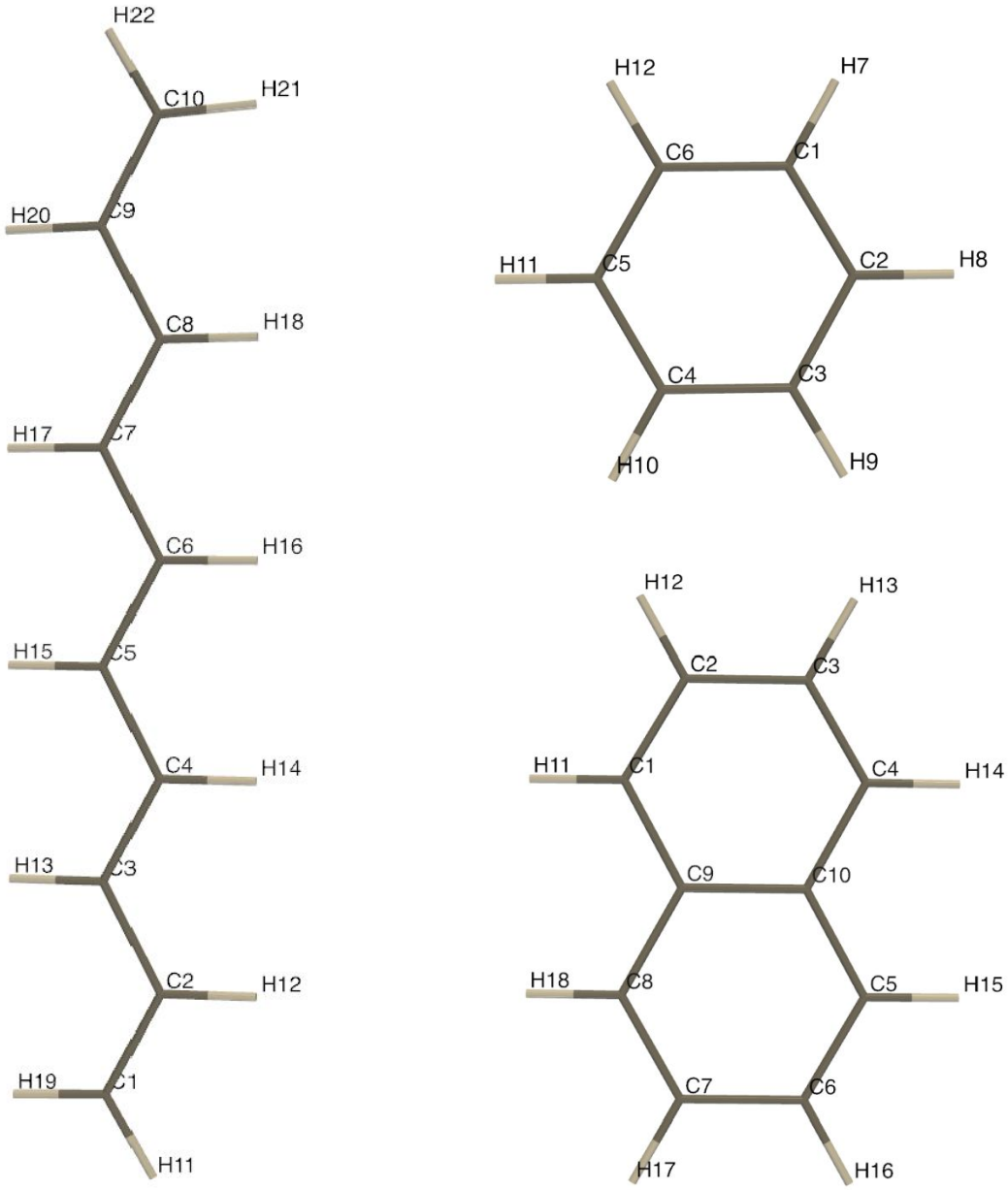

Figure 1. Molecular structure and the numbering of atoms in 1,3,5,7,9-decapentaene (left), benzene (top right) and naphthalene (bottom right). The 1,3,5,7,9-decapentaene radical considered in this work is obtained from 1,3,5,7,9-decapentaene by removing atom H19.

The π-TSP effect on the FC contribution to spin-spin couplings

The calculated Fermi-contact contributions to ^{n}J(C-C) couplings are presented in Tables 1 (for 1,3,5,7,9-decapentaene), 2 (for benzene) and 3 (naphthalene). Other contributions to ^{n}J(C-C) couplings for the considered systems can be found in Tables S1-S4 in ESI. In Tables 1-3, the first column indicates the number of bonds separating the coupled carbons. The values in the second column show the ^{n}J(C-C) values obtained with all orbitals participating in the transmission of spin-polarization, and the third column gives the results when the π-TSP effect is switched off, that is, when the π-orbitals do not polarize other orbitals *via* the exchange interaction. The last column gives the differences between the values in the second and third columns, in other words it gives the contributions to ^{n}J(C-C) solely due to the transmission of spin-polarization by the π-system (*via* the π-channel). The π-TSP effect listed in the last column of Table 1 is also shown graphically in Figure 2. Additionally, Figure S1 in ESI shows the values calculated with two finer grids used for numerical integration and confirms the numerical stability of the results. The π-TSP effect on ^{n}J(C1- C_{n+1}) is always positive for an odd number of bonds separating the coupled carbon atoms (***n*** = 1, 3, 5, …) and negative for an even number (***n*** = 2, 4, 6, …). When π-TSP is excluded (column 3 in Table 1, π-TSP switched OFF) the C – C couplings are positive for ***n*** from 1 to 5, which disagrees with the Dirac vector model. The sign alternation in column 3 is observed only for ***n*** > 4.

Table 1. The π-TSP effect on $^{n}J^{FC}$(C1- C_{n+1}) in 1,3,5,7,9-decapentaene. The values are given in Hz.

n[a]	π-TSP switched ON	π-TSP switched OFF	ΔJ [b]
1	77.44	74.88	2.56
2	1.86	3.40	-1.53
3	7.43	6.41	1.02
4	-0.72	0.11	-0.83
5	1.04	0.34	0.70
6	-0.70	-0.14	-0.56
7	0.73	0.19	0.54
8	-0.54	-0.12	-0.42
9	0.52	0.14	0.38

[a] ***n*** is the number of bonds separating C and C_{n+1} .

[b] ΔJ is the difference between the values of the SSCCs (Hz) in the second (π-TSP switch-ON) and the third (π-TSP switch-OFF) columns, and as such represents the quantitative effect of π-TSP.

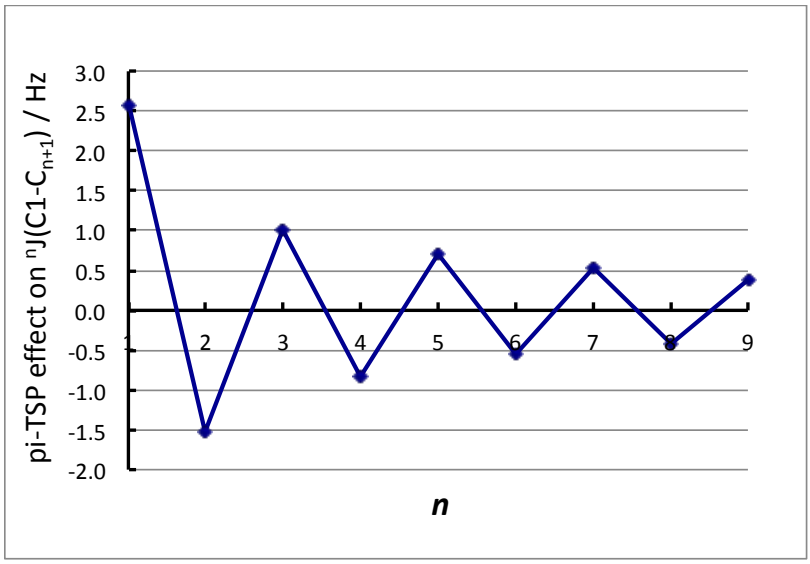

Figure 2. The π-TSP effect on ${}^{n}J^{FC}$(C1- C_{n+1}) in 1,3,5,7,9-decapentaene as a function of the number of bonds separating two carbons (in Hz).

The decay of the π-transmitted spin-polarization contribution to ${}^{n}J$ (C1- C_{n+1}) in 1,3,5,7,9-decapentaene with increasing ***n*** is much slower than the decay of the usual σ-bond-transmitted polarization (see Table 1). While the latter tends to die off after ca. 5 bonds, the π-TSP contributions continue to oscillate even up to nine bonds (see Figure 2), and for ***n*** > 3 they actually give the dominant contribution to the *J*-values (see Table 1). These findings agree with previous works.[11,13]

Similar trends are also observed for a classic π-system, benzene (see Table 2). Without π-TSP there is no sign alternation of the values of the C – C couplings (Table 2, column 3), whereas the π-TSP contribution is positive for ***n*** = 1 and 3 and negative for ***n*** = 2. The magnitude of the π-TSP contribution to ${}^{2}J$ (C1- C3) is bigger than the *J* value calculated without π-TSP (-0.97 Hz versus 0.71 Hz), making π-TSP responsible for the sign alternation of the total *J* values seen in the second column in Table 2.

Table 2. The π-TSP effect on ${}^{n}J^{FC}$(C1- C_{n+1}) in benzene. The values are given in Hz.

n[a]	π-TSP switched ON	π-TSP switched OFF	ΔJ [b]
1	62.94	61.43	1.51
2	-0.33	0.71	-1.04
3	7.80	6.96	0.84

[a] ***n*** is the number of bonds separating C and C_{n+1} .

[b] ΔJ is the difference between the values of the SSCCs (Hz) in the second (π-TSP switch-ON) and the third (π-TSP switch-OFF) columns, and as such represents the quantitative effect of π-TSP.

Naphthalene provides a suitable model for analyzing the π-TSP effect on $^{n}J^{FC}$(C1-C_{n+1}) in an aromatic compound for a larger range of ***n*** (from 1 to 5, see Table 3) than that in benzene. Unlike benzene, naphthalene contains carbon-carbon bonds which are not symmetry-equivalent (see for instance their bond lengths in the optimized structure in Figure S2 in ESI); and, except for ***n*** = 5, there are multiple topologically different SSCC pathways through the same number of bonds. This results in multiple different *J* values for the same ***n***. For example, for ***n*** = 1, values of SSCC ranging from 55.8 to 68.0 Hz are found. For ***n*** = 2 values of SSCC ranging from –0.03 to 3.8 Hz are obtained; in addition, ^{4}J(C2-C7) and ^{4}J(C1-C6) have opposite signs (Table 3).

Overall, there is no sign alternation of total *J*(C-C) values with increasing number of bonds, i.e. they do not obey the Dirac vector model. In contrast, the π-TSP effect shown in the last column of Table 3 displays remarkably stable sign alternation with increasing number of bonds. It displays much smaller variation in the *J* values for the same ***n*** and decays more slowly. ^{5}J(C2-C6) is mainly caused by the π-TSP effect (the last row in Table 3).

Table 3. The π-TSP effect on $^{n}J^{FC}$(C-C) in naphthalene. The values are given in Hz.

n[a]		π-TSP switched ON	π-TSP switched OFF	Δ *J* [b]
1	C1-C2	67.97	66.37	1.60
	C1-C9	61.28	60.01	1.26
	C2-C3	59.07	57.70	1.37
	C9-C10	55.82	54.60	1.22
2	C1-C8	3.78	4.64	-0.86
	C1-C10	1.14	2.08	-0.93
	C2-C9	0.36	1.27	-0.91
	C1-C3	-0.03	0.95	-0.98
3	C3-C9	6.45	5.78	0.67
	C1-C4	5.33	4.60	0.73
	C1-C5	2.35	1.97	0.38
4	C2-C7	0.52	0.95	-0.43
	C1-C6	-0.50	-0.24	-0.26
5	C2-C6	0.46	0.07	0.39

[a] ***n*** is the number of bonds separating C and C_{n+1}.

[b] Δ*J* is the difference between the values of SSCCs (Hz) in the second (π-TSP switch-ON) and the third (π-TSP switch-OFF) columns, and as such represents the quantitative effect of π-TSP.

In all three examples, the sign of the π-TSP effect on $^{n}J^{FC}(C1\text{-}C_{n+1})$ is positive for an odd ***n*** and negative otherwise. It decays more slowly with increasing number of bonds than the effect of spin-polarization transmitted by other channels. The π-TSP effect may be significant even for short range couplings such as $^{2}J^{FC}(C1\text{-}C_3)$ in naphthalene and it becomes dominant for ***n*** > 4 in 1,3,5,7,9-decapentaene and naphthalene.

Besides the FC term, there is another spin-mediated contribution to spin-spin couplings, the spin-dipolar contribution (SD). It also displays the sign alternating pattern with increasing the number of bonds (see Figure S3 in ESI). This indicates that the pi-TSP effect likely plays an important role for the SD contribution for long-range spin-spin couplings, too.

The π-TSP effect on the spin-density induced by the FC operator

Spin-polarization is often illustrated by plots of the spin-density induced by the FC operator on one of the coupled nuclei. Besides the total spin-density, we can also separately plot the spin-density caused by the π-TSP effect, i.e. the difference in the spin-densities obtained with and without π-TSP, and the spin-polarization of the valence π-orbitals only, i.e., the summed spin-polarization of the valence of π-orbitals.

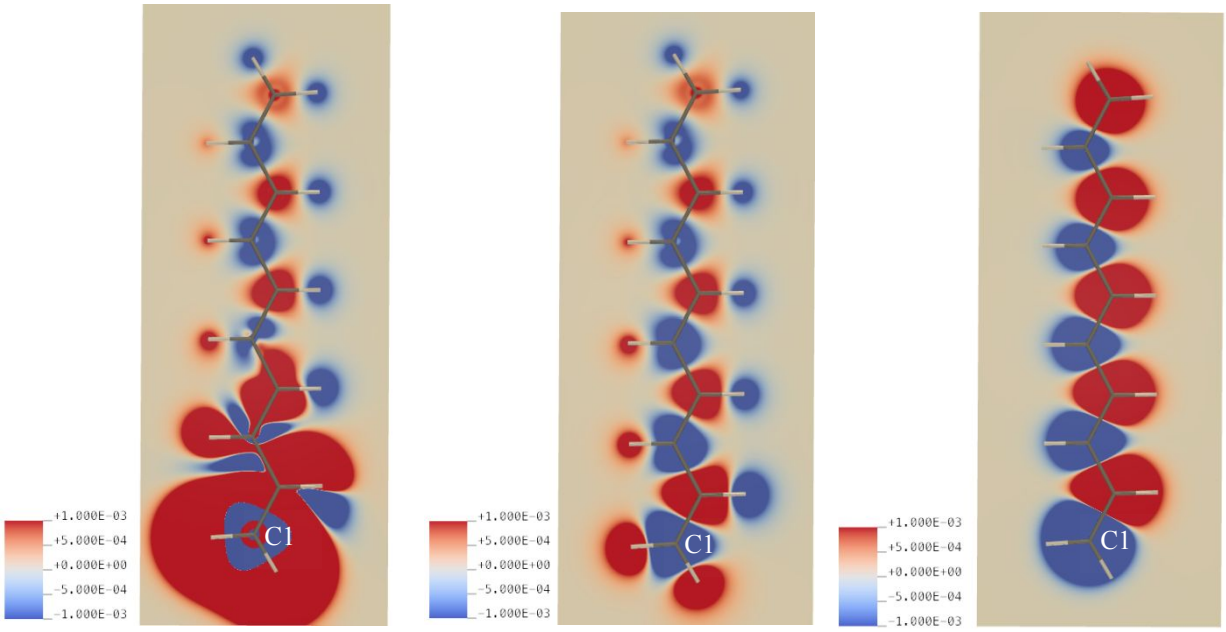

Figure 3. The spin-density in 1,3,5,7,9-decapentaene induced by FC(C1) (color-coded according to the density values given in a.u.). The total spin-density (left) and spin-polarization only due to the π-TSP

effect (middle) are shown in the molecular plane. The spin-polarization of the group of π-orbitals is shown in the plane 0.5 Å below the molecular plane (right).

As seen in Figure 3 (comparing left and middle), the long-range spin-polarization (***n*** > 4) in the molecular plane of 1,3,5,7,9-decapentaene is mainly caused by the π-TSP effect, consistent with the calculated results in Table 1. Interestingly, the π-TSP effect is not limited to carbon atoms, as hydrogen atoms are also affected (Figure 3, middle), displaying positive spin-density in their proximity if they are separated by an odd number of bonds from C1 and negative otherwise for ***n*** > 3. The π-orbitals have values of zero at the carbon positions and thus the π-MO density and the induced spin-density of π-MOs are zero in the molecular plane, too. In order to visualize the spin-polarization of the π-orbitals, a cross-section is shown in the plane 0.5 Å below the molecular plane (a cross section in the plane 0.5 Å above the molecular plane would show exactly the same spin density). A 3d-plot of the spin-polarization of the valence π-orbitals is given in ESI (Figure S4). The plots in Figure 3 display a clear sign alternation of the long-range spin-polarization, in agreement with the spin-spin coupling values in Table 1. In previous works, the sign alternation of the π-TSP effect on the values of spin-spin couplings was implicitly attributed to the Dirac vector model.[11,13] However, the Dirac vector model considers the propagation of the FC-induced spin-polarization through a chain of σ-bonds only.

The Dirac vector model explains the sign alternation as follows: let us assume that the g-value of the first nucleus ***A*** is positive and its spin is up. Then, due to the FC mechanism on nucleus ***A***, FC(A), the probability of finding the electron that has spin up (α-electron) in the proximity of nucleus ***A*** is lower than that of finding the electron with its spin down (β-electron). In other words, the α-electron is trying to avoid nucleus ***A*** and thus "slides" slightly towards the other side of the bond, whereas the β-electron moves in the opposite direction — closer to nucleus ***A*** — creating spin-polarization. Due to Hund's rule, the probability of finding the α-electron of the next bond will be higher in the proximity of the second nucleus. Consequently, the β-electron of the second bond will shift towards the third nucleus, and so on. Therefore, the sign of the spin density near a nucleus in a chain depends on the number of bonds separating it from nucleus ***A***: it is positive for an odd number of bonds, and negative otherwise.

However, the Dirac vector model assumes that each bond in a chain possesses two electrons and that these electrons are localized in the space between the two bonded atoms: if one of the electrons goes closer to one end of the bond, the other one has nowhere to go except for shifting to another end.

Clearly, these assumptions are not valid for delocalized bonding situations such as π-systems. In benzene, for example, the π-electrons are delocalized and there are only six π-electrons for six bonds. Therefore, the classic Dirac vector model cannot be readily extended to such systems. Nonetheless, the sign alternation of the π-TSP effect on the FC-induced spin-density and of the spin-polarization of π-orbitals in benzene is clearly seen in Figure 5, middle and right.

The sign alternation of the spin-polarization of π-orbitals can be explained from the point of view of perturbation theory. Let us consider first the spin-polarization of σ-orbitals from this point of view, with FC(A) taken as the perturbation. A closed-shell doubly-occupied σ-orbital becomes polarized by admixing vacant orbitals with opposite signs into its α- and β-components (with the admixture having opposite signs in each case). In the classic picture, the biggest contribution to the perturbation of an occupied σ-orbital is expected from its corresponding antibonding σ^*-orbital. The bonding orbital has the same sign at the positions of the bonded nuclei, whereas the signs of the antibonding orbital at these points are opposite. Consequently, the resulting spin-density will have opposite signs at the positions of the nuclei in accord with the Dirac vector model. In this model, the explanation of the sign alternation of spin-polarization for a classical σ-bond neither relies on the localization of its electrons between two bonded nuclei, nor requires the presence of two electrons in a particular bond. Therefore, it is applicable to the spin-polarization of π-orbitals as well. In planar systems, the π-orbitals can be admixed only with low-lying vacant π-orbitals, which are mainly their antibonding counterparts. The signs of the bonding and antibonding π-orbitals in the proximities of the bonded nuclei obey the same rules as the signs of the σ-orbitals, which leads to the sign alternation of the spin polarization of π-orbitals. The above reasoning can be expressed as follows:

$$\pi'_\alpha \approx \pi + \tau\pi^* \qquad (2)$$

$$\pi'_\beta \approx \pi - \tau\pi^* \qquad (3)$$

$$\rho_\alpha - \rho_\beta \approx (\pi + \tau\pi^*)^2 - (\pi - \tau\pi^*)^2 = 4\tau\,\pi\,\pi^*. \qquad (4)$$

In equations 2 – 4, π is a closed-shell π-orbital, π^* is its antibonding counterpart, ρ_α and ρ_β are the α and β densities of the polarized π-orbital, and τ is the admixing coefficient. Equation 4 shows that the sign of the spin density of the polarized π-orbital at any point is determined by the product of the unperturbed (unpolarized) bonding and antibonding π-orbitals and the sign of the admixing coefficient. The sign of the admixing coefficient ensures that, in the proximity of the first nucleus, the nuclear and

electron spins have opposite orientation (assuming that the g-value of the first nucleus is positive). The π and π^* orbitals are constructed as the bonding and antibonding combinations of atomic p-orbitals. This means that their product always has opposite signs in the proximities of two neighboring atoms.

Note that if an occupied MO is antibonding between two neighboring atoms and it admixes a vacant MO which is bonding, their product would also have the opposite signs in the proximities of the two neighboring atoms. As an example, the sign-alternating effect of the product between the HOMO and LUMO for 1,3,5,7,9-decapentaene is shown in Figure 4. The HOMO and LUMO are both a mixture of bonding and antibonding with respect to individual C – C bonds, but the HOMO is overall slightly more bonding than antibonding and the LUMO is vice versa. Both orbitals have a similar number of nodes but shifted, so the nodes of the two orbitals are in antiphase with each other. Therefore, their product contributes to the sign- alternating pattern.

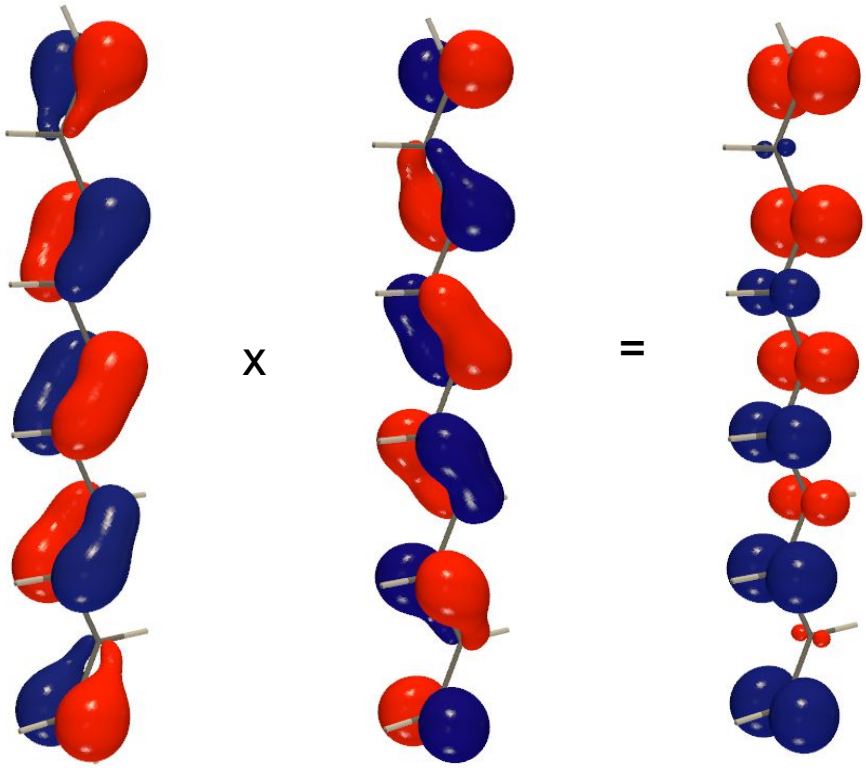

Figure 4. The HOMO and LUMO for 1,3,5,7,9-decapentaene (left and middle, correspondingly) and their product (right) contributing to the sign-alternating pattern of the FC-induced spin density. The isosurface value is 0.05 a.u. for MOs and 0.0025 a.u. for their product.

The polarized π-orbitals transmit spin-polarization to σ-orbitals. Due to Hund's rule, the sign of the spin-density of such polarized σ-orbitals in the proximity of the nuclei will be consistent with the sign of the spin-density of the π-orbitals. This explains the sign alternation seen in the π-TSP effect in Figure 3, middle.

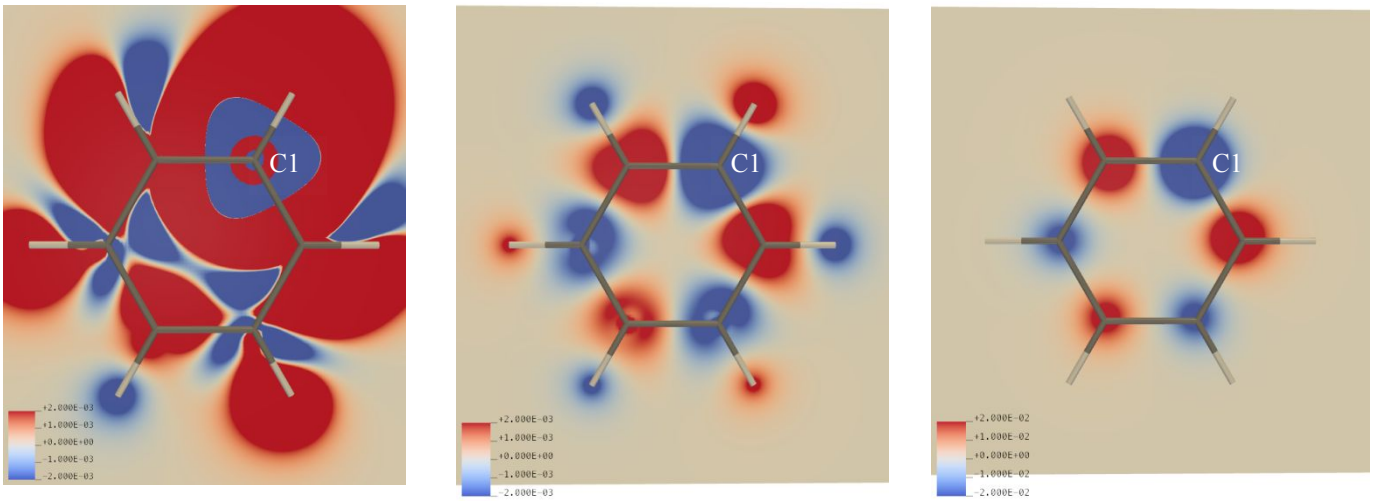

Figure 5. The spin-density in benzene induced by FC(C1) (color-coded according to the density values given in a.u.). The total spin-density (left) and spin-polarization only due to the π-TSP effect (middle) are shown in the molecular plane. The spin-polarization of the group of π-orbitals is shown in the plane 0.5 Å below the molecular plane (right).

The plots for the spin-polarization in our next example, benzene, are shown in Figure 5. The sign alternation and the shapes of the lobes in the middle plot in Figure 5 resemble those for 1,3,5,7,9-decapentaene (Figure 3, middle and right). However, the π-TSP effect is less important, relative to the total spin-density, in benzene (Figure 5, left) than in 1,3,5,7,9-decapentaene, because in benzene the carbons atoms are separated by three bonds at most, i.e. there are no long-range C-C couplings. The spin-polarization of the π-orbitals themselves shows the same sign alternation pattern as in the previous system (Figure 5, right). Thus, we can conclude that while the transmission of spin-polarization via π-orbitals in benzene is easily observed, it does not play a central role in spin-spin couplings between carbons due to the presence of only short-range couplings.

In this respect, naphthalene, a system that can be viewed as the fusion of a pair of benzene rings, would be more informative for analyzing the π-TSP effect on the spin-polarization, due to the presence of several long-range C – C couplings through up to five bonds.

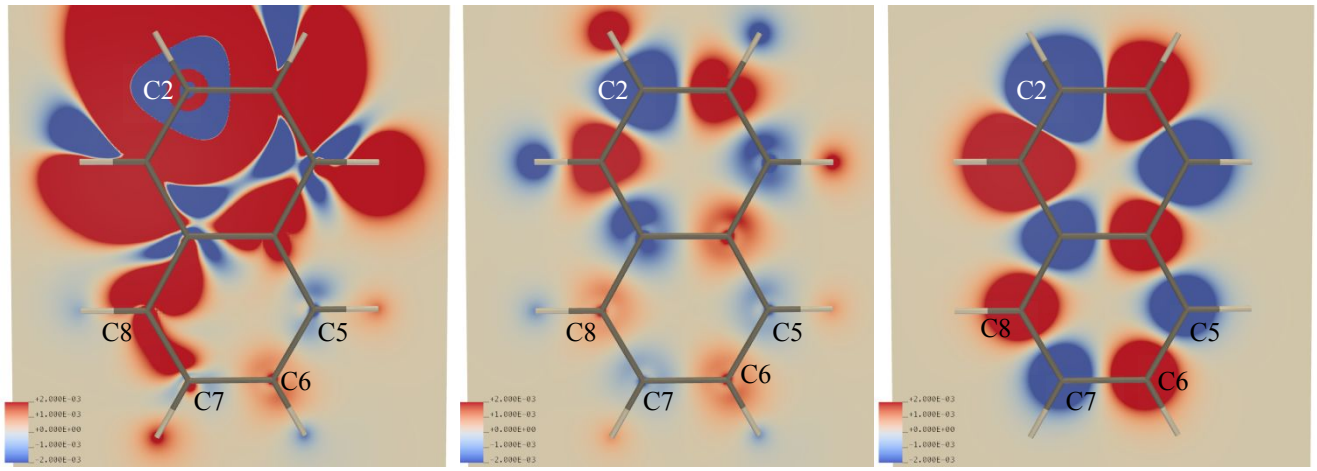

Figure 6. The spin-density in naphthalene induced by FC(C2) (color-coded according to the density values given in a.u.). The total spin-density (left) and spin-polarization only due to the π-TSP effect (middle) are shown in the molecular plane. The spin-polarization of the group of π-orbitals is shown in the plane 0.5 Å below the molecular plane (right).

The spin-polarization induced by FC(C2) in naphthalene (Figure 6, left) in the first ring (containing C2) is similar to that in benzene (Figure 5, left). The induced spin-density at C5 and C6 is mainly due to π-TSP (compare the right and middle plots in Figure 6). The sign alternation due to the π-TSP effect is clearly seen in the second ring (Figure 6, middle). The π-TSP effect on the spin-density in naphthalene (Figure 6, middle) is again consistent with the spin-polarization of the π-orbitals (Figure 6, right), and it extends to hydrogen atoms. ^{5}J(C2-C6) is essentially the result of the π-TSP effect whereas ^{4}J(C2-C7) and ^{4}J(C2-C5) are also affected by the π-TSP effect but to a smaller extent, which is consistent with the data in Table 3.

In all of the examples just listed, the spin-polarization of the π-orbitals follows the sign-alternating pattern, resulting in the sign alternation of the total spin-density induced by FC(C) even in areas that are rather remote from the center of perturbation (***n*** > 4). However, exceptions to this rule

can occur. An example of this is the cyclobutadienyl dication, where an additional effect conflicts with the usual sign alternation. The doubly-degenerate LUMO is nonbonding and its product with the HOMO does not display consistent sign alternation on adjacent carbon atoms, but does show sign alternation between carbons separated by two bonds (see Figures S5 and S6 in ESI). The π-TSP effect on the FC induced spin-density in the cyclobutadienyl dication and spin-polarization of the π-orbitals taken together are shown in Figure 7. The planar form of the cyclooctatetraenyl dication is another example where similar findings relating to sign alternation are obtained. The π-TSP effect on the spin density in the cyclooctatetraenyl dication induced by FC(C1) and the spin-polarization of the group of π-orbitals are shown in Figure S7 in ESI. The HOMO, LUMO and their products are plotted in Figure S8 in ESI. The overall HOMO contribution to the spin density is seen in Figure S9 in ESI.

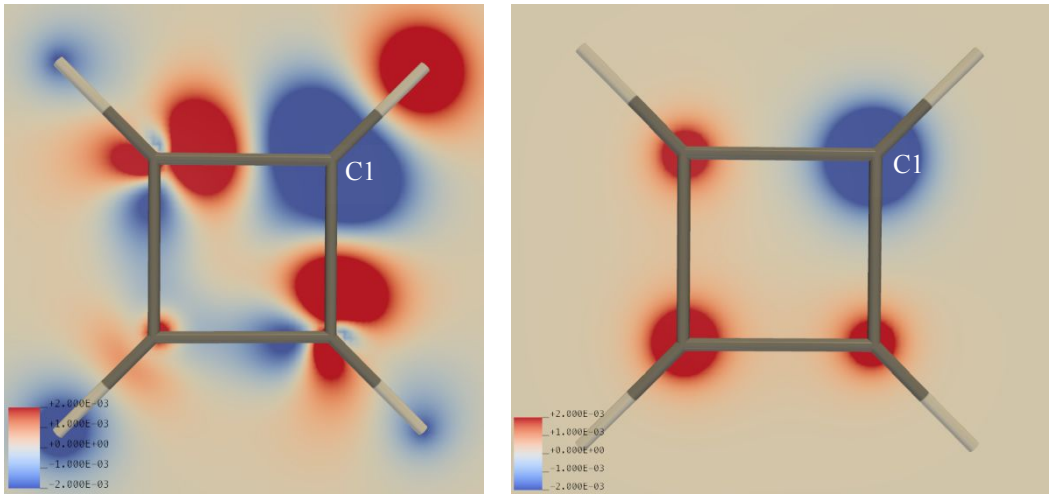

Figure 7. The π-TSP effect on the spin density in cyclobutadiene dication induced by FC(C1) (left; color-coded according to the density values given in a.u.) and spin-polarization of the group of π-orbitals in the plane 0.5 Å below the molecular plane (right).

The π-TSP effect on CDD

The plots of the FC-induced spin-density show the propagation of spin-polarization through the whole molecule, but they do not provide information about the magnetic interaction of a particular pair

of nuclei. This can be achieved by plotting the CDD (see section Computational Methods), which shows what parts of the electron density are involved in the interaction of the two nuclear magnetic moments and nothing else. This way, one can see how π-TSP affects the spin-spin coupling pathways. Figure 8 shows the total CDD for ^{9}J(C1-C10) in 1,3,5,7,9-decapentaene (left) and which part of the CDD is the result of π-TSP (middle). Comparison of the plots shows that the π-TSP effect is responsible for the main changes in the electron density due to the interaction of the nuclear magnetic moments of C1 and C10. On decreasing the number of bonds separating the coupled nuclei, the relative role of π-TSP diminishes (see Figure S10 in ESI). For ***n*** = 4 it is no longer dominant, though π-TSP affects the CDD even at C10 (Figure S10 in ESI, middle). Interestingly, the transmission of spin-polarization by the π- and σ-channels have opposite effects on the CDD at C8 (compare the middle and right plots in Figure S10 in ESI).

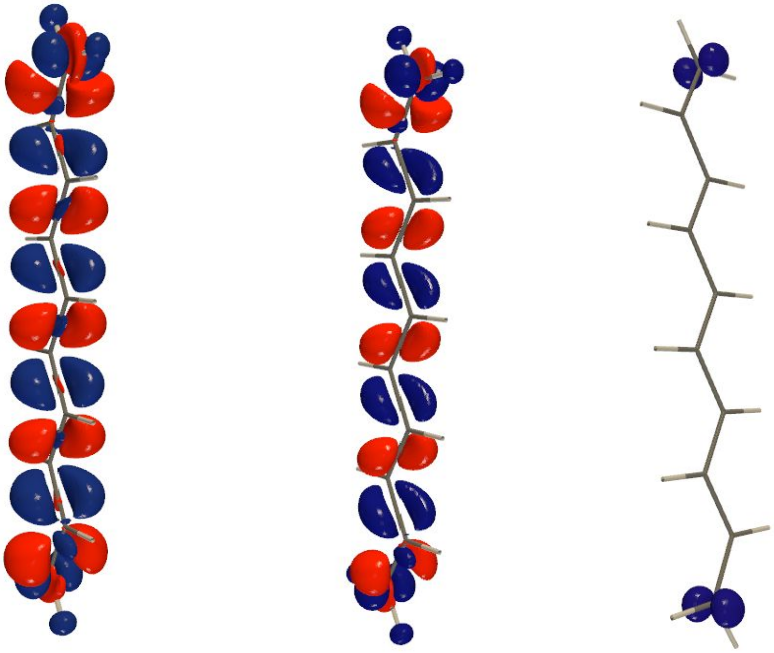

Figure 8. CDD for ^{9}J(C1-C10) in 1,3,5,7,9-decapentaene: total (left), and due the π-TSP effect (middle) and the CDD when the π-TSP effect is switched off (right). The isosurface value in all plots is 0.001 a.u.

For ^{3}J(C1-C4) in benzene, the π-TSP effect on CDD is much less important than other channels for the transmission of spin-polarization (see Figure 9). To visualize the π-TSP effect for ^{3}J(C1-C4) we have to use an isosurface value ten times smaller than that for the total CDD.

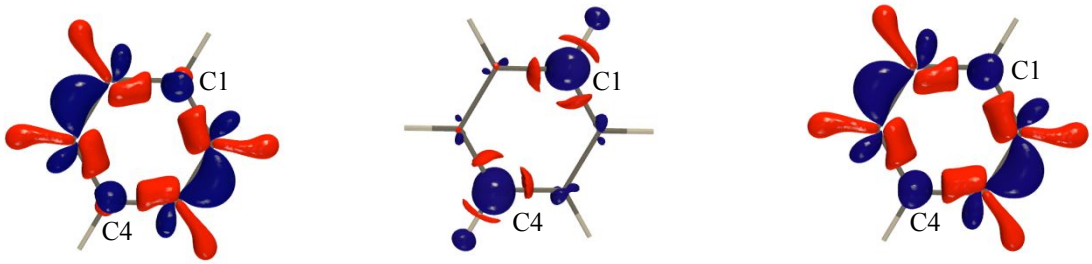

Figure 9. CDD for ^{3}J(C1-C4) in benzene: total (left), due to the π-TSP effect (middle) and the CDD when the π-TSP effect is switched off (right). The isosurface value in the right and left plots is 0.02 a.u. In order to show the π-TSP effect (middle) we used a smaller isosurface value of 0.002 a.u.

The CDDs for long-range C-C couplings in naphthalene are shown in Figures S11-S13 in ESI. The CDD for ^{5}J(C2-C6) in Figure S11 (ESI) is dominated by π-TSP, but its effect diminishes for ^{4}J(C2-C7) and ^{4}J(C1-C6) and (Figures S12 and S13, ESI). Interestingly, the interaction between C2 and C7 occurs along a single zig-zag pathway (Figure S12, left, ESI), but neither the total CDD nor the part thereof arising due to the π-TSP effect resemble their counterparts for ^{4}J(C1-C5) in 1,3,5,7,9-decapentaene in Figure S10 in ESI. The relative role of the π-TSP effect in the CDD of the latter is more important than for ^{4}J(C2-C7) in naphthalene.

The π-TSP effect on Hyperfine Coupling

The π-TSP effect on the EPR hyperfine coupling constant (HFCC) has received much less attention in the literature than its effect on NMR spin-spin couplings. The tools described above also allow one to analyze this phenomenon. The FC contribution to NMR spin-spin couplings and the EPR hyperfine coupling constant use the same operator, so some similarities between these two properties are expected. To illustrate the resemblances and dissimilarities of the π-TSP effect on EPR hyperfine coupling with C-C spin-spin couplings in 1,3,5,7,9-decapentaene, we considered a model system made by removing H19 without reoptimizing the structure (i.e., keeping the rest of the structure unchanged, in

order to facilitate the deconvolution of the main effect under scrutiny from other changes due to structural relaxation; the calculated ^{13}C HFCCs for the optimized structure are collected in Table S5 in ESI).[30] The calculated HFCC results are presented in Table 4, where the second column contains ^{13}C HFCCs obtained with all orbitals participating in the transmission of spin-polarization. The third column shows the results when the π-TSP effect is switched off, that is, when the π-orbitals do not polarize other orbitals *via* the exchange interaction. The last column contains the differences between the values in the second and third columns, in other words the contributions to ^{13}C HFCC solely due to the transmission of spin-polarization by the π-system. Just as in Table 1, the last column displays a remarkably stable sign alternation, also shown in Figure 10. The graph in Figure 10 strikingly resembles the graph for the π-TSP effect on $^{n}J^{FC}$(C1-C$_{n+1}$) in 1,3,5,7,9-decapentaene in Figure 2, since the transmission of spin-polarization via the system of π-orbitals is the same (π-channel).

Table 4. The π-TSP effect on ^{13}C HFCC in the 1,3,5,7,9-decapentaene-1-yl radical. The values are given in MHz.

Carbon	π-TSP switched ON	π-TSP switched OFF	Difference
1	441.39	434.46	6.94
2	2.64	9.16	-6.53
3	44.33	39.61	4.72
4	-5.74	-2.35	-3.40
5	3.40	0.27	3.13
6	-2.88	-0.56	-2.32
7	2.54	0.28	2.26
8	-2.35	-0.63	-1.72
9	1.82	0.18	1.64
10	-1.70	-0.41	-1.28

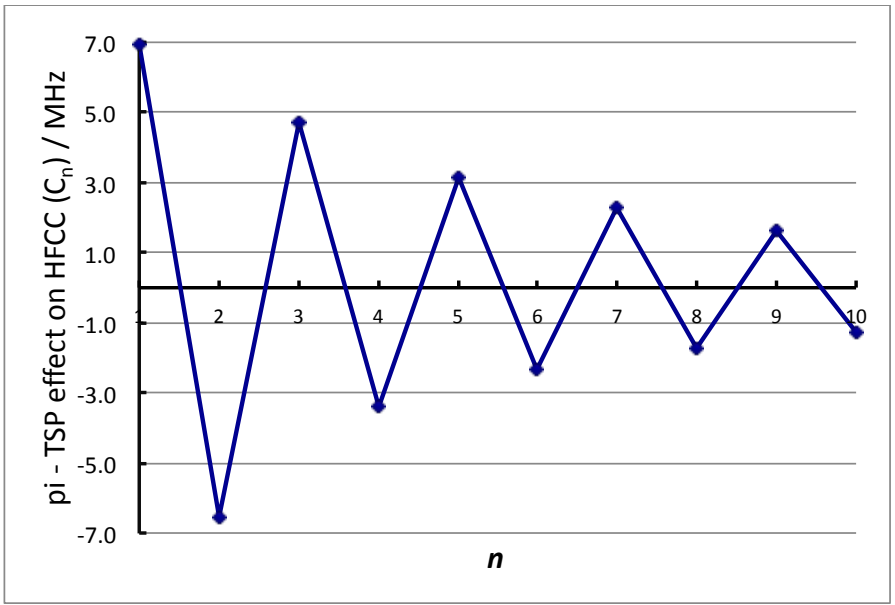

Figure 10. The π-TSP effect on ^{13}C HFCC (in MHz) in the 1,3,5,7,9-decapentaen-1-yl radical. The values on the horizontal axis correspond to the numbering of carbons in Figure 1, left.

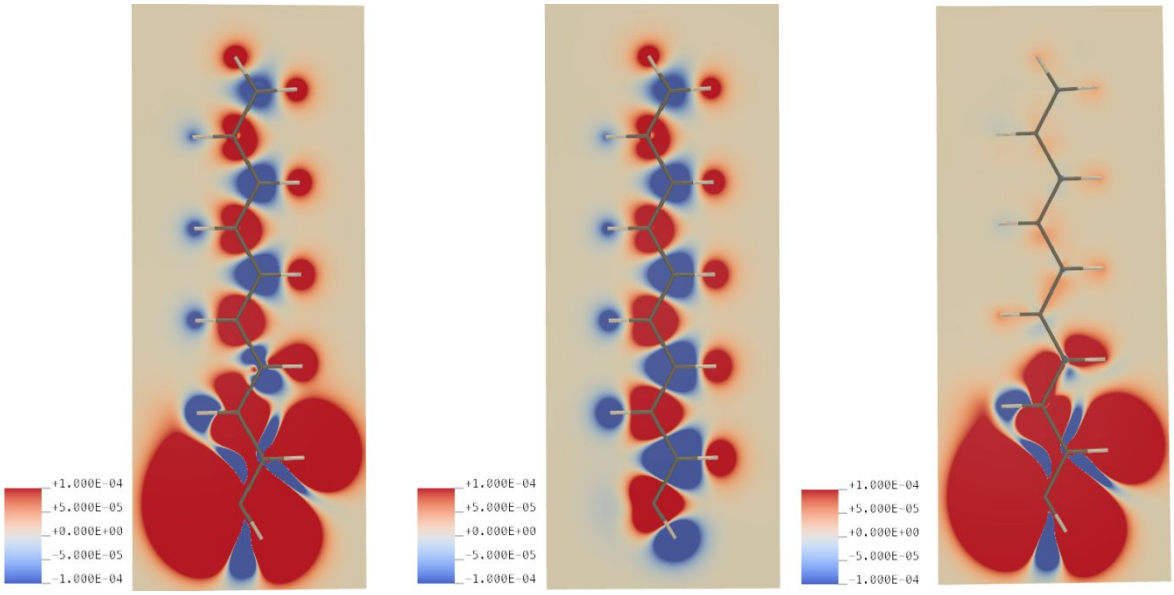

Figure 11. The spin-density of the 1,3,5,7,9-decapentaene-1-yl radical in the radical plane: total (left), the spin-density due-to the π-TSP effect (middle) and when the π-TSP effect is switched off (right).

The distribution of spin-density in the 1,3,5,7,9-decapentaen-1-yl radical is shown in Figure 11, left. The π-TSP effect on the spin-density is visualized in the middle plot of Figure 11. The spin-density in the absence of the π-TSP effect (Figure 11, right) can be associated with the SOMO contribution (the density of the SOMO is presented in Figure 12). It is interesting to note the significant delocalization of the SOMO in space. Still, it is clear that long-range hyperfine couplings are, as expected, due to the π-TSP effect.

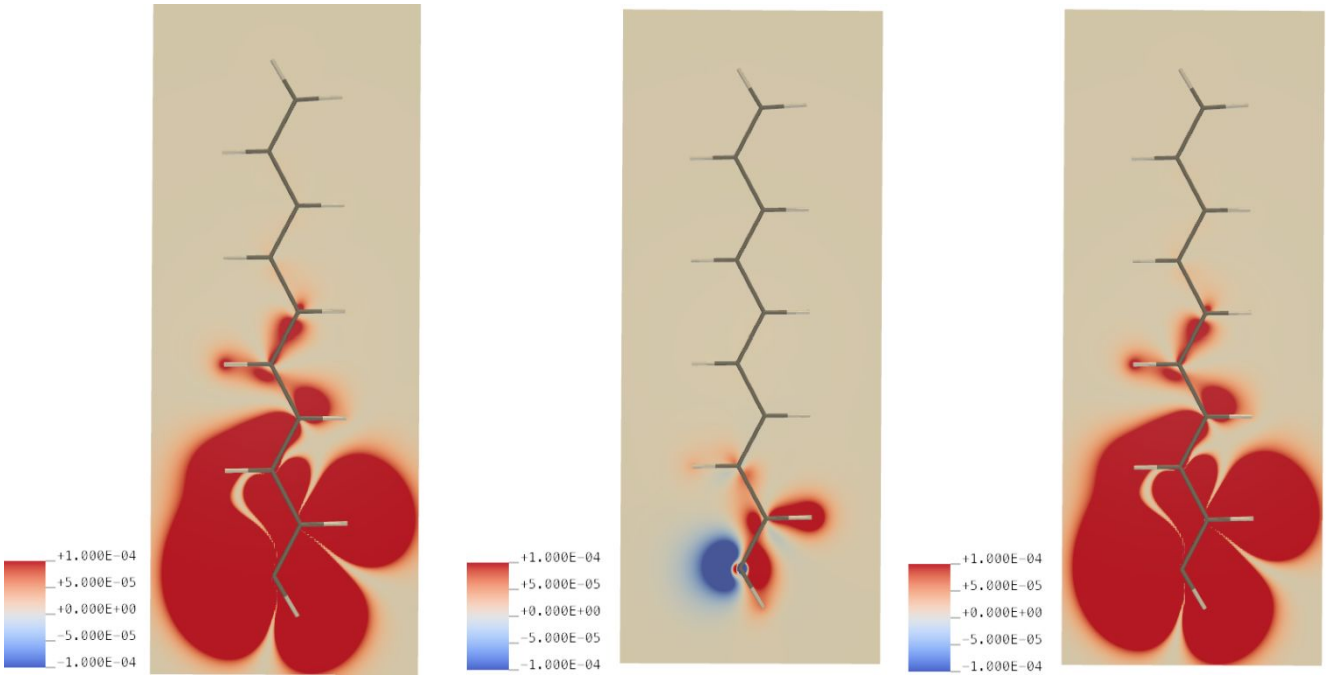

Figure 12. The SOMO density in the 1,3,5,7,9-decapentaen-1-yl radical (left), the π-TSP effect on the density of the SOMO (middle) and the SOMO density when the π-TSP effect is switched off (right).

The C10 hyperfine coupling pathway is plotted in Figure 13, a. It shows the changes in the spin-density due to its interaction with the C10 nuclear magnetic moment. The total pathway looks very similar to the CDD for ^{9}J(C1-C10) in 1,3,5,7,9-decapentaene (Figure 8, left) except for the observed interchange of the colors (red ↔ blue) due to the opposite signs of the carbon and electron magnetic moments.[14] With the exception of areas near C10 and to a lesser extent near C1, the dominant contribution to HFDD comes from the differences in the spin-polarization of valence π-orbitals when the C10 nuclear magnetic moment is up and down. The π-orbitals can be polarized by the exchange interaction either with other π-orbitals (the π-TSP effect shown in Figure 13, b) or with *s*- and *σ*-orbitals (Figure 13 c and d). The latter effect is less important and it is seen only when plotted with a smaller isosurface value (Figure 13, d). The HFDDs in Figures 13, a-c are also shown as color maps in the plane 0.5 Å below the radical plane in Figure S14 in SI.

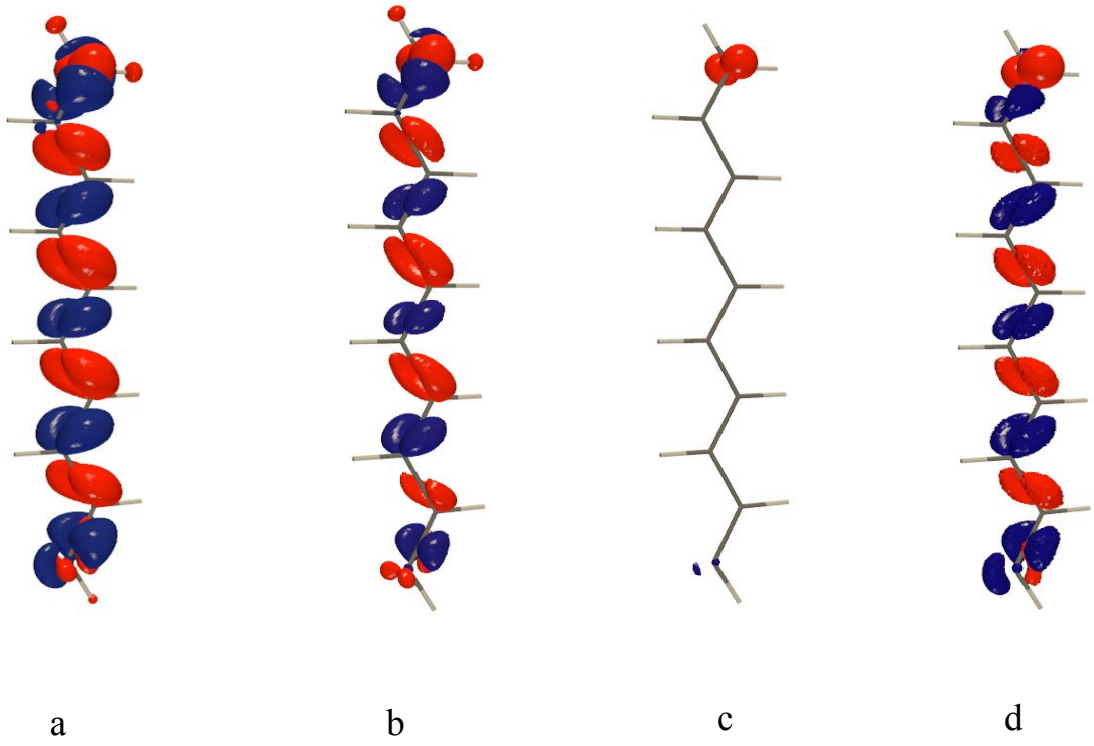

Figure 13. The C10 HFDD in the 1,3,5,7,9-decapentaen-1-yl radical (a); the π-TSP effect on the C10 HFDD (b) and the C10 HFDD when the π-TSP effect is switched off (c and d). The isosurface value is 0.0002 a.u. in plots a, b, and c and 0.0001 a.u. in plot d.

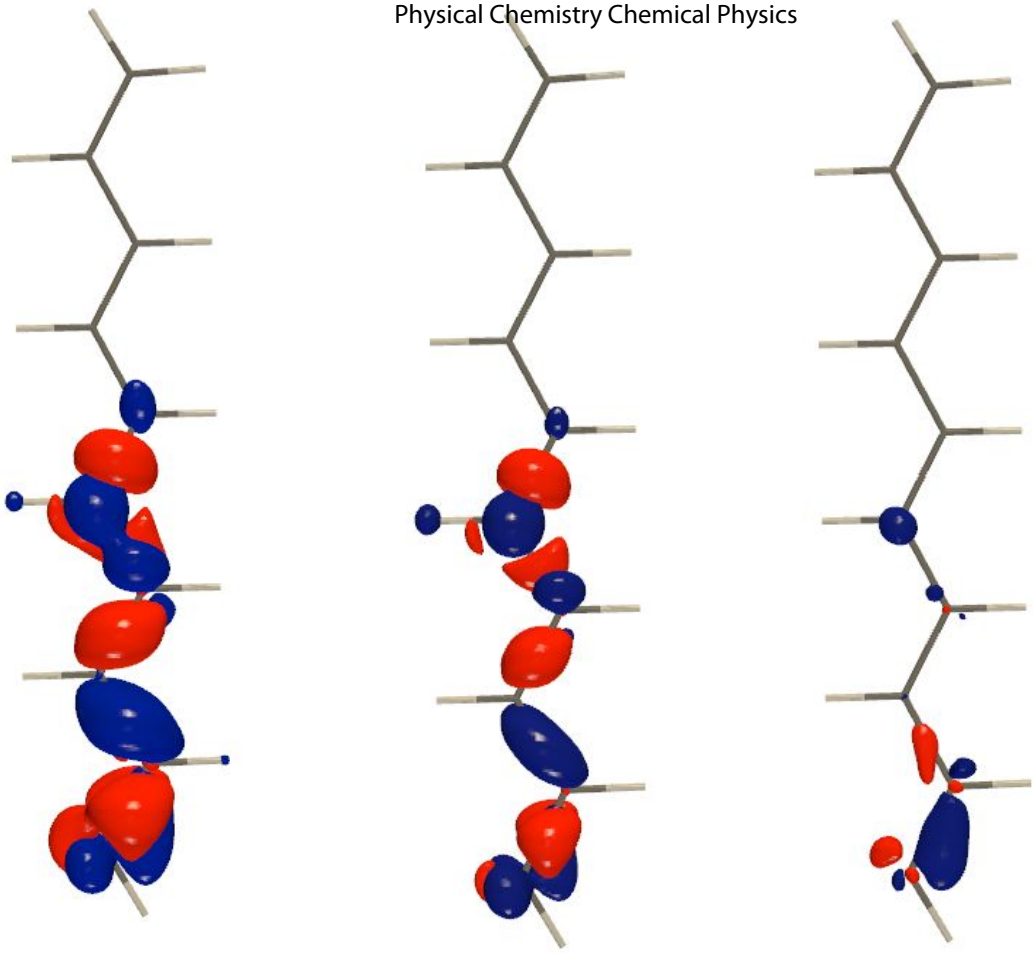

Figure 14. The C5 HFDD in the 1,3,5,7,9-decapentaen-1-yl radical (a); the π-TSP effect on the C5 HFDD and the C5 HFDD (b) when the π-TSP effect is switched off (c). The isosurface value is 0.0003 a.u. in all plots.

The π-TSP effect on the C5 HFDD in the 1,3,5,7,9-decapentaen-1-yl radical is shown in Figure 14. The differences between the CDD for ^{4}J(C1-C5) and C5 HFDD (and the corresponding π-TSP effects) are now more noticeable (compare with Figure S10 in ESI) than for their long-range counterparts in Figures 8 and 13. The π-TSP effect on the C5 HFDD is significant, which is consistent with the HFCC values in Table 4.

Conclusions

We have presented a new DFT-based approach assessing the effect of the transmission of spin-polarization by π-orbitals (π-TSP) and applicable to the analysis of molecular properties that depend on

the effects of spin-polarization (i.e, NMR spin-spin couplings, EPR hyperfine couplings, etc.). This approach does not depend on a particular perturbation theory or analysis based on contributions from an arbitrary choice of MOs (although these are useful for analysis and rationalization), but is based on evaluating the magnetic resonance properties of interest directly from total electron densities and spin densities. Specifically, we have studied the mechanism of propagation of spin polarization in planar unsaturated hydrocarbons (with clear σ/π separation), calling special attention to the way the π -MOs contribute to the transmission of spin density along the bonds. Orbitals transmit spin-polarization via their exchange-correlation interaction with other orbitals. With a simple manipulation, namely averaging the α and β densities from the π-MOs within the total densities for the calculation of the exchange-correlation contribution to the Fock matrix, the contribution of these π-MOs to the spin polarization can be switched off. This approach has been applied to estimating the π-TSP effect on different aspects of the Fermi-contact contribution to NMR spin-spin couplings and EPR hyperfine structure coupling constants: specifically, the π-TSP effect on the distribution of spin-density, spin-spin coupling pathways and pathways of EPR hyperfine couplings. To the best of our knowledge, the sign alternation of the π-TSP effect on spin-spin couplings is here for the first time explained based on perturbation theory and Hund's rule. We have also identified exceptions to this pattern, where – for identifiable reasons – spin-polarization delocalization effects occur across a cyclic π-system, interfering with the usual sign-alternating pattern.

Electronic Supplementary Information

Calculated *J*(C-C) in 1,3,5,7,9-decapentaene, benzene and naphthalene; the bond lengths in the optimized structure of naphthalene; the FC and SD contributions to *J*(C-C) in 1,3,5,7,9-decapentaene calculated with different DFT functionals; 3d plot of spin-polarization of the group of π-orbitals in 1,3,5,7,9-decapentaene; MO contributions to spin polarization for cyclobutadieneyl and cyclooctatetraenyl dications to illustrate the interference with the sign alternating pattern; CDDs for J(C-C) in naphthalene; calculated 13C HFCCs in the 1,3,5,7,9-decapentaene-1-yl radical for the optimized structure; color maps of the C10 HFDD; optimized structures used in this work.

Conflicts of interest

There are no conflicts to declare.

Acknowledgments

We acknowledge the support from Slovak-French PHC Stefanik project "Spin Coupling Advanced Level Perception" (SCALP). OM, VM and JRA acknowledge the support from Slovak grant agencies APVV (grants No. SK-FR-19-0001 and APVV-19-0516) and VEGA (grant No. 2/0135/21). This work was also supported by the CNRS, the Université de Bourgogne, the Conseil Régional BFC (CHIMENE project), the PIA-excellence ISITE-BFC program (COMICS project) and the FEDER, which are all sincerely thanked. MB thanks EastCHEM and the School of Chemistry in St Andrews for support and access to a computing facility maintained by Dr H. Früchtl.

CORRESPONDING AUTHORS

Olga L. Malkina – Institute of Inorganic Chemistry, Slovak Academy of Sciences, Dúbravská cesta 9, 84 536 Bratislava, Slovakia; Email: olga.malkin@savba.sk

Vladimir G. Malkin – Institute of Inorganic Chemistry, Slovak Academy of Sciences, Dúbravská cesta 9, 84 536 Bratislava, Slovakia; Email: vladimir.malkin@savba.sk

1 W. Kutzelnigg, U. Fleischer, M. Schindler, in *NMR-Basic Principles and Progress*, Vol. 23, Eds. P. Diehl, E. Fluck, H. Günther, R. Kosfeld, J. Seelig (Springer Verlag, Heidelberg, 1990), p. 165-262.
2 P. v. R. Schleyer, Ch. Maerker, A. Dransfeld. H. Jiao, N. J. R. van E. Hommes, P. v. R. Schleyer, H. Jiao, N.J.R. van E. Hommes, *J. Am. Chem. Soc*., 1996, 118, 6317-6318; P. v. R. Schleyer, V.G. Malkin, O.L. Malkina, *J. Am. Chem. Soc*., 1997, **119**, 12669-126709; H. Fallah-Bagher-Shaidaei, C. S Wannere, C. Corminboeuf, R. Puchta, P. v. R. Schleyer, *Org. Lett.* 2006, **8(5),** 863-866; Z. F Chen, C. S. Wannere, C. Corminboeuf, R. Puchta, P. v. R. Schleyer, *Chem. Rev.* 2005, **105(10),** 3842-3888.
3 H. Fliegl, R. Valiev, F. Pichierri and D. Sundholm, *Chemical Modelling*, 2018, **14**, 2018, 1-42.
4 R. K. Harris, Nuclear Magnetic Resonance Spectroscopy, 1983, Pitman Books Limited.
5 J. A. Pople, P. Gill, N. C. Handy, *Int. J. Quantum. Chem*. 1995, **56(4)**, 303-305.
6 H. M. McConnell, *Journal of Molecular Spectroscopy* 1995, **1**, 11-17.
7 H. M. McConnell*, J. Chem. Phys*. 1959, **30**, 126.
8 M. J. Barfield, *Chem. Phys*. 1968, **49**, 2145-2153; Erratum: Ibid.1969, **51**, 2291-2292.
9 J. Kowalewski, Calculations of Nuclear Spin-Spin Coupling Constants in *Progress in NMR Spectroscopy*, 1977, **I I**, l-78, Pergamon Press.
10 H. Fukui, T. Tsuji, and K. Miura, *J. Am. Chem. Soc.* 1981, **103**, 3652.
11 A.R. Engelmann, Scuseria and Contreras, *JOURNAL OF MAGNETIC RESONANCE* 1982, **9**, 21-29.
12 V. G. Malkin, O. L. Malkina, D. R. Salahub, *Chem. Phys. Lett.* 1994, **221**, 91.
13 J. Gräfenstein, T. Tuttle and D. Cremer, *Phys . Chem. Chem. Phys*, 2005, **7**, 452 – 462.
14 V. G. Malkin, O. L. Malkina, G. M. Zhidomirov, *J. Phys. Chem. A*, 2017, **121 (18)**, 3580–3587.
15 C. Sire, H. Cattey, A. Tsivery, J.-C. Hierso, J. Roger, *Advanced Synthesis & Catalysis*, 2022, **364**, 440-452; O. L. Malkina, J.-C. Hierso, V. G. Malkin, *Am. Chem. Soc*, 2022, **144**, 10768-10784.
16 S. Mom, M. Beaupérin, D. Roy, S. Royer, R. Amardeil, H. Cattey, H. Doucet, J.-C. Hierso, *Inorganic Chemistry*, 2011, **50**, 11592-11603; T.-A. Nguyen, M.-J. Penouilh, H. Cattey, N. Pirio, P. Fleurat-Lessard, J.-C. Hierso, J. Roger, *Organometallics*, 2021, **40**, 3571-3584.
17 E. Duval, S. Koide, *Phys. Lett.*, 1964, **8(6)**, 314-315.
18 L. A. Eriksson, V. G. Malkin, O. L. Malkina, D. R. Salahub D.R., J. Chem. Phys., 1993, **99**, 9756.
19 O.L. Malkina, V.G. Malkin, *Angew. Chem. Int. Edition*, 2003, **42**, 4335-4338.
20 M. Karplus, *J. Chem. Phys*., 1960, **33**, 1842; M. Barfield, J. Chem. Phys. 1970, 74, 621-626.
21 Gaussian 03, Revision A.1, Frisch, M. J.; Trucks, G. W.; Schlegel, H. B.; Scuseria, G. E.; Robb, M. A.; Cheeseman, J. R.; Zakrzewski, V. G.; Montgomery, Jr., J. A.; Stratmann, R. E.; Burant, J. C. et al., Gaussian, Inc., Pittsburgh PA, 2003.
22 M. Bremer, P. v. R. Schleyer, U. Fleischer *Am. Chem. Soc*, 1989, **111**, 1147; H.-U. Siehl, *Adv; Org. Chem.* 2008, **42**, 152.
23 D. R. Salahub, R. Foumier, P. Mlynarski, I. Papai, A. St-Amant, J. Ushio, In *Density Functional Methods in Chemistry*; Labanowski, J.K.; Andzelm, J. W., Eds.; Springer: Berlin, 1991; p 77.
24 V. G. Malkin, O. L. Malkina, deMon-NMR program, version 2021.
25 J. P. Perdew, Y. Wang, Y. *Phys. Rev. B,* 1986, **33**, 8800- 8802.
26 J. P. Perdew, Y. Wang, *Phys. Rev. B* 1989, **40**, 3399.
27 J. P. Perdew*Phys. Rev. B* 1986, **33**, 8822–8824.
28 J. P. Perdew, *Phys. Rev. B* 1986, **34**, 7406.

29 M. D. Hanwell, D. E. Curtis, D. C. Lonie, T. Vandermeersch, E. Zurek, G. R. Hutchison, Avogadro: An Advanced Semantic Chemical Editor, Visualization, and Analysis Platform. *Journal of Cheminformatics* 2012, 4-17.
30 Spin contamination is small in this radical, e.g. <Ŝ2>=0.77 at P86/lGLO-II.

Electronic Supplementary Material

Transmission of spin-polarization by π-orbitals: an approach to assessing its effect on NMR spin-spin coupling and EPR hyperfine structure

Olga L. Malkina,*[,a] Florian Lemken[a], James R. Asher[a,b], Jean-Cyrille Hierso[c], Michael Bűhl[d], Vladimir G. Malkin*[a]

[a] *Institute of Inorganic Chemistry, Slovak Academy of Sciences, Dúbravská cesta 9, SK-84536 Bratislava, Slovakia*

[b] *Faculty of Natural Sciences, Department of Inorganic Chemistry, Comenius University, Mlynská dolina CH2, SK-84215 Bratislava, Slovakia*

[c] *Institut de Chimie Moléculaire de l'Université de Bourgogne (ICMUB, UMR CNRS 6302), Université Bourgogne–Franche-Comté (UBFC), 9 avenue Alain Savary, 21078 Dijon Cedex, France*

[d] *EaStChem School of Chemistry, University of St Andrews, St Andrews, Fife KY16 9ST, UK*

Table S1. Calculated ^{n}J (C1- C_{n+1}) in 1,3,5,7,9-decapentaene in Hz calculated using the P86 exchange-correlation functional.

n	FC	PSO	DSO	SUM[a]
1	77.44	-8.60	0.14	68.98
2	1.86	0.16	-0.05	1.97
3	7.43	0.62	-0.08	7.97
4	-0.72	0.02	-0.04	-0.74
5	1.04	-0.11	-0.04	0.89
6	-0.70	0.02	-0.02	-0.70
7	0.73	0.05	-0.02	0.76
8	-0.54	0.01	-0.01	-0.54
9	0.52	0.01	-0.01	0.52

a) The calculation of the SD term is not implemented in the deMon program.

Table S2. Calculated ^{n}J(C1- C_{n+1}) in benzene in Hz calculated using the P86 exchange-correlation functional.

n	FC	PSO	DSO	SUM[a]
2	62.94	-6.61	0.21	56.54
3	-0.33	0.04	-0.02	-0.31
4	7.80	0.46	-0.01	8.25

a) The calculation of the SD term is not implemented in the deMon program.

Table S3. Calculated ^{n}J(C1- C_{n+1}) in naphthalene in Hz calculated using the P86 exchange-correlation functional.

n		FC	PSO	DSO	SUM[a]
1	C1-C2	67.97	-7.46	0.22	60.73
	C1-C9	61.28	-5.38	0.28	56.18
	C2-C3	59.07	-5.43	0.22	53.86
	C9-C10	55.82	-5.45	0.33	50.7
2	C1-C8	3.78	-0.05	0.01	3.74
	C1-C10	1.14	-0.03	0.03	1.14
	C2-C9	0.36	-0.02	0.02	0.36
	C1-C3	-0.03	0.08	-0.01	0.04
3	C3-C9	6.45	0.21	0.03	6.69
	C1-C4	5.33	0.34	0.01	5.68
	C1-C5	2.35	-0.21	-0.06	2.08
4	C2-C7	0.52	0.05	-0.06	0.51
	C1-C6	-0.50	0.01	-0.06	-0.55
5	C2-C6	0.46	0.01	-0.05	0.42

a) The calculation of the SD term is not implemented in the deMon program

Table S4. ^{n}J (C1- C_{n+1}) in 1,3,5,7,9-decapentaene in Hz calculated[a] using the BP86 and B3LYP exchange-correlation functionals.

n	V_{xc}	FC	SD	PSO	DSO	Total
1	BP86	70.88	3.01	-8.56	0.14	65.47
	B3LYP	83.76	4.69	-9.18	0.13	79.41
2	BP86	2.44	-1.85	0.17	-0.05	0.70
	B3LYP	-0.90	-4.00	0.17	-0.05	-4.78
3	BP86	6.92	2.64	0.65	-0.08	10.12
	B3LYP	9.77	4.53	0.66	-0.08	14.88
4	BP86	-0.37	-1.11	0.02	-0.04	-1.51
	B3LYP	-2.83	-2.84	0.02	-0.04	-5.69
5	BP86	0.68	1.79	-0.11	-0.04	2.32
	B3LYP	2.99	3.61	-0.11	-0.04	6.46
6	BP86	-0.48	-0.65	0.02	-0.02	-1.14
	B3LYP	-2.38	-1.89	0.02	-0.02	-4.28
7	BP86	0.45	1.47	0.05	-0.02	1.95
	B3LYP	2.26	3.06	0.05	-0.02	5.35
8	BP86	-0.39	-0.37	0.01	-0.01	-0.77
	B3LYP	-1.70	-1.06	0.01	-0.01	-2.77
9	BP86	0.30	1.18	0.00	-0.01	1.46
	B3LYP	1.56	2.39	0.01	-0.01	3.94

a) IGLO-II basis set (ref. 1), G03 package (ref. 21).

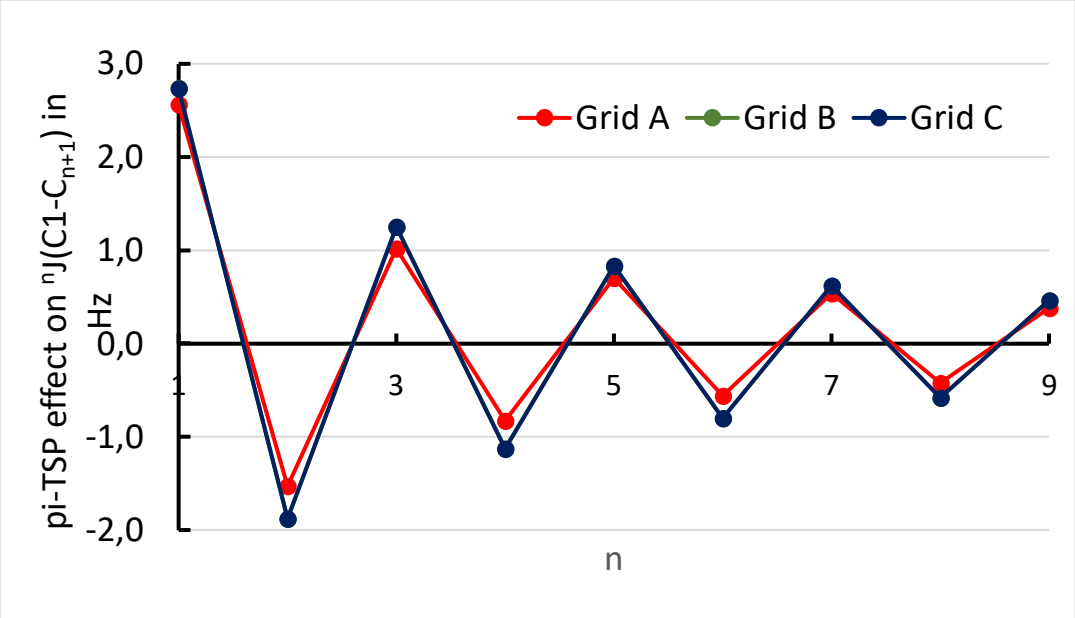

Figure S1. The π-TSP effect on ${}^{n}J^{FC}$(C1- C_{n+1}) in 1,3,5,7,9-decapentaene as a function of the number of bonds separating two carbons (in Hz) calculated using three different grids for numerical integration. Grid A: about 3000 points/atom during the main SCF procedure,then an extra SCF iteration with about 10500 points/atom; Grid B: about 10500 points/atom; Grid C: about 20000 points/atom.

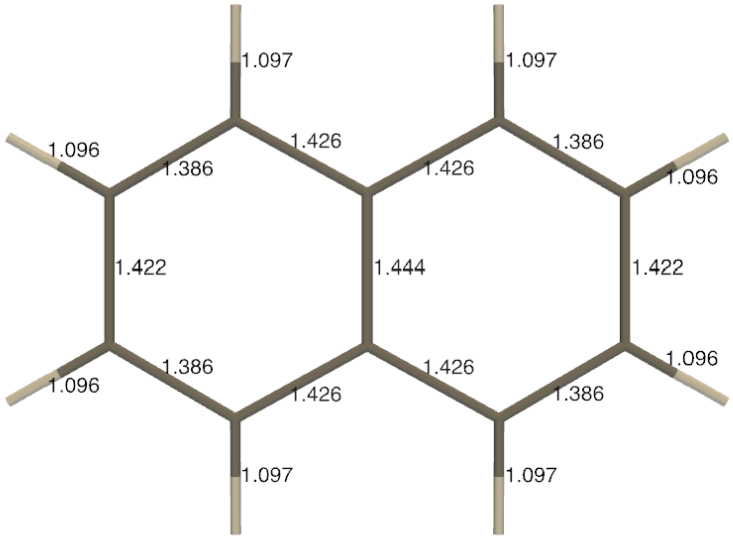

Figure S2. The bond lengths in the optimized structure of naphthalene.

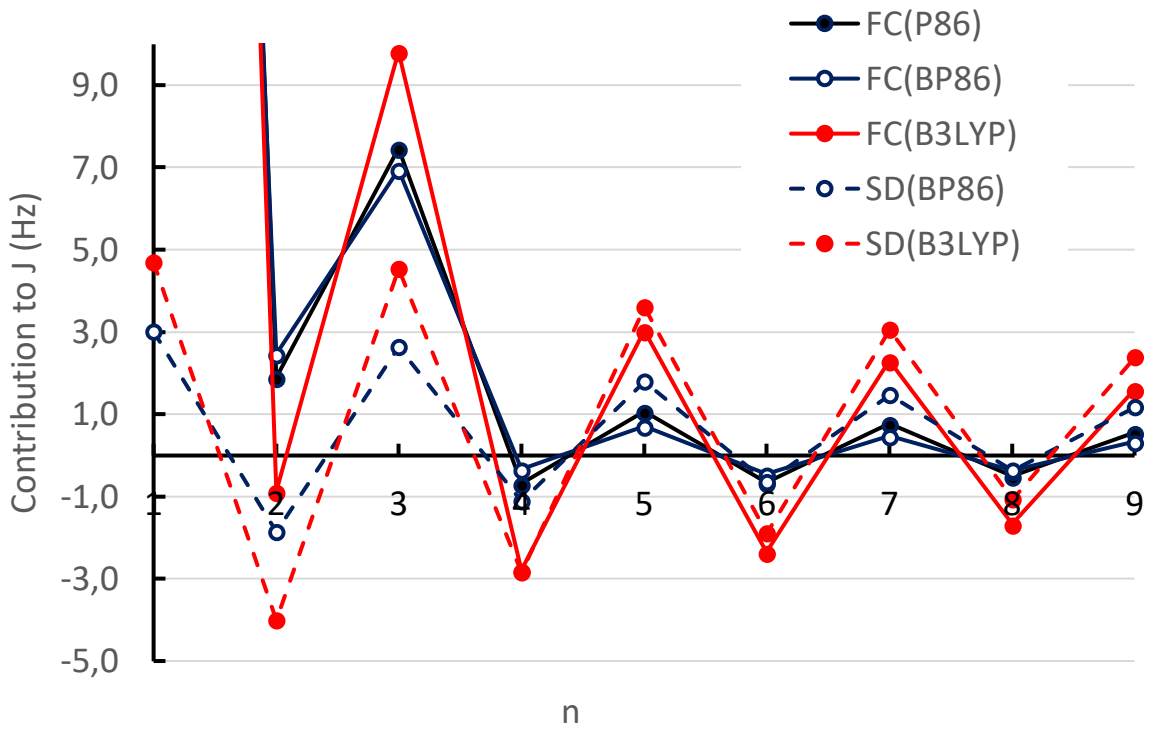

Figure S3. The FC and SD contributions to ^{n}J (C1- C_{n+1}) in 1,3,5,7,9-decapentaene calculated with different exchange-correlation functionals. The B3LYP and BP86 results were obtained using the G03 package (ref. 21).

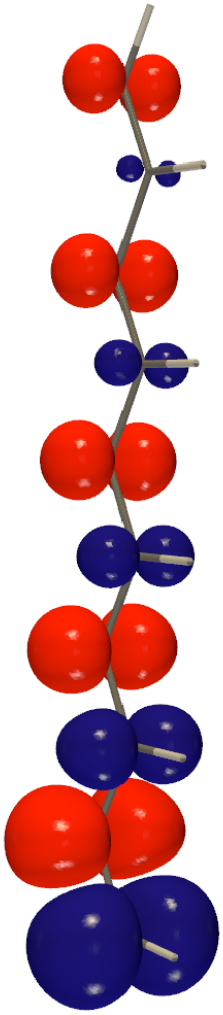

Figure S4. Spin-polarization of π-orbitals taken together in 1,3,5,7,9-decapentaene due to FC(C1). The isosurface value is 0.007 a.u.

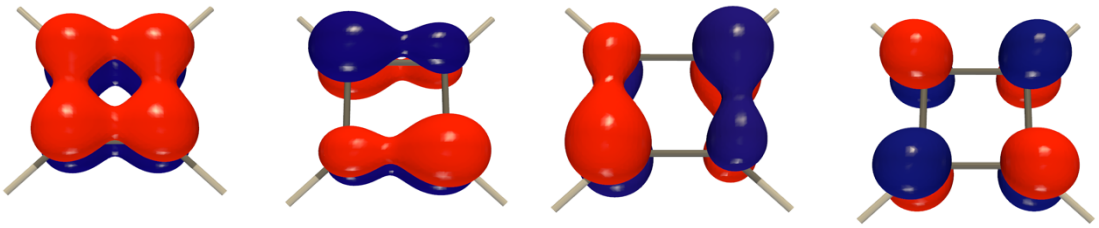

MO11 MO14 MO15 MO16

Figure S5. The occupied π-orbital (MO11) and the lowest vacant π-orbitals (MO14, MO15 and MO16) of a cyclobutadienyl dication. The isosurface value 0.1 a.u. .

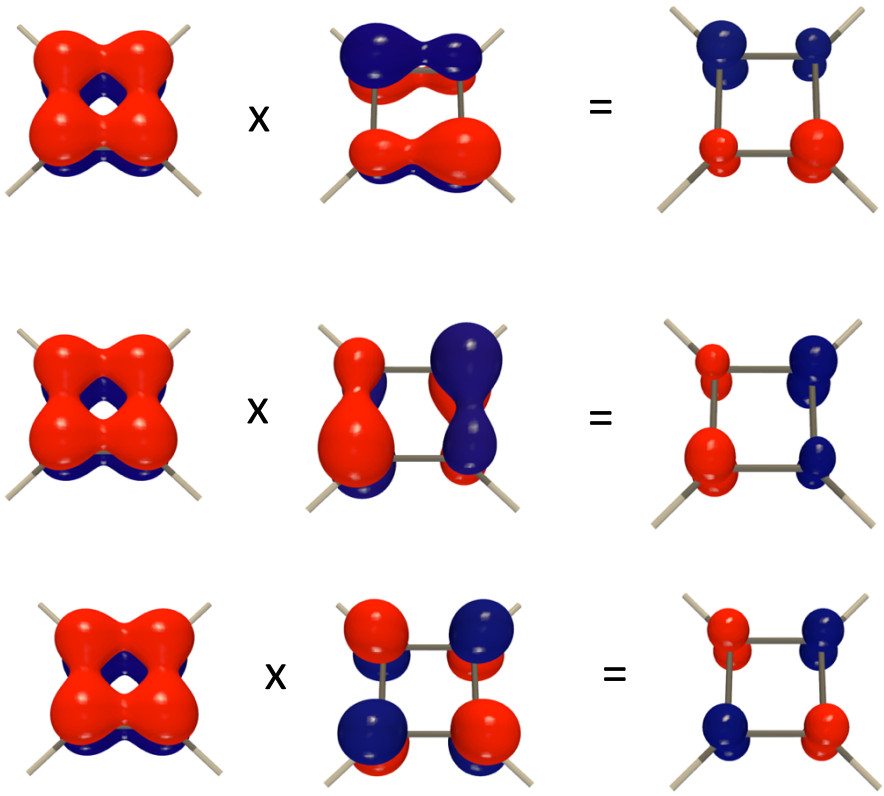

MO11 x MO14 + MO11 x MO15 + MO11 x MO16 =

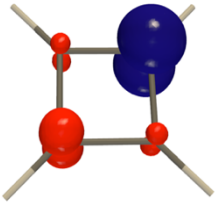

Figure S6. The contributions of the products of the occupied π-orbital with low-lying vacant π -orbitals to the spin-density induced by FC(C1) in a cyclobutadienyl dication. The isosurface value is 0.1 a.u. for MOs and 0.02 a.u. for their products.

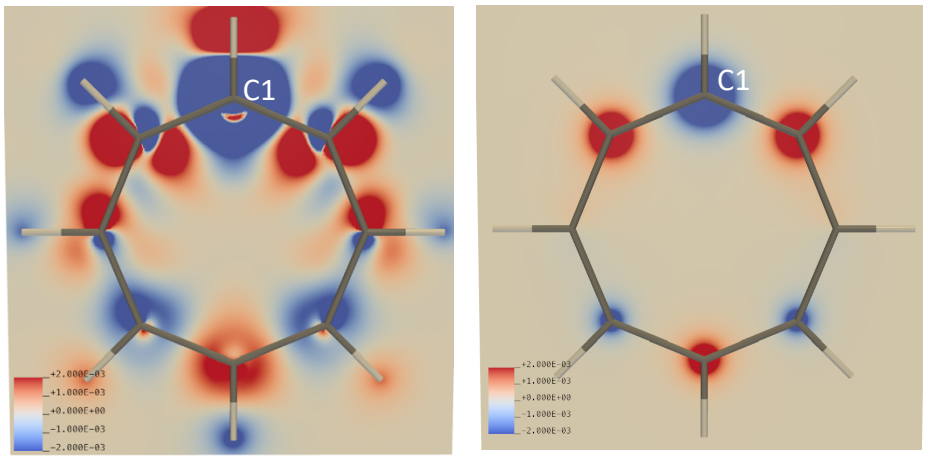

Figure S7. The π-TSP effect on the spin density in a cyclooctatetranyl dication induced by FC(C1) (left; color-coded according to the density values given in a.u.) in the dication plane and the total spin-polarization of the π-orbitals in the plane 0.5 Å below the molecular plane; right).

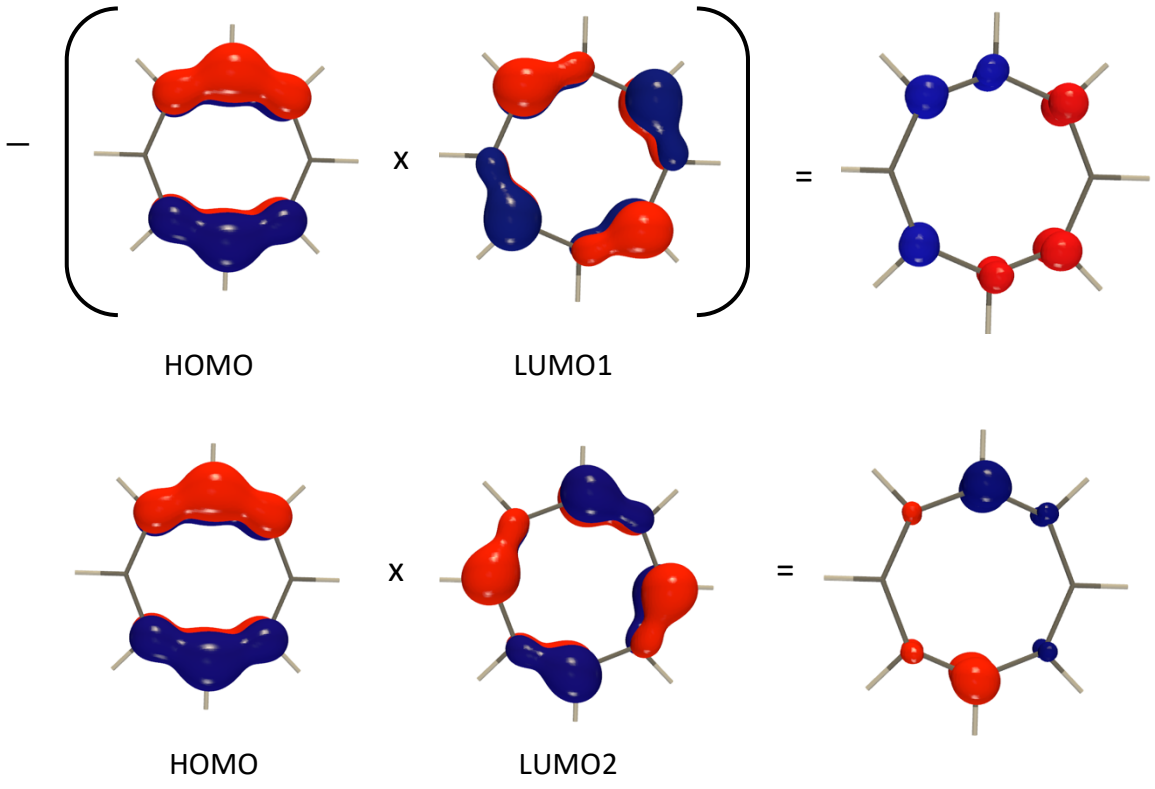

Figure S8. The products of the HOMO and LUMO orbitals for a cyclooctatetranyl dication. The first product is taken with a negative sign because the corresponding coefficient τ is negative (see Eqs. 2-4 in the main text). The isosurface value is 0.07 a.u. for MOs and 0.01 a.u for their products.

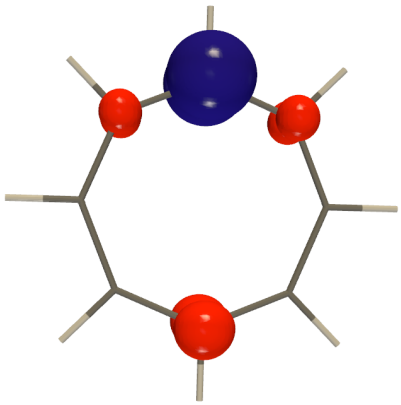

Figure S9. The overall contribution of the HOMO to the spin density induced by FC(C1) in a cyclooctatetranyl dication (compare with Figure S5, left). The isosurface value is 0.01.

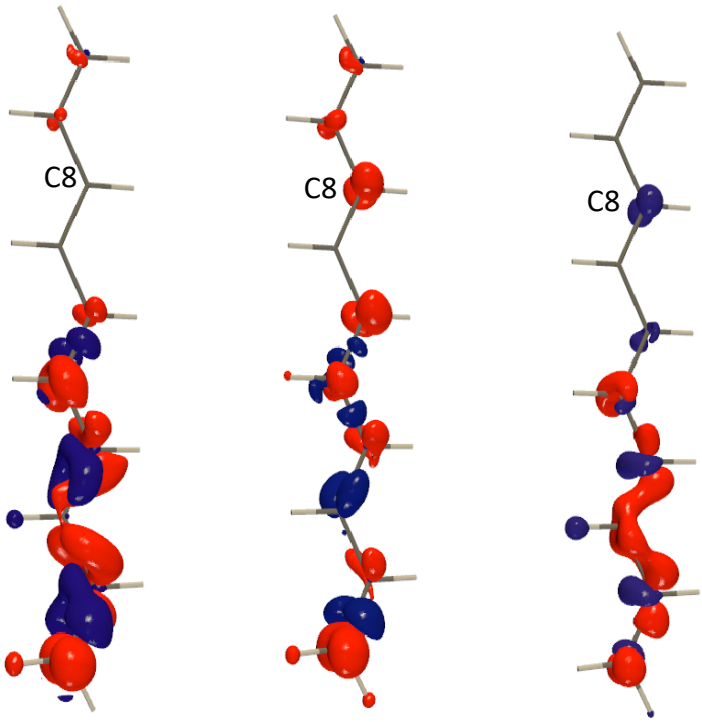

Figure S10. The CDD for ^{4}J(C1-C5) in 1,3,5,7,9-decapentaene: total (left), due the π-TSP effect (middle) and the CDD when the π-TSP effect is switched off (right). The isosurface value in all plots is 0.004 a.u.

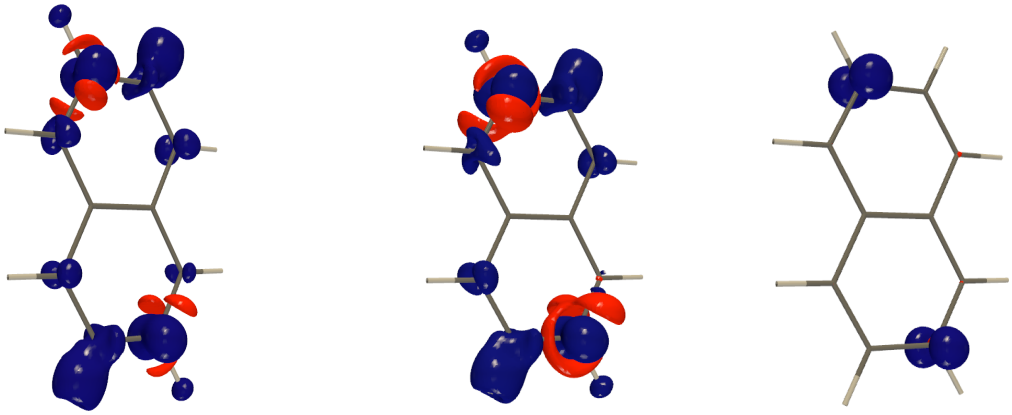

Figure S11. CDD for ^{5}J(C2-C6) in naphthalene: total (left), due the π-TSP effect (middle) and the CDD when the π-TSP effect is switched off (right). The isosurface value in all plots is 0.001 a.u.

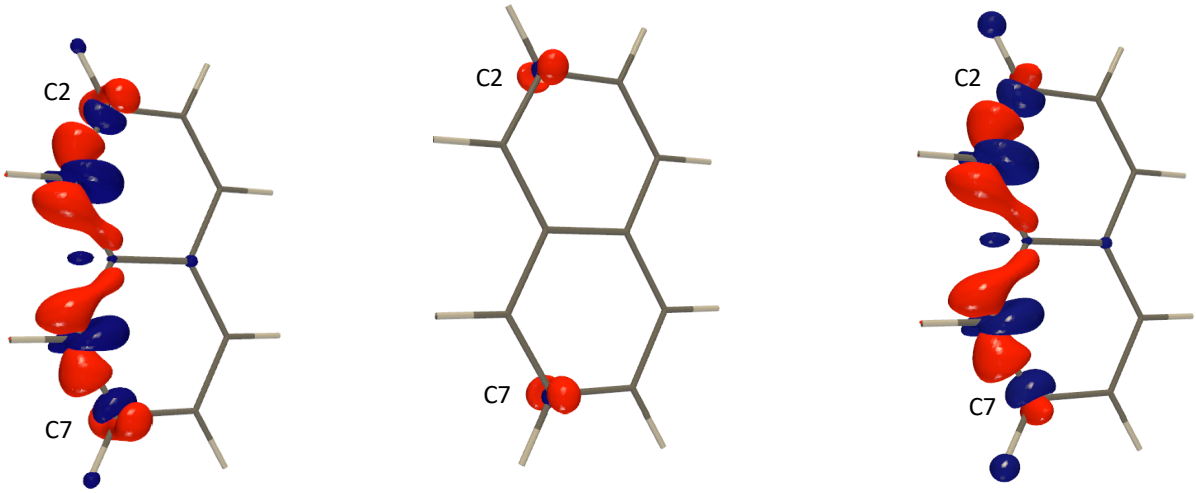

Figure S12. CDD for ^{4}J(C2-C7) in naphthalene: total (left), due the π-TSP effect (middle) and the CDD when the π-TSP effect is switched off (right). The isosurface value in all plots is 0.004 a.u.

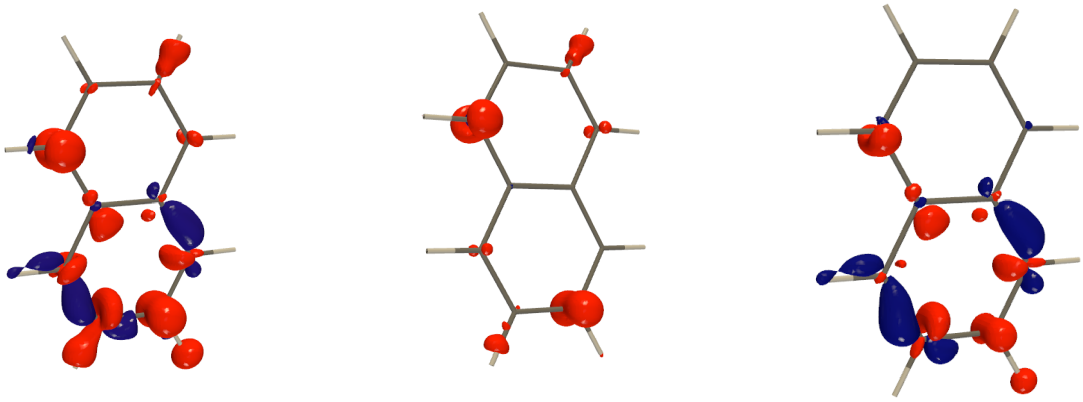

Figure S13. CDD for ^{4}J(C1-C6) in naphthalene: total (left) due the π-TSP effect (middle) and the CDD when the π-TSP effect is switched off (right). The isosurface value in all plots is 0.002 a.u.

Table S5. The π-TSP effect on ^{13}C HFCC in the 1,3,5,7,9-decapentaene-1-yl radical for the optimized structure. The values are given in MHz.

Carbon	π-TSP ON	π-TSP OFF	Difference
1	337.30	322.82	14.48
2	-3.31	2.39	-5.70
3	87.76	87.36	0.40
4	0.33	4.74	-4.41
5	5.73	2.65	3.07
6	-2.15	0.64	-2.79
7	2.72	0.01	2.71
8	-2.30	-1.05	-1.25
9	1.84	0.25	1.58
10	-1.73	-1.65	-0.08

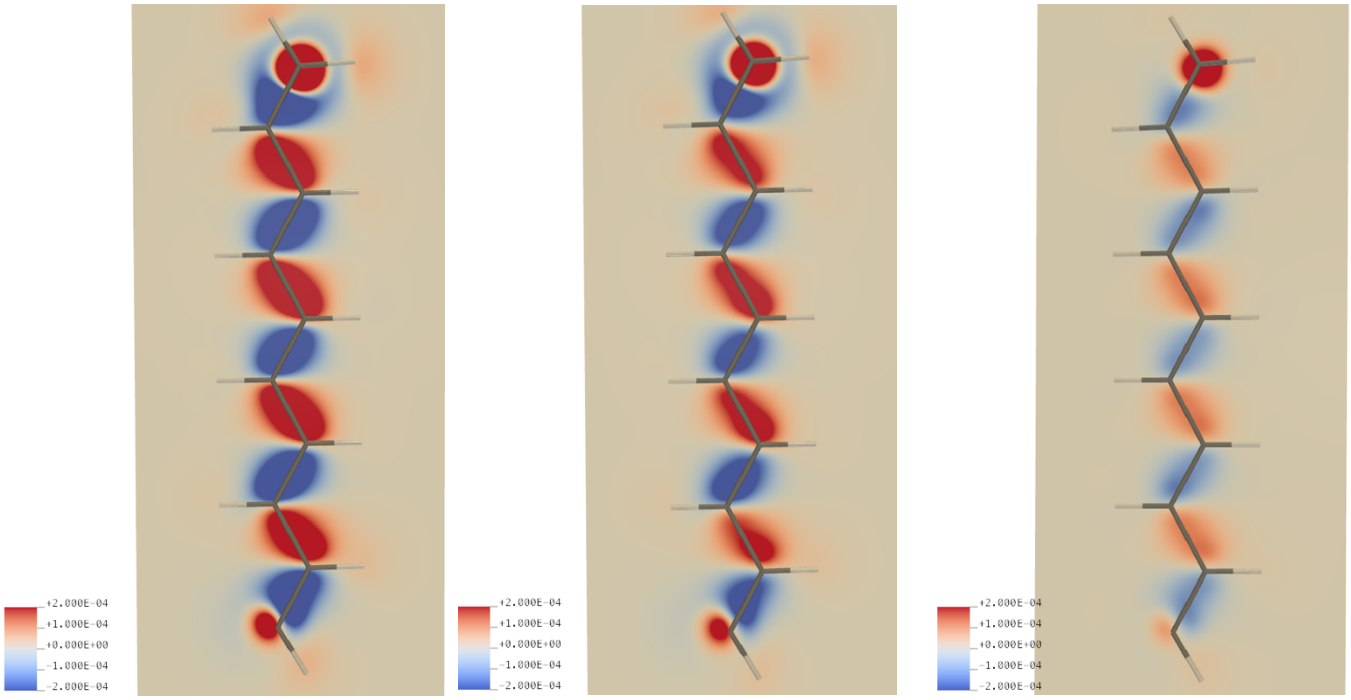

Figure S14. The C10 HFDD in the 1,3,5,7,9-decapentaen-1-yl radical (a); the π-TSP effect on the C10 HFDD (b) and the C10 HFDD when the π-TSP effect is switched off (c and d). The plots show HFDDs in the plane 0.5 Å below the radical plane.

Cartesian coordinates of the optimized structures used in this work (in Å):

1,3,5,7,9-decapentaene

C	5.57155652	0.22658449	0.00000000
C	4.36600585	-0.39674599	0.00000000
C	3.09207900	0.28462510	0.00000000
C	1.87752333	-0.35288057	0.00000000
C	0.60895764	0.31650229	0.00000000
C	-0.60666635	-0.32524946	0.00000000
C	-1.87524579	0.34410891	0.00000000
C	-3.08975700	-0.29350101	0.00000000
C	-4.36380817	0.38766895	0.00000000
C	-5.56925882	-0.23586894	0.00000000
H	6.51054405	-0.33548276	0.00000000
H	4.33296253	-1.49643498	0.00000000
H	3.11286760	1.38489525	0.00000000
H	1.86263989	-1.45364347	0.00000000
H	0.62183181	1.41703940	0.00000000
H	-0.61953786	-1.42578655	0.00000000
H	-1.86041124	1.44487033	0.00000000
H	-3.11035372	-1.39377864	0.00000000
H	5.64918963	1.32065942	0.00000000
H	-4.33100048	1.48735752	0.00000000

H	-5.64674361	-1.32995336	0.00000000
H	-6.50835102	0.32600995	0.00000000

Benzene

C	1.21636673	0.70226966	0.00000000
C	0.00000000	1.40453931	0.00000000
C	-1.21636673	0.70226966	0.00000000
C	-1.21636673	-0.70226966	0.00000000
C	0.00000000	-1.40453931	0.00000000
C	1.21636673	-0.70226966	0.00000000
H	2.16549152	1.25024712	0.00000000
H	0.00000000	2.50049422	0.00000000
H	-2.16549152	1.25024711	0.00000000
H	-2.16549152	-1.25024712	0.00000000
H	0.00000000	-2.50049422	0.00000000
H	2.16549152	-1.25024711	0.00000000

Naphthalene

C	-1.24872214	1.41037019	0.00000000
C	-2.44596401	0.71120114	0.00000000
C	-2.44596401	-0.71120114	0.00000000
C	-1.24872214	-1.41037019	0.00000000
C	1.24872214	-1.41037019	0.00000000
C	2.44596401	-0.71120114	0.00000000
C	2.44596401	0.71120114	0.00000000
C	1.24872214	1.41037019	0.00000000
C	0.00000000	0.72204322	0.00000000
C	0.00000000	-0.72204322	0.00000000
H	-1.24451964	2.50721371	0.00000000
H	-3.39819664	1.25308018	0.00000000
H	-3.39819664	-1.25308018	0.00000000
H	-1.24451964	-2.50721371	0.00000000
H	1.24451964	-2.50721371	0.00000000
H	3.39819664	-1.25308018	0.00000000
H	3.39819664	1.25308018	0.00000000
H	1.24451964	2.50721371	0.00000000

1,3,5,7,9-decapentaen-1-yl radical

C	-2.40149636	-5.01194437	0.00000000
C	-2.36081202	-3.67617444	0.00000000
C	-1.15104000	-2.86688171	0.00000000
C	-1.15759986	-1.49581841	0.00000000
C	0.02317277	-0.68074443	0.00000000
C	0.01494579	0.69367383	0.00000000
C	1.19470635	1.50971314	0.00000000

C	1.18921531	2.88132298	0.00000000
C	2.38146967	3.69733141	0.00000000
C	2.38341658	5.05445237	0.00000000
H	-3.31264099	-3.11772101	0.00000000
H	-0.18930342	-3.39833737	0.00000000
H	-2.12723114	-0.97493033	0.00000000
H	0.99313506	-1.20066202	0.00000000
H	-0.95523966	1.21331677	0.00000000
H	2.16430738	0.98846773	0.00000000
H	0.22257379	3.40725204	0.00000000
H	-1.68561535	-5.83685490	0.00000000
H	3.34204371	3.16095891	0.00000000
H	1.44789566	5.62698300	0.00000000
H	3.31468574	5.62919382	0.00000000

Cyclobutadienyl dication

C	0.72997582	0.72997582	0.00000000
C	-0.72997582	0.72997582	0.00000000
C	0.72997582	-0.72997582	0.00000000
C	-0.72997582	-0.72997582	0.00000000
H	1.51268973	1.51268973	0.00000000
H	-1.51268973	1.51268973	0.00000000
H	1.51268973	-1.51268973	0.00000000
H	-1.51268973	-1.51268973	0.00000000

Cyclooctatetranyl dication

C	1.85403202	0.00000045	0.00000000
C	1.31099830	-1.31099894	0.00000000
C	0.00000045	-1.85403202	0.00000000
C	-1.31099894	-1.31099830	0.00000000
C	-1.85403202	-0.00000045	0.00000000
C	-1.31099830	1.31099894	0.00000000
C	-0.00000045	1.85403202	0.00000000
C	1.31099894	1.31099830	0.00000000
H	2.95368374	0.00001701	0.00000000
H	2.08855777	-2.08858182	0.00000000
H	0.00001701	-2.95368374	0.00000000
H	-2.08858182	-2.08855777	0.00000000
H	-2.95368374	-0.00001701	0.00000000
H	-2.08855777	2.08858182	0.00000000
H	-0.00001701	2.95368374	0.00000000
H	2.08858182	2.08855777	0.00000000

Transmission of spin-polarization by π-orbitals: an approach to assessing its effect on NMR spin-spin coupling and EPR hyperfine structure

Olga L. Malkina,*[,a] Florian Lemken[a], James R. Asher[a,b], Jean-Cyrille Hierso[c], Michael Bűhl[d], Vladimir G. Malkin*[a]

[a]*Institute of Inorganic Chemistry, Slovak Academy of Sciences, Dúbravská cesta 9, SK-84536 Bratislava, Slovakia*

[b] *Faculty of Natural Sciences, Department of Inorganic Chemistry, Comenius University, Mlynská dolina CH2, SK-84215 Bratislava, Slovakia*

[c] *Institut de Chimie Moléculaire de l'Université de Bourgogne (ICMUB, UMR CNRS 6302), Université Bourgogne–Franche-Comté (UBFC), 9 avenue Alain Savary, 21078 Dijon Cedex, France*

[d] *EaStChem School of Chemistry, University of St Andrews, St Andrews, Fife KY16 9ST, UK*

** Corresponding authors; e-mail: olga.malkin@savba.sk, vladimir.malkin@savba.sk*

Dedicated to the memory of Prof. Paul von Ragué Schleyer

A new approach to assessing the effect of the transmission of spin-polarization by π-orbitals (π-TSP) is presented. In order to switch off the π-TSP effect, we artificially average the α- and β-densities of the valence π-orbitals when calculating the exchange-correlation contribution to the Fock matrix in the unrestricted Kohn-Sham framework. The π-TSP effect is then evaluated as the difference between the results obtained with switched-on and switched-off options. This approach is applied to estimate the π-TSP effect on the Fermi-contact contribution to spin-spin couplings and EPR hyperfine structure coupling constants. The π-TSP effect on the distribution of spin-density, spin-spin coupling pathways and pathways of EPR hyperfine couplings is demonstrated for benzene, naphthalene, 1,3,5,7,9-decapentaene and 1,3,5,7,9-decapentaen-1-yl radical. The sign alternation of the spin-polarization transmitted by π-orbitals is explained in a theoretical framework based on perturbation theory. However, the delocalized nature of the π-system can interfere with the sign alternation in certain cases, two of which – cyclobutadiene dication and cyclooctatetraene dication – are examined, and an explanation for which is provided.

Introduction

The accurate description, modeling and understanding of the nature of the chemical bonds remains one of the most important issues in theoretical chemistry. Obviously, bond types are directly relevant to the stability and reactivity of the compounds, and are of primary importance concerning various molecular physical properties. For example, the impact of σ- and π-bonds on NMR shielding was studied early on by Kutzelnigg *et al*.[1] The special concept of the nucleus-independent chemical shift (NICS) was introduced to measure aromaticity by examining ring-current effects stemming from delocalized π-electrons.[2] The NICS concept generated numerous discussions, resulting in further improvements and alternative approaches.[3] The effect of the transmission of spin-polarization by π-bonds (π-TSP) on NMR indirect spin-spin coupling constants (SSCC) is more difficult to assess. For instance, when a delocalized planar system is considered, the commonly-used analyses of contributions from molecular orbitals (MO) to the Fermi Contact (FC) part of spin-spin coupling would show zero contribution from π-MOs because they have values of zero at the positions of the coupled nuclei.[4] Thus, the direct FC contribution from the π-bonds to *J*(C-C) in benzene is zero since the π-MOs have zero s-character on both coupled nuclei. However, the lack of contributions from the π-bonds is a shortcoming only of the commonly-used analyses. Indeed, the π-bonds are actively involved in the transmission of spin-polarization (π-TSP) between two carbon nuclei in benzene: the s-orbital is polarized due to Fermi-contact interaction on the first carbon, which in turn polarizes all orbitals around the carbon, including π-MOs. Then the π-MOs further transfer the polarization to the second carbon and polarize its s-orbital. Finally, the polarized s-orbital interacts with the nuclear magnetic moment of the second carbon *via* the FC mechanism. π-orbitals are delocalized and easily polarized, and they can transmit spin-polarization more efficiently and farther than sigma-orbitals. This kind of dynamic spin-polarization has also been invoked to explain the occurrence of nonzero hyperfine coupling constants on the H atoms in the planar methyl radical, and to advocate the use of the spin-unrestricted formalism in Kohn-Sham DFT.[5] The assessment of this intricate spin transmission phenomenon, however, requires a more advanced analysis.

Different ways to estimate its effect have been used in the past. In 1957 McConnell used empirical data on hyperfine splitting in aromatic free radicals to estimate the contribution of π-electrons to *J*(H-H) in aromatic molecules based on the effective "π-electron spin - proton spin interaction Hamiltonian".[6] Later he used valence bond (VB) theory to predict the negative contribution from π-electrons to *J*(H-H)

through an even number of bonds.[7] VB was also used by Barfield [8] to study the π-TSP effect on long-range proton-proton coupling. A thorough review of early works on π-TSP is available. [9]

The appearance of semi-empirical methods attracted new interest to π-TSP. Fukui, Tsuji, and Miura[10] used the SOS2-INDO expression (sum-over-states including single and double excitations at the INDO level) for the calculation of *J*-coupling. The separation of excitations into three categories (from σ to σ* orbitals, from π to π* orbitals and mixed π-σ* and σ-π* transitions) allowed them to obtain the π-contribution to spin-spin coupling constants. Engelmann, Scuseria and Contreras based their analysis on the SCPT-INDO expression.[11] The unperturbed MOs were separated into π- and σ- subspaces. SCPT (self-consistent perturbation theory) part was applied either to all MOs or only to the σ-subspace. The difference in the results showed the effect of π-orbitals on SSCC. Despite the limited accuracy of semi-empirical methods, these early works provided consistent qualitative conclusions: 1) π-TSP decayed more slowly than the spin-polarization transmitted by σ-orbitals, and 2) the contribution of π-orbitals to *J*-couplings was positive through an odd number of bonds and negative otherwise, though no satisfactory explanation of this phenomenon was given.

Interest in the π-TSP effect on SSCC was renewed with the development of DFT-based methods for calculating *J*-coupling.[12] Gräfenstein, Tuttle and Cremer followed the ideas of Fukui *et al*.[10] using the CP-DFT (coupled perturbed density functional) equations written in terms of localized molecular orbitals (LMOs).[13] Excluding different combinations of LMOs from the equations, they were able to estimate the effect of the π-mechanism on long-range C–C, C–H and H–H SSCC in polyenes. The practical applications of this promising approach were somewhat hindered by the necessity of hand-picking the relevant combinations of LMOs, and it was difficult to extend this approach to the analysis of other properties. However, the authors reached many interesting conclusions, which overall agreed with previous findings made at the semi-empirical level. The sign alternation of the contribution of π-orbitals to J^{FC}-couplings with an increasing number of bonds separating the coupled nuclei was linked to the Dirac vector model for long-range spin-spin couplings, albeit without explanation. Therefore, it remains unclear how the Dirac vector model proposed for explaining the sign alternation of long-range J^{FC}-couplings in a chain of σ-bonds can be applied to the π-mechanism.

Our motivation for addressing the topic of π-TSP is as follows: a) though the π-TSP effect on the EPR hyperfine coupling constants (HFCCs) was discussed long ago,[4,6] its detailed analysis has received much less attention than the influence of π-TSP on NMR spin-spin coupling; b) deeper insight into π-TSP can

be gained by the methods of visualization of pathways of NMR spin-spin couplings and EPR hyperfine couplings that are now available;[14] c) to the best of our knowledge, a consistent explanation for the sign alternation of the π-TSP effect along the bonds on SSCCs and HFCCs is still lacking; d) deeper understanding of π-TSP may be beneficial for further analyzing spin-spin transmission pathways in transition metal complexes that include aromatic moieties in their ancillary ligands (phenyl, naphthyl, *etc.*)[15] or that possess benzene and olefins as ligands themselves (metallocenes, *etc.*).[16]

The aim of this work is to present an approach that allows one to switch the π-TSP effect off and on easily, and which is applicable to the analysis of molecular properties that depend on the effects of spin-polarization (SSCC, HFCC). We apply this approach to show the π-TSP effect on different aspects of NMR spin-spin couplings and EPR hyperfine coupling constants. We consider the following systems: benzene, naphthalene, 1,3,5,7,9-decapentaene, and a 1,3,5,7,9-decapentaene-1-yl radical, which is obtained by removing one of the hydrogens from 1,3,5,7,9-decapentaene. We also explain the sign alternation of the contribution of π-orbitals to J^{FC}-couplings with increasing number of bonds and its relation to the Dirac vector model.[17] We furthermore identify two exceptions to the rule – cyclobutadiene dication and cyclooctatetraene dication – and discuss the reasons for this.

Computational methods

We analyzed the π-TSP effect on the FC contribution to the NMR spin-spin coupling and on the EPR hyperfine coupling constant. The FC contribution to SSCC is calculated using single finite perturbation theory (FPT) as described previously.[12] The isotropic HFCC of a particular nucleus is obtained from an unperturbed SCF calculation as the value of the spin-density at the position of the nucleus multiplied by a well-defined constant.[18]

For visualization of spin-spin coupling pathways, we used an approach based on double finite perturbation theory.[19] In this approach, the nuclear magnetic moments of the two interacting nuclei are included as finite perturbations. We perform two SCF calculations, with parallel and antiparallel orientation of the nuclear magnetic moments, as a simulation of experimental NMR measurement. Due to the FC interactions caused by the nuclear magnetic moments, the electron density distribution depends on their relative orientation. The difference between the electron densities obtained from these two calculations, called the Coupling Deformation Density (CDD), shows which parts of the electronic structure are involved in the magnetic interaction of the two nuclei. Mathematically, CDD is

the bilinear response of the total electron density to the nuclear magnetic moments, and it is expressed as follows:

$$\rho_{MN}(r) = \frac{\rho^{\uparrow\uparrow}(r) - \rho^{\uparrow\downarrow}(r)}{\lambda_1 \lambda_2} \quad (1)$$

where λ_1 and λ_2 are the perturbation parameters used in double finite perturbation theory (DFPT), and $\rho^{\uparrow\uparrow}(r)$ and $\rho^{\uparrow\downarrow}(r)$ are doubly-perturbed electron densities (*i.e*. the densities corresponding to the parallel and antiparallel orientation of the nuclear magnetic moments involved in the spin-spin coupling). From the physical point of view, CDD, being the difference between two electron densities, is an observable.

Analogously to the visualization of spin-spin coupling pathways, we have also developed an approach for the visualization of hyperfine coupling pathways.[14] The magnetic moment of a nucleus of interest is there included as a finite perturbation. The difference between the spin-densities for the two opposite orientations of the nuclear magnetic moment (Hyperfine Deformation Density, HFDD) shows the hyperfine coupling pathway. Again, from the physical point of view, HFDD is an observable.

In order to assess the π-TSP effect on the properties described above, we have to be able to switch it on and off, preferably in the same manner for both unperturbed and perturbed calculations: that is, without relying on the explicit expressions for particular properties, as was done in previous works.[11,13] Orbitals transmit spin-polarization *via* their exchange-correlation interaction with other orbitals.[20] In the DFT framework, this means through the contribution of the spin-density of the polarized orbitals to the exchange-correlation potential. In order to switch off the π-TSP effect, we artificially average the α- and β-densities of the valence π-orbitals for calculating the exchange-correlation potential. In this approach, the π-orbitals are still polarized by core and σ-orbitals but they cannot contribute to further transmission of the spin-polarization. In this case, the contribution to SSCC or HFCC due to the π-TSP effect vanishes. Herein, we consider planar systems where the π-orbitals are easily identifiable even in their canonical form. For more complex systems, localized molecular orbitals can be used. The difference between the results obtained using the switch on and switch off options is considered to be the π-TSP effect.

Computational details

All calculations have been carried out using density functional theory. The structures of 1,3,5,7,9-decapentaene, benzene, naphthalene, and the planar forms of cyclobutadienyl and cyclooctatetranyl dications were optimized at the RI-BP86-D3/6-31G* level using the G03 package [21]. We are aware that the planar form of cyclobutadienyl dication is a saddle point. It is well known that the puckered minimum is significantly more stable (by 9.6 kcal/mol at RI-BP86-D3 level, according to our calculations; this is similar to ab initio results reported earlier[22]). However, the planar form is interesting as the simplest model for a Hückel aromatic system where the sign alternation can be studied. The cartesian coordinates of the optimized structures are given in ESI. For better comparison of NMR spin-spin coupling and hyperfine coupling pathways, the structure of a 1,3,5,7,9-decapentaene radical was obtained by removing H19 from 1,3,5,7,9-decapentaene (see Fig. 1) without relaxation of the structure. The property calculations were done with a local modified version of the deMon-KS code.[23,24] In these calculations we employed the Perdew86 exchange-correlation functional in its spin-unrestricted formalism,[25, 26, 27, 28] and the IGLO-II basis set.[1] The grid for numerical integration contained about 3000 points per atom during the main SCF procedure. After reaching the SCF convergence, however, an extra iteration with about 10500 points per atom was performed in order to increase the accuracy of the molecular orbital coefficients. Visualization has been done with AVOGADRO 1.1.1.[29] On the isosurface plots, blue and red colors correspond to positive and negative values, respectively.

Results and discussion

To investigate the π-TSP effect we selected three systems, a long-chain linear olefin, a simple aromatic, and a fused-ring extended π-aromatic: 1,3,5,7,9-decapentaene, benzene and naphthalene, respectively. Their atom numbering is shown in Figure 1. We first analyzed the π-TSP effect on the FC contribution to *J*(C-C) in these systems. Then we considered and compared how the transmission of spin-polarization by π-orbitals affects the spin-density (induced by the FC operator on one of the carbon atoms), again in all three systems. Additionally, we examined the π-TSP effect on the induced spin density for the cyclobutadiene dication, an example with a noticeable deviation from the sign alternation pattern. We

subsequently addressed the π-TSP effect on the general NMR spin-spin coupling pathways. Finally, we analyzed the π-TSP effect on different aspects of the ^{13}C hyperfine couplings.

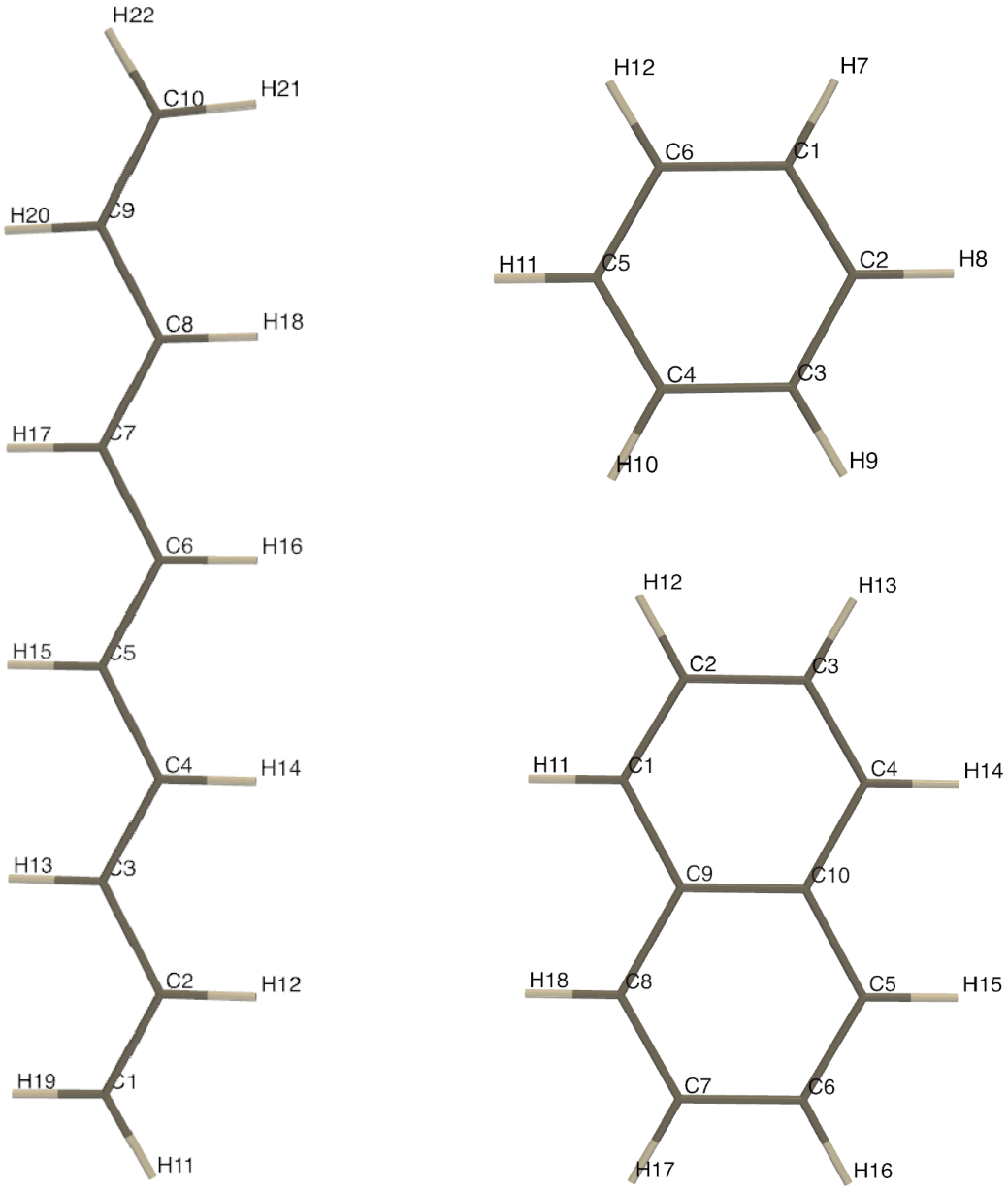

Figure 1. Molecular structure and the numbering of atoms in 1,3,5,7,9-decapentaene (left), benzene (top right) and naphthalene (bottom right). The 1,3,5,7,9-decapentaene radical considered in this work is obtained from 1,3,5,7,9-decapentaene by removing atom H19.

The π-TSP effect on the FC contribution to spin-spin couplings

The calculated Fermi-contact contributions to ^{n}J(C-C) couplings are presented in Tables 1 (for 1,3,5,7,9-decapentaene), 2 (for benzene) and 3 (naphthalene). Other contributions to ^{n}J(C-C) couplings for the considered systems can be found in Tables S1-S4 in ESI. In Tables 1-3, the first column indicates the number of bonds separating the coupled carbons. The values in the second column show the ^{n}J(C-C) values obtained with all orbitals participating in the transmission of spin-polarization, and the third column gives the results when the π-TSP effect is switched off, that is, when the π-orbitals do not polarize other orbitals *via* the exchange interaction. The last column gives the differences between the values in the second and third columns, in other words it gives the contributions to ^{n}J(C-C) solely due to the transmission of spin-polarization by the π-system (*via* the π-channel). The π-TSP effect listed in the last column of Table 1 is also shown graphically in Figure 2. Additionally, Figure S1 in ESI shows the values calculated with two finer grids used for numerical integration and confirms the numerical stability of the results. The π-TSP effect on ^{n}J(C1- C_{n+1}) is always positive for an odd number of bonds separating the coupled carbon atoms (***n*** = 1, 3, 5, …) and negative for an even number (***n*** = 2, 4, 6, …). When π-TSP is excluded (column 3 in Table 1, π-TSP switched OFF) the C – C couplings are positive for ***n*** from 1 to 5, which disagrees with the Dirac vector model. The sign alternation in column 3 is observed only for ***n*** > 4.

Table 1. The π-TSP effect on $^{n}J^{FC}$(C1- C_{n+1}) in 1,3,5,7,9-decapentaene. The values are given in Hz.

n[a]	π-TSP switched ON	π-TSP switched OFF	Δ *J* [b]
1	77.44	74.88	2.56
2	1.86	3.40	-1.53
3	7.43	6.41	1.02
4	-0.72	0.11	-0.83
5	1.04	0.34	0.70
6	-0.70	-0.14	-0.56
7	0.73	0.19	0.54
8	-0.54	-0.12	-0.42
9	0.52	0.14	0.38

[a] ***n*** is the number of bonds separating C and C_{n+1} .

[b] Δ*J* is the difference between the values of the SSCCs (Hz) in the second (π-TSP switch-ON) and the third (π-TSP switch-OFF) columns, and as such represents the quantitative effect of π-TSP.

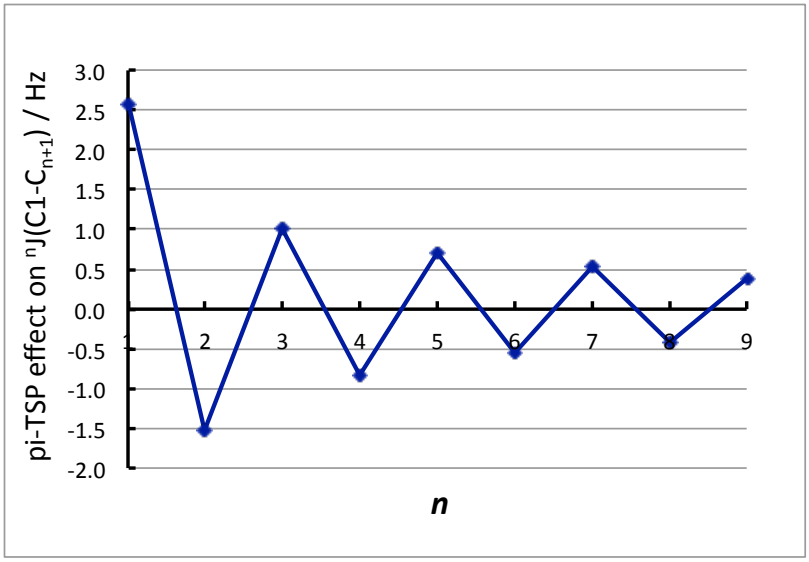

Figure 2. The π-TSP effect on $^{n}J^{FC}$(C1- C_{n+1}) in 1,3,5,7,9-decapentaene as a function of the number of bonds separating two carbons (in Hz).

The decay of the π-transmitted spin-polarization contribution to ^{n}J (C1- C_{n+1}) in 1,3,5,7,9-decapentaene with increasing ***n*** is much slower than the decay of the usual σ-bond-transmitted polarization (see Table 1). While the latter tends to die off after ca. 5 bonds, the π-TSP contributions continue to oscillate even up to nine bonds (see Figure 2), and for ***n*** > 3 they actually give the dominant contribution to the *J*-values (see Table 1). These findings agree with previous works.[11,13]

Similar trends are also observed for a classic π-system, benzene (see Table 2). Without π-TSP there is no sign alternation of the values of the C – C couplings (Table 2, column 3), whereas the π-TSP contribution is positive for ***n*** = 1 and 3 and negative for ***n*** = 2. The magnitude of the π-TSP contribution to ^{2}J (C1- C3) is bigger than the *J* value calculated without π-TSP (-0.97 Hz versus 0.71 Hz), making π-TSP responsible for the sign alternation of the total *J* values seen in the second column in Table 2.

Table 2. The π-TSP effect on $^{n}J^{FC}$(C1- C_{n+1}) in benzene. The values are given in Hz.

n[a]	π-TSP switched ON	π-TSP switched OFF	Δ *J* [b]
1	62.94	61.43	1.51
2	-0.33	0.71	-1.04
3	7.80	6.96	0.84

[a] ***n*** is the number of bonds separating C and C_{n+1} .

[b] Δ*J* is the difference between the values of the SSCCs (Hz) in the second (π-TSP switch-ON) and the third (π-TSP switch-OFF) columns, and as such represents the quantitative effect of π-TSP.

Naphthalene provides a suitable model for analyzing the π-TSP effect on $^{n}J^{FC}$(C1-C_{n+1}) in an aromatic compound for a larger range of ***n*** (from 1 to 5, see Table 3) than that in benzene. Unlike benzene, naphthalene contains carbon-carbon bonds which are not symmetry-equivalent (see for instance their bond lengths in the optimized structure in Figure S2 in ESI); and, except for ***n*** = 5, there are multiple topologically different SSCC pathways through the same number of bonds. This results in multiple different *J* values for the same ***n***. For example, for ***n*** = 1, values of SSCC ranging from 55.8 to 68.0 Hz are found. For ***n*** = 2 values of SSCC ranging from –0.03 to 3.8 Hz are obtained; in addition, ^{4}J(C2-C7) and ^{4}J(C1-C6) have opposite signs (Table 3).

Overall, there is no sign alternation of total *J*(C-C) values with increasing number of bonds, i.e. they do not obey the Dirac vector model. In contrast, the π-TSP effect shown in the last column of Table 3 displays remarkably stable sign alternation with increasing number of bonds. It displays much smaller variation in the *J* values for the same ***n*** and decays more slowly. ^{5}J(C2-C6) is mainly caused by the π-TSP effect (the last row in Table 3).

Table 3. The π-TSP effect on $^{n}J^{FC}$(C-C) in naphthalene. The values are given in Hz.

n[a]		π-TSP switched ON	π-TSP switched OFF	Δ *J* [b]
1	C1-C2	67.97	66.37	1.60
	C1-C9	61.28	60.01	1.26
	C2-C3	59.07	57.70	1.37
	C9-C10	55.82	54.60	1.22
2	C1-C8	3.78	4.64	-0.86
	C1-C10	1.14	2.08	-0.93
	C2-C9	0.36	1.27	-0.91
	C1-C3	-0.03	0.95	-0.98
3	C3-C9	6.45	5.78	0.67
	C1-C4	5.33	4.60	0.73
	C1-C5	2.35	1.97	0.38
4	C2-C7	0.52	0.95	-0.43
	C1-C6	-0.50	-0.24	-0.26
5	C2-C6	0.46	0.07	0.39

[a] ***n*** is the number of bonds separating C and C_{n+1}.

[b] Δ*J* is the difference between the values of SSCCs (Hz) in the second (π-TSP switch-ON) and the third (π-TSP switch-OFF) columns, and as such represents the quantitative effect of π-TSP.

In all three examples, the sign of the π-TSP effect on $^{n}J^{FC}(C1\text{-}C_{n+1})$ is positive for an odd ***n*** and negative otherwise. It decays more slowly with increasing number of bonds than the effect of spin-polarization transmitted by other channels. The π-TSP effect may be significant even for short range couplings such as $^{2}J^{FC}(C1\text{-}C_3)$ in naphthalene and it becomes dominant for ***n*** > 4 in 1,3,5,7,9-decapentaene and naphthalene.

Besides the FC term, there is another spin-mediated contribution to spin-spin couplings, the spin-dipolar contribution (SD). It also displays the sign alternating pattern with increasing the number of bonds (see Figure S3 in ESI). This indicates that the pi-TSP effect likely plays an important role for the SD contribution for long-range spin-spin couplings, too.

The π-TSP effect on the spin-density induced by the FC operator

Spin-polarization is often illustrated by plots of the spin-density induced by the FC operator on one of the coupled nuclei. Besides the total spin-density, we can also separately plot the spin-density caused by the π-TSP effect, i.e. the difference in the spin-densities obtained with and without π-TSP, and the spin-polarization of the valence π-orbitals only, i.e., the summed spin-polarization of the valence of π-orbitals.

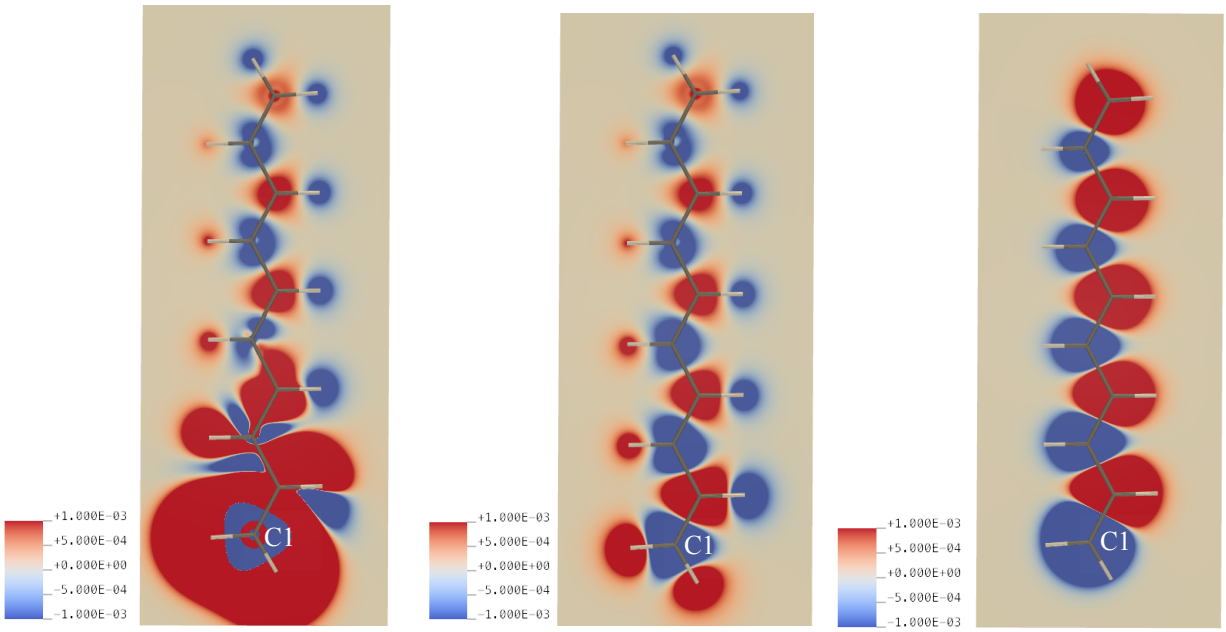

Figure 3. The spin-density in 1,3,5,7,9-decapentaene induced by FC(C1) (color-coded according to the density values given in a.u.). The total spin-density (left) and spin-polarization only due to the π-TSP

effect (middle) are shown in the molecular plane. The spin-polarization of the group of π-orbitals is shown in the plane 0.5 Å below the molecular plane (right).

As seen in Figure 3 (comparing left and middle), the long-range spin-polarization (***n*** > 4) in the molecular plane of 1,3,5,7,9-decapentaene is mainly caused by the π-TSP effect, consistent with the calculated results in Table 1. Interestingly, the π-TSP effect is not limited to carbon atoms, as hydrogen atoms are also affected (Figure 3, middle), displaying positive spin-density in their proximity if they are separated by an odd number of bonds from C1 and negative otherwise for ***n*** > 3. The π-orbitals have values of zero at the carbon positions and thus the π-MO density and the induced spin-density of π-MOs are zero in the molecular plane, too. In order to visualize the spin-polarization of the π-orbitals, a cross-section is shown in the plane 0.5 Å below the molecular plane (a cross section in the plane 0.5 Å above the molecular plane would show exactly the same spin density). A 3d-plot of the spin-polarization of the valence π-orbitals is given in ESI (Figure S4). The plots in Figure 3 display a clear sign alternation of the long-range spin-polarization, in agreement with the spin-spin coupling values in Table 1. In previous works, the sign alternation of the π-TSP effect on the values of spin-spin couplings was implicitly attributed to the Dirac vector model.[11,13] However, the Dirac vector model considers the propagation of the FC-induced spin-polarization through a chain of σ-bonds only.

The Dirac vector model explains the sign alternation as follows: let us assume that the g-value of the first nucleus ***A*** is positive and its spin is up. Then, due to the FC mechanism on nucleus ***A***, FC(A), the probability of finding the electron that has spin up (α-electron) in the proximity of nucleus ***A*** is lower than that of finding the electron with its spin down (β-electron). In other words, the α-electron is trying to avoid nucleus ***A*** and thus "slides" slightly towards the other side of the bond, whereas the β-electron moves in the opposite direction — closer to nucleus ***A*** — creating spin-polarization. Due to Hund's rule, the probability of finding the α-electron of the next bond will be higher in the proximity of the second nucleus. Consequently, the β-electron of the second bond will shift towards the third nucleus, and so on. Therefore, the sign of the spin density near a nucleus in a chain depends on the number of bonds separating it from nucleus ***A***: it is positive for an odd number of bonds, and negative otherwise.

However, the Dirac vector model assumes that each bond in a chain possesses two electrons and that these electrons are localized in the space between the two bonded atoms: if one of the electrons goes closer to one end of the bond, the other one has nowhere to go except for shifting to another end.

Clearly, these assumptions are not valid for delocalized bonding situations such as π-systems. In benzene, for example, the π-electrons are delocalized and there are only six π-electrons for six bonds. Therefore, the classic Dirac vector model cannot be readily extended to such systems. Nonetheless, the sign alternation of the π-TSP effect on the FC-induced spin-density and of the spin-polarization of π-orbitals in benzene is clearly seen in Figure 5, middle and right.

The sign alternation of the spin-polarization of π-orbitals can be explained from the point of view of perturbation theory. Let us consider first the spin-polarization of σ-orbitals from this point of view, with FC(A) taken as the perturbation. A closed-shell doubly-occupied σ-orbital becomes polarized by admixing vacant orbitals with opposite signs into its α- and β-components (with the admixture having opposite signs in each case). In the classic picture, the biggest contribution to the perturbation of an occupied σ-orbital is expected from its corresponding antibonding σ^*-orbital. The bonding orbital has the same sign at the positions of the bonded nuclei, whereas the signs of the antibonding orbital at these points are opposite. Consequently, the resulting spin-density will have opposite signs at the positions of the nuclei in accord with the Dirac vector model. In this model, the explanation of the sign alternation of spin-polarization for a classical σ-bond neither relies on the localization of its electrons between two bonded nuclei, nor requires the presence of two electrons in a particular bond. Therefore, it is applicable to the spin-polarization of π-orbitals as well. In planar systems, the π-orbitals can be admixed only with low-lying vacant π-orbitals, which are mainly their antibonding counterparts. The signs of the bonding and antibonding π-orbitals in the proximities of the bonded nuclei obey the same rules as the signs of the σ-orbitals, which leads to the sign alternation of the spin polarization of π-orbitals. The above reasoning can be expressed as follows:

$$\pi'_\alpha \approx \pi + \tau\pi^* \qquad (2)$$

$$\pi'_\beta \approx \pi - \tau\pi^* \qquad (3)$$

$$\rho_\alpha - \rho_\beta \approx (\pi + \tau\pi^*)^2 - (\pi - \tau\pi^*)^2 = 4\tau\,\pi\,\pi^*. \qquad (4)$$

In equations 2 – 4, π is a closed-shell π-orbital, π^* is its antibonding counterpart, ρ_α and ρ_β are the α and β densities of the polarized π-orbital, and τ is the admixing coefficient. Equation 4 shows that the sign of the spin density of the polarized π-orbital at any point is determined by the product of the unperturbed (unpolarized) bonding and antibonding π-orbitals and the sign of the admixing coefficient. The sign of the admixing coefficient ensures that, in the proximity of the first nucleus, the nuclear and

electron spins have opposite orientation (assuming that the g-value of the first nucleus is positive). The π and π^* orbitals are constructed as the bonding and antibonding combinations of atomic p-orbitals. This means that their product always has opposite signs in the proximities of two neighboring atoms.

Note that if an occupied MO is antibonding between two neighboring atoms and it admixes a vacant MO which is bonding, their product would also have the opposite signs in the proximities of the two neighboring atoms. As an example, the sign-alternating effect of the product between the HOMO and LUMO for 1,3,5,7,9-decapentaene is shown in Figure 4. The HOMO and LUMO are both a mixture of bonding and antibonding with respect to individual C – C bonds, but the HOMO is overall slightly more bonding than antibonding and the LUMO is vice versa. Both orbitals have a similar number of nodes but shifted, so the nodes of the two orbitals are in antiphase with each other. Therefore, their product contributes to the sign-alternating pattern.

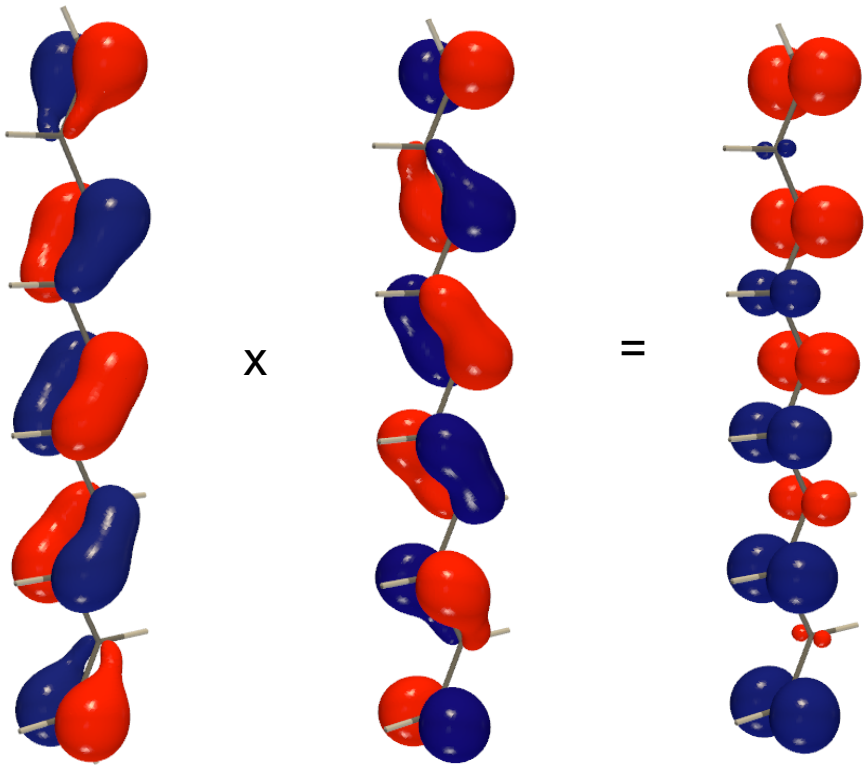

Figure 4. The HOMO and LUMO for 1,3,5,7,9-decapentaene (left and middle, correspondingly) and their product (right) contributing to the sign-alternating pattern of the FC-induced spin density. The isosurface value is 0.05 a.u. for MOs and 0.0025 a.u. for their product.

The polarized π-orbitals transmit spin-polarization to σ-orbitals. Due to Hund's rule, the sign of the spin-density of such polarized σ-orbitals in the proximity of the nuclei will be consistent with the sign of the spin-density of the π-orbitals. This explains the sign alternation seen in the π-TSP effect in Figure 3, middle.

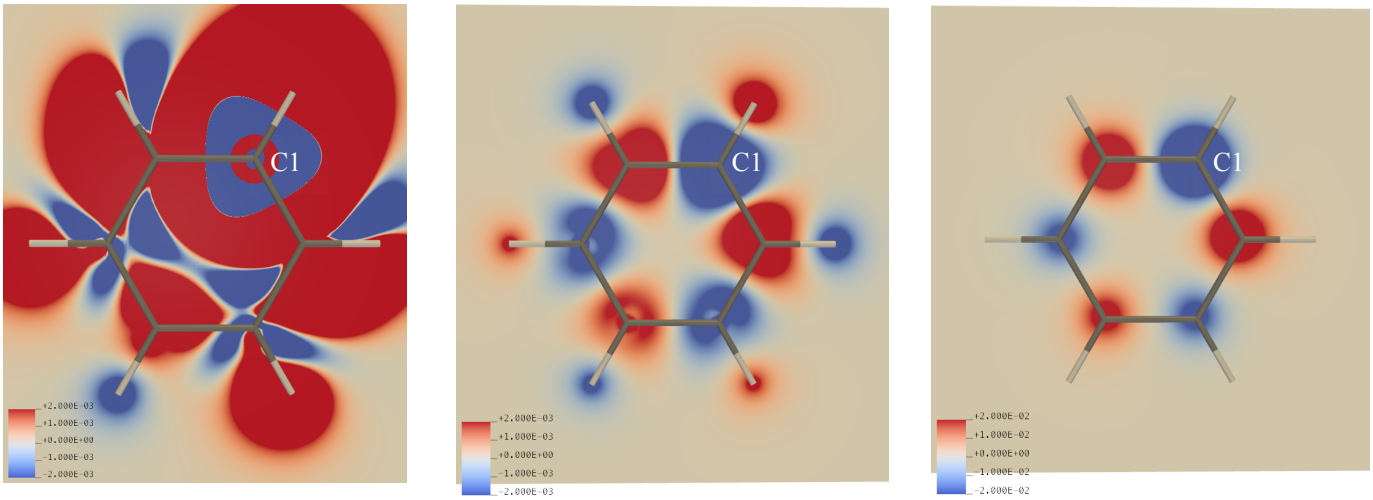

Figure 5. The spin-density in benzene induced by FC(C1) (color-coded according to the density values given in a.u.). The total spin-density (left) and spin-polarization only due to the π-TSP effect (middle) are shown in the molecular plane. The spin-polarization of the group of π-orbitals is shown in the plane 0.5 Å below the molecular plane (right).

The plots for the spin-polarization in our next example, benzene, are shown in Figure 5. The sign alternation and the shapes of the lobes in the middle plot in Figure 5 resemble those for 1,3,5,7,9-decapentaene (Figure 3, middle and right). However, the π-TSP effect is less important, relative to the total spin-density, in benzene (Figure 5, left) than in 1,3,5,7,9-decapentaene, because in benzene the carbons atoms are separated by three bonds at most, i.e. there are no long-range C-C couplings. The spin-polarization of the π-orbitals themselves shows the same sign alternation pattern as in the previous system (Figure 5, right). Thus, we can conclude that while the transmission of spin-polarization via π-orbitals in benzene is easily observed, it does not play a central role in spin-spin couplings between carbons due to the presence of only short-range couplings.

In this respect, naphthalene, a system that can be viewed as the fusion of a pair of benzene rings, would be more informative for analyzing the π-TSP effect on the spin-polarization, due to the presence of several long-range C – C couplings through up to five bonds.

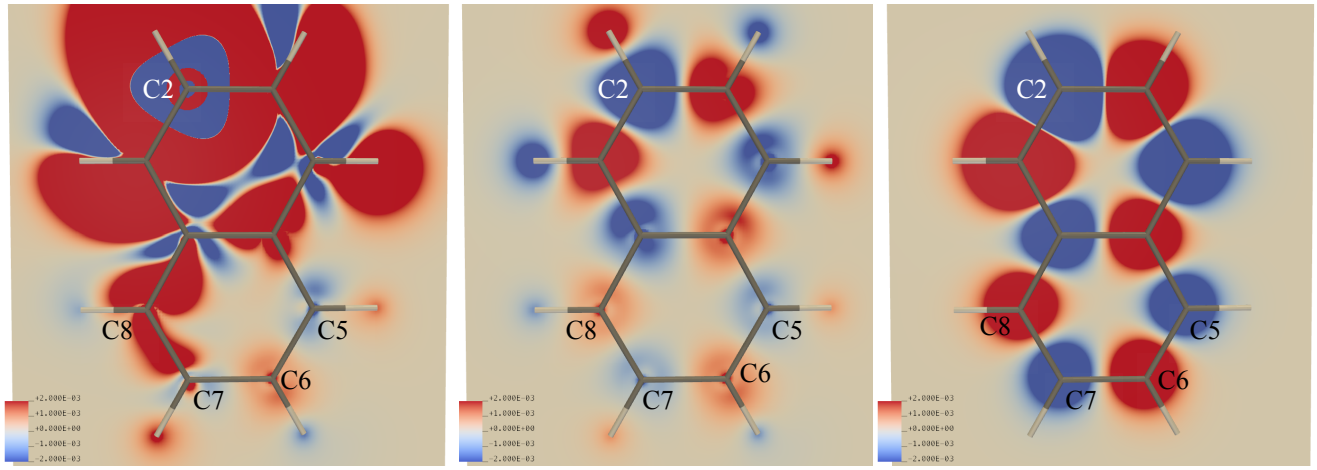

Figure 6. The spin-density in naphthalene induced by FC(C2) (color-coded according to the density values given in a.u.). The total spin-density (left) and spin-polarization only due to the π-TSP effect (middle) are shown in the molecular plane. The spin-polarization of the group of π-orbitals is shown in the plane 0.5 Å below the molecular plane (right).

The spin-polarization induced by FC(C2) in naphthalene (Figure 6, left) in the first ring (containing C2) is similar to that in benzene (Figure 5, left). The induced spin-density at C5 and C6 is mainly due to π-TSP (compare the right and middle plots in Figure 6). The sign alternation due to the π-TSP effect is clearly seen in the second ring (Figure 6, middle). The π-TSP effect on the spin-density in naphthalene (Figure 6, middle) is again consistent with the spin-polarization of the π-orbitals (Figure 6, right), and it extends to hydrogen atoms. ^{5}J(C2-C6) is essentially the result of the π-TSP effect whereas ^{4}J(C2-C7) and ^{4}J(C2-C5) are also affected by the π-TSP effect but to a smaller extent, which is consistent with the data in Table 3.

In all of the examples just listed, the spin-polarization of the π-orbitals follows the sign-alternating pattern, resulting in the sign alternation of the total spin-density induced by FC(C) even in areas that are rather remote from the center of perturbation ($n > 4$). However, exceptions to this rule

can occur. An example of this is the cyclobutadienyl dication, where an additional effect conflicts with the usual sign alternation. The doubly-degenerate LUMO is nonbonding and its product with the HOMO does not display consistent sign alternation on adjacent carbon atoms, but does show sign alternation between carbons separated by two bonds (see Figures S5 and S6 in ESI). The π-TSP effect on the FC induced spin-density in the cyclobutadienyl dication and spin-polarization of the π-orbitals taken together are shown in Figure 7. The planar form of the cyclooctatetraenyl dication is another example where similar findings relating to sign alternation are obtained. The π-TSP effect on the spin density in the cyclooctatetraenyl dication induced by FC(C1) and the spin-polarization of the group of π-orbitals are shown in Figure S7 in ESI. The HOMO, LUMO and their products are plotted in Figure S8 in ESI. The overall HOMO contribution to the spin density is seen in Figure S9 in ESI.

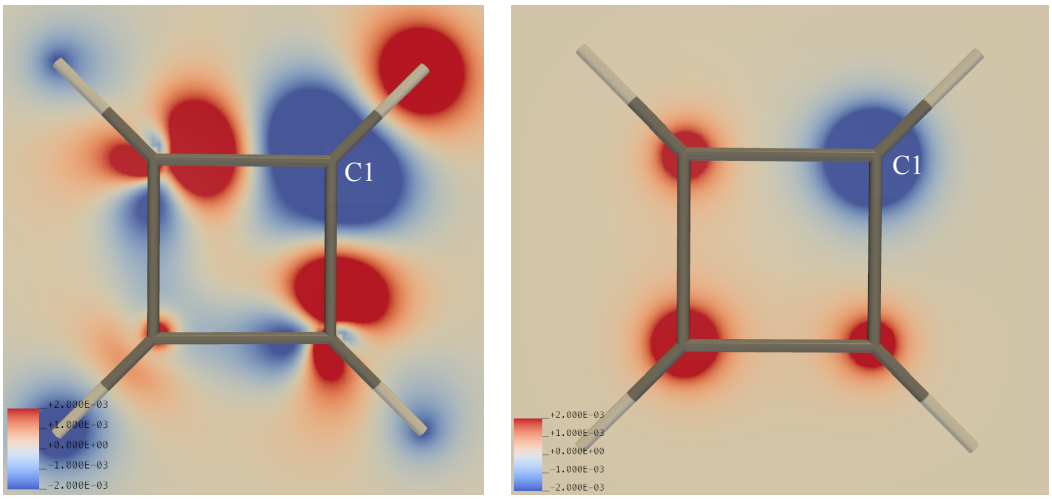

Figure 7. The π-TSP effect on the spin density in cyclobutadiene dication induced by FC(C1) (left; color-coded according to the density values given in a.u.) and spin-polarization of the group of π-orbitals in the plane 0.5 Å below the molecular plane (right).

The π-TSP effect on CDD

The plots of the FC-induced spin-density show the propagation of spin-polarization through the whole molecule, but they do not provide information about the magnetic interaction of a particular pair

of nuclei. This can be achieved by plotting the CDD (see section Computational Methods), which shows what parts of the electron density are involved in the interaction of the two nuclear magnetic moments and nothing else. This way, one can see how π-TSP affects the spin-spin coupling pathways. Figure 8 shows the total CDD for ^{9}J(C1-C10) in 1,3,5,7,9-decapentaene (left) and which part of the CDD is the result of π-TSP (middle). Comparison of the plots shows that the π-TSP effect is responsible for the main changes in the electron density due to the interaction of the nuclear magnetic moments of C1 and C10. On decreasing the number of bonds separating the coupled nuclei, the relative role of π-TSP diminishes (see Figure S10 in ESI). For ***n*** = 4 it is no longer dominant, though π-TSP affects the CDD even at C10 (Figure S10 in ESI, middle). Interestingly, the transmission of spin-polarization by the π- and σ-channels have opposite effects on the CDD at C8 (compare the middle and right plots in Figure S10 in ESI).

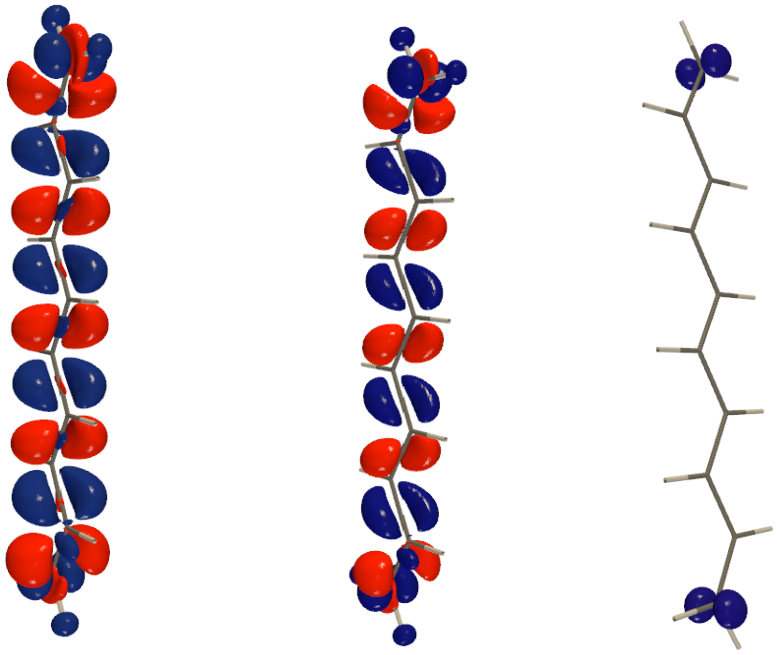

Figure 8. CDD for ^{9}J(C1-C10) in 1,3,5,7,9-decapentaene: total (left), and due the π-TSP effect (middle) and the CDD when the π-TSP effect is switched off (right). The isosurface value in all plots is 0.001 a.u.

For ^{3}J(C1-C4) in benzene, the π-TSP effect on CDD is much less important than other channels for the transmission of spin-polarization (see Figure 9). To visualize the π-TSP effect for ^{3}J(C1-C4) we have to use an isosurface value ten times smaller than that for the total CDD.

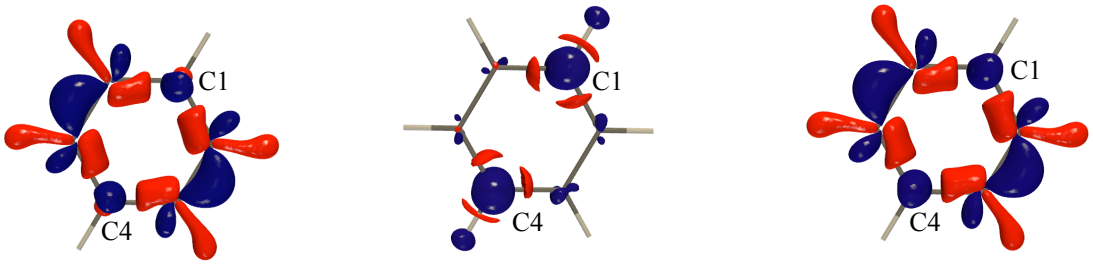

Figure 9. CDD for ^{3}J(C1-C4) in benzene: total (left), due to the π-TSP effect (middle) and the CDD when the π-TSP effect is switched off (right). The isosurface value in the right and left plots is 0.02 a.u. In order to show the π-TSP effect (middle) we used a smaller isosurface value of 0.002 a.u.

The CDDs for long-range C-C couplings in naphthalene are shown in Figures S11-S13 in ESI. The CDD for ^{5}J(C2-C6) in Figure S11 (ESI) is dominated by π-TSP, but its effect diminishes for ^{4}J(C2-C7) and ^{4}J(C1-C6) and (Figures S12 and S13, ESI). Interestingly, the interaction between C2 and C7 occurs along a single zig-zag pathway (Figure S12, left, ESI), but neither the total CDD nor the part thereof arising due to the π-TSP effect resemble their counterparts for ^{4}J(C1-C5) in 1,3,5,7,9-decapentaene in Figure S10 in ESI. The relative role of the π-TSP effect in the CDD of the latter is more important than for ^{4}J(C2-C7) in naphthalene.

The π-TSP effect on Hyperfine Coupling

The π-TSP effect on the EPR hyperfine coupling constant (HFCC) has received much less attention in the literature than its effect on NMR spin-spin couplings. The tools described above also allow one to analyze this phenomenon. The FC contribution to NMR spin-spin couplings and the EPR hyperfine coupling constant use the same operator, so some similarities between these two properties are expected. To illustrate the resemblances and dissimilarities of the π-TSP effect on EPR hyperfine coupling with C-C spin-spin couplings in 1,3,5,7,9-decapentaene, we considered a model system made by removing H19 without reoptimizing the structure (i.e., keeping the rest of the structure unchanged, in

order to facilitate the deconvolution of the main effect under scrutiny from other changes due to structural relaxation; the calculated ^{13}C HFCCs for the optimized structure are collected in Table S5 in ESI).[30] The calculated HFCC results are presented in Table 4, where the second column contains ^{13}C HFCCs obtained with all orbitals participating in the transmission of spin-polarization. The third column shows the results when the π-TSP effect is switched off, that is, when the π-orbitals do not polarize other orbitals *via* the exchange interaction. The last column contains the differences between the values in the second and third columns, in other words the contributions to ^{13}C HFCC solely due to the transmission of spin-polarization by the π-system. Just as in Table 1, the last column displays a remarkably stable sign alternation, also shown in Figure 10. The graph in Figure 10 strikingly resembles the graph for the π-TSP effect on $^{n}J^{FC}$(C1-C_{n+1}) in 1,3,5,7,9-decapentaene in Figure 2, since the transmission of spin-polarization via the system of π-orbitals is the same (π-channel).

Table 4. The π-TSP effect on ^{13}C HFCC in the 1,3,5,7,9-decapentaene-1-yl radical. The values are given in MHz.

Carbon	π-TSP switched ON	π-TSP switched OFF	Difference
1	441.39	434.46	6.94
2	2.64	9.16	-6.53
3	44.33	39.61	4.72
4	-5.74	-2.35	-3.40
5	3.40	0.27	3.13
6	-2.88	-0.56	-2.32
7	2.54	0.28	2.26
8	-2.35	-0.63	-1.72
9	1.82	0.18	1.64
10	-1.70	-0.41	-1.28

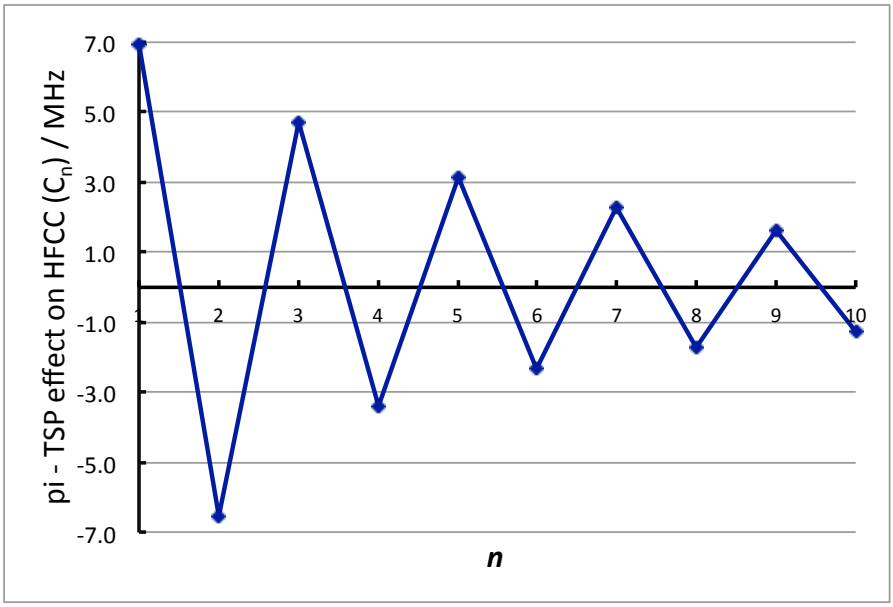

Figure 10. The π-TSP effect on ^{13}C HFCC (in MHz) in the 1,3,5,7,9-decapentaen-1-yl radical. The values on the horizontal axis correspond to the numbering of carbons in Figure 1, left.

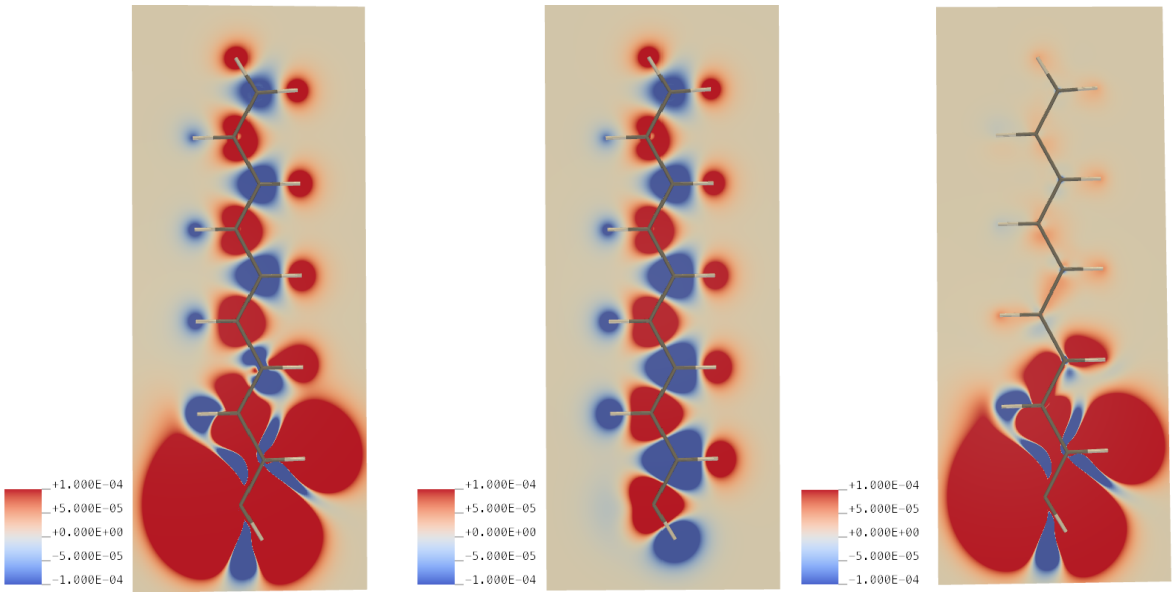

Figure 11. The spin-density of the 1,3,5,7,9-decapentaene-1-yl radical in the radical plane: total (left), the spin-density due-to the π-TSP effect (middle) and when the π-TSP effect is switched off (right).

The distribution of spin-density in the 1,3,5,7,9-decapentaen-1-yl radical is shown in Figure 11, left. The π-TSP effect on the spin-density is visualized in the middle plot of Figure 11. The spin-density in the

absence of the π-TSP effect (Figure 11, right) can be associated with the SOMO contribution (the density of the SOMO is presented in Figure 12). It is interesting to note the significant delocalization of the SOMO in space. Still, it is clear that long-range hyperfine couplings are, as expected, due to the π-TSP effect.

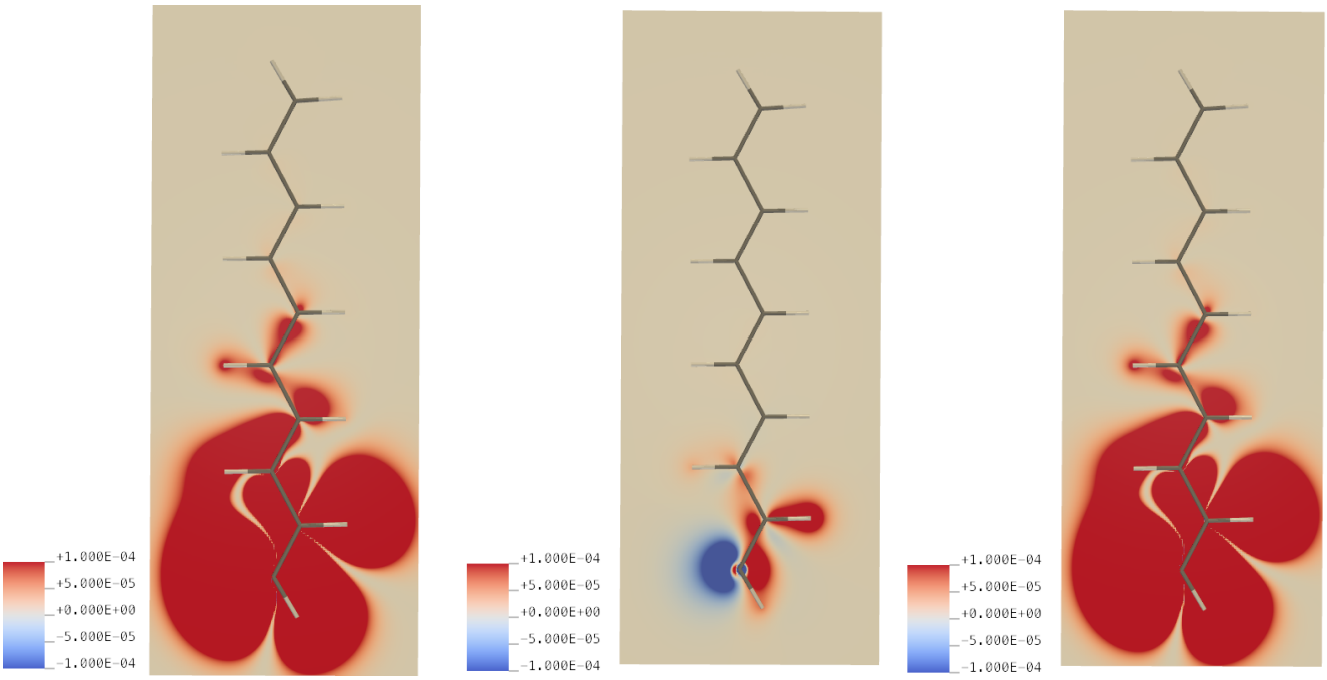

Figure 12. The SOMO density in the 1,3,5,7,9-decapentaen-1-yl radical (left), the π-TSP effect on the density of the SOMO (middle) and the SOMO density when the π-TSP effect is switched off (right).

The C10 hyperfine coupling pathway is plotted in Figure 13, a. It shows the changes in the spin-density due to its interaction with the C10 nuclear magnetic moment. The total pathway looks very similar to the CDD for ^{9}J(C1-C10) in 1,3,5,7,9-decapentaene (Figure 8, left) except for the observed interchange of the colors (red ↔ blue) due to the opposite signs of the carbon and electron magnetic moments.[14] With the exception of areas near C10 and to a lesser extent near C1, the dominant contribution to HFDD comes from the differences in the spin-polarization of valence π-orbitals when the C10 nuclear magnetic moment is up and down. The π-orbitals can be polarized by the exchange interaction either with other π-orbitals (the π-TSP effect shown in Figure 13, b) or with *s*- and *σ*-orbitals (Figure 13 c and d). The latter effect is less important and it is seen only when plotted with a smaller isosurface value (Figure 13, d). The HFDDs in Figures 13, a-c are also shown as color maps in the plane 0.5 Å below the radical plane in Figure S14 in SI.

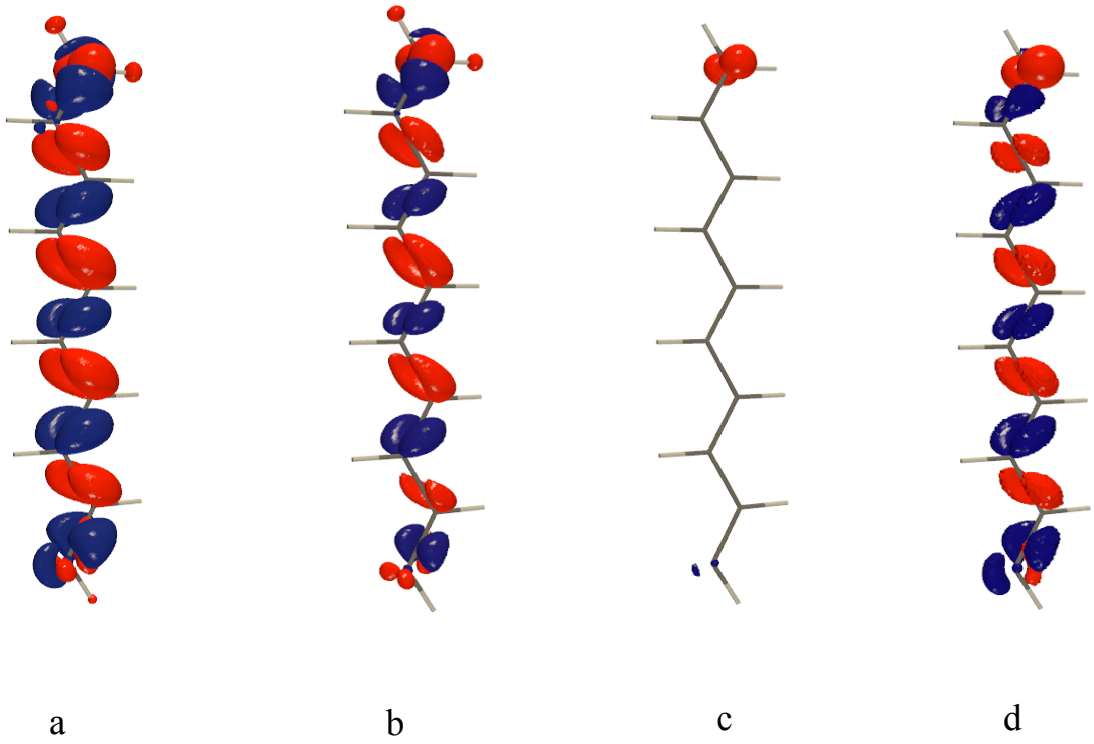

Figure 13. The C10 HFDD in the 1,3,5,7,9-decapentaen-1-yl radical (a); the π-TSP effect on the C10 HFDD (b) and the C10 HFDD when the π-TSP effect is switched off (c and d). The isosurface value is 0.0002 a.u. in plots a, b, and c and 0.0001 a.u. in plot d.

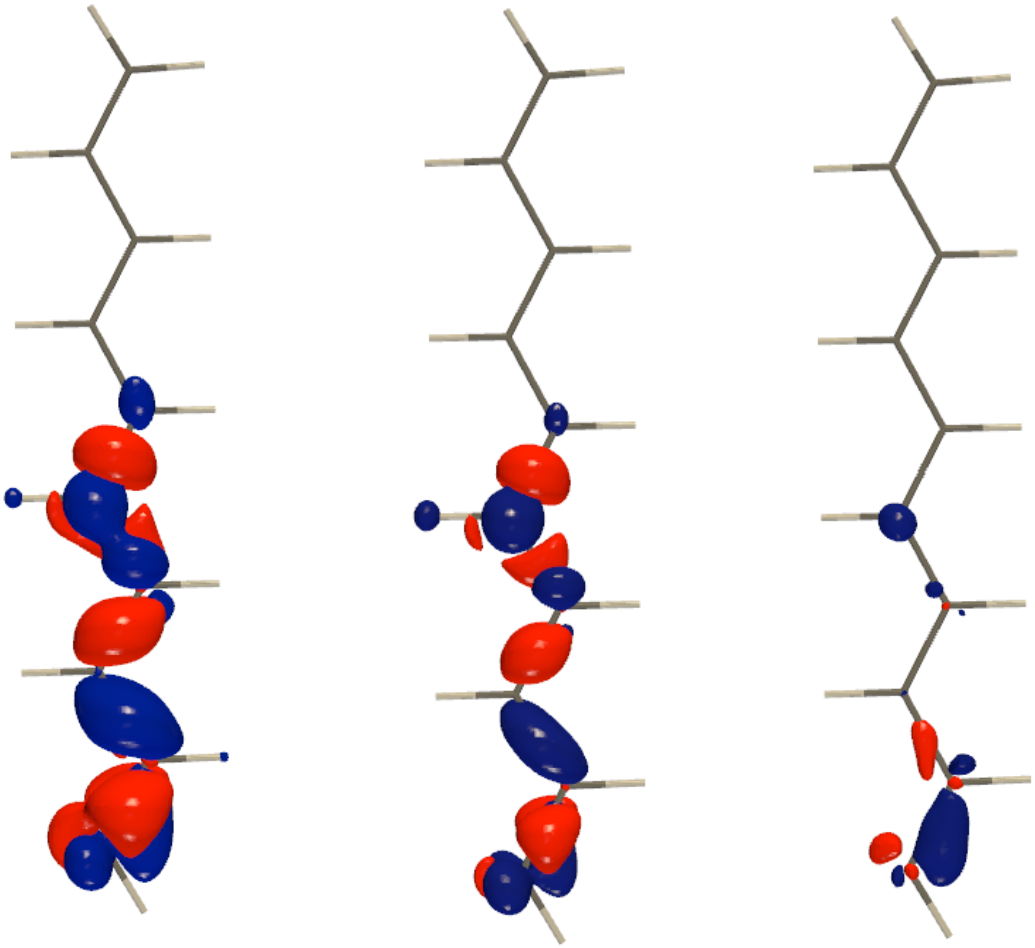

Figure 14. The C5 HFDD in the 1,3,5,7,9-decapentaen-1-yl radical (a); the π-TSP effect on the C5 HFDD and the C5 HFDD (b) when the π-TSP effect is switched off (c). The isosurface value is 0.0003 a.u. in all plots.

The π-TSP effect on the C5 HFDD in the 1,3,5,7,9-decapentaen-1-yl radical is shown in Figure 14. The differences between the CDD for ^{4}J(C1-C5) and C5 HFDD (and the corresponding π-TSP effects) are now more noticeable (compare with Figure S10 in ESI) than for their long-range counterparts in Figures 8 and 13. The π-TSP effect on the C5 HFDD is significant, which is consistent with the HFCC values in Table 4.

Conclusions

We have presented a new DFT-based approach assessing the effect of the transmission of spin-polarization by π-orbitals (π-TSP) and applicable to the analysis of molecular properties that depend on the effects of spin-polarization (i.e, NMR spin-spin couplings, EPR hyperfine couplings, etc.). This approach does not depend on a particular perturbation theory or analysis based on contributions from an arbitrary choice of MOs (although these are useful for analysis and rationalization), but is based on evaluating the magnetic resonance properties of interest directly from total electron densities and spin densities. Specifically, we have studied the mechanism of propagation of spin polarization in planar unsaturated hydrocarbons (with clear σ/π separation), calling special attention to the way the π -MOs contribute to the transmission of spin density along the bonds. Orbitals transmit spin-polarization via their exchange-correlation interaction with other orbitals. With a simple manipulation, namely averaging the α and β densities from the π-MOs within the total densities for the calculation of the exchange-correlation contribution to the Fock matrix, the contribution of these π-MOs to the spin polarization can be switched off. This approach has been applied to estimating the π-TSP effect on different aspects of the Fermi-contact contribution to NMR spin-spin couplings and EPR hyperfine structure coupling constants: specifically, the π-TSP effect on the distribution of spin-density, spin-spin coupling pathways and pathways of EPR hyperfine couplings. To the best of our knowledge, the sign alternation of the π-TSP effect on spin-spin couplings is here for the first time explained based on perturbation theory and Hund's rule. We have also identified exceptions to this pattern, where – for identifiable reasons – spin-polarization delocalization effects occur across a cyclic π-system, interfering with the usual sign-alternating pattern.

Electronic Supplementary Information

Calculated *J*(C-C) in 1,3,5,7,9-decapentaene, benzene and naphthalene; the bond lengths in the optimized structure of naphthalene; the FC and SD contributions to *J*(C-C) in 1,3,5,7,9-decapentaene calculated with different DFT functionals; 3d plot of spin-polarization of the group of π-orbitals in 1,3,5,7,9-decapentaene; MO contributions to spin polarization for cyclobutadieneyl and cyclooctatetraenyl dications to illustrate the interference with the sign alternating pattern; CDDs for J(C-C) in naphthalene; calculated 13C HFCCs in the 1,3,5,7,9-decapentaene-1-yl radical for the optimized structure; color maps of the C10 HFDD; optimized structures used in this work.

Conflicts of interest

There are no conflicts to declare.

Acknowledgments

We acknowledge the support from Slovak-French PHC Stefanik project "Spin Coupling Advanced Level Perception" (SCALP). OM, VM and JRA acknowledge the support from Slovak grant agencies APVV (grants No. SK-FR-19-0001 and APVV-19-0516) and VEGA (grant No. 2/0135/21). This work was also supported by the CNRS, the Université de Bourgogne, the Conseil Régional BFC (CHIMENE project), the PIA-excellence ISITE-BFC program (COMICS project) and the FEDER, which are all sincerely thanked. MB thanks EastCHEM and the School of Chemistry in St Andrews for support and access to a computing facility maintained by Dr H. Früchtl.

CORRESPONDING AUTHORS

Olga L. Malkina – Institute of Inorganic Chemistry, Slovak Academy of Sciences, Dúbravská cesta 9, 84 536 Bratislava, Slovakia; Email: olga.malkin@savba.sk

Vladimir G. Malkin – Institute of Inorganic Chemistry, Slovak Academy of Sciences, Dúbravská cesta 9, 84 536 Bratislava, Slovakia; Email: vladimir.malkin@savba.sk

1 W. Kutzelnigg, U. Fleischer, M. Schindler, in *NMR-Basic Principles and Progress*, Vol. 23, Eds. P. Diehl, E. Fluck, H. Günther, R. Kosfeld, J. Seelig (Springer Verlag, Heidelberg, 1990), p. 165-262.
2 P. v. R. Schleyer, Ch. Maerker, A. Dransfeld. H. Jiao, N. J. R. van E. Hommes, P. v. R. Schleyer, H. Jiao, N.J.R. van E. Hommes, *J. Am. Chem. Soc*., 1996, 118, 6317-6318; P. v. R. Schleyer, V.G. Malkin, O.L. Malkina, *J. Am. Chem. Soc*., 1997, **119**, 12669-126709; H. Fallah-Bagher-Shaidaei, C. S Wannere, C. Corminboeuf, R. Puchta, P. v. R. Schleyer, *Org. Lett.* 2006, **8(5),** 863-866; Z. F Chen, C. S. Wannere, C. Corminboeuf, R. Puchta, P. v. R. Schleyer, *Chem. Rev.* 2005, **105(10),** 3842-3888.
3 H. Fliegl, R. Valiev, F. Pichierri and D. Sundholm, *Chemical Modelling*, 2018, **14**, 2018, 1-42.
4 R. K. Harris, Nuclear Magnetic Resonance Spectroscopy, 1983, Pitman Books Limited.
5 J. A. Pople, P. Gill, N. C. Handy, *Int. J. Quantum. Chem*. 1995, **56(4)**, 303-305.
6 H. M. McConnell, *Journal of Molecular Spectroscopy* 1995, **1**, 11-17.
7 H. M. McConnell*, J. Chem. Phys*. 1959, **30**, 126.
8 M. J. Barfield, *Chem. Phys*. 1968, **49**, 2145-2153; Erratum: Ibid.1969, **51**, 2291-2292.
9 J. Kowalewski, Calculations of Nuclear Spin-Spin Coupling Constants in *Progress in NMR Spectroscopy*, 1977, **I I**, l-78, Pergamon Press.
10 H. Fukui, T. Tsuji, and K. Miura, *J. Am. Chem. Soc.* 1981, **103**, 3652.
11 A.R. Engelmann, Scuseria and Contreras, *JOURNAL OF MAGNETIC RESONANCE* 1982, **9**, 21-29.
12 V. G. Malkin, O. L. Malkina, D. R. Salahub, *Chem. Phys. Lett.* 1994, **221**, 91.
13 J. Gräfenstein, T. Tuttle and D. Cremer, *Phys . Chem. Chem. Phys*, 2005, **7**, 452 – 462.
14 V. G. Malkin, O. L. Malkina, G. M. Zhidomirov, *J. Phys. Chem. A*, 2017, **121 (18)**, 3580–3587.
15 C. Sire, H. Cattey, A. Tsivery, J.-C. Hierso, J. Roger, *Advanced Synthesis & Catalysis*, 2022, **364**, 440-452; O. L. Malkina, J.-C. Hierso, V. G. Malkin, *Am. Chem. Soc*, 2022, **144**, 10768-10784.
16 S. Mom, M. Beaupérin, D. Roy, S. Royer, R. Amardeil, H. Cattey, H. Doucet, J.-C. Hierso, *Inorganic Chemistry*, 2011, **50**, 11592-11603; T.-A. Nguyen, M.-J. Penouilh, H. Cattey, N. Pirio, P. Fleurat-Lessard, J.-C. Hierso, J. Roger, *Organometallics*, 2021, **40**, 3571-3584.
17 E. Duval, S. Koide, *Phys. Lett.*, 1964, **8(6)**, 314-315.
18 L. A. Eriksson, V. G. Malkin, O. L. Malkina, D. R. Salahub D.R., J. Chem. Phys., 1993, **99**, 9756.
19 O.L. Malkina, V.G. Malkin, *Angew. Chem. Int. Edition*, 2003, **42**, 4335-4338.
20 M. Karplus, *J. Chem. Phys*., 1960, **33**, 1842; M. Barfield, J. Chem. Phys. 1970, 74, 621-626.
21 Gaussian 03, Revision A.1, Frisch, M. J.; Trucks, G. W.; Schlegel, H. B.; Scuseria, G. E.; Robb, M. A.; Cheeseman, J. R.; Zakrzewski, V. G.; Montgomery, Jr., J. A.; Stratmann, R. E.; Burant, J. C. et al., Gaussian, Inc., Pittsburgh PA, 2003.
22 M. Bremer, P. v. R. Schleyer, U. Fleischer *Am. Chem. Soc*, 1989, **111**, 1147; H.-U. Siehl, *Adv; Org. Chem.* 2008, **42**, 152.
23 D. R. Salahub, R. Foumier, P. Mlynarski, I. Papai, A. St-Amant, J. Ushio, In *Density Functional Methods in Chemistry*; Labanowski, J.K.; Andzelm, J. W., Eds.; Springer: Berlin, 1991; p 77.
24 V. G. Malkin, O. L. Malkina, deMon-NMR program, version 2021.
25 J. P. Perdew, Y. Wang, Y. *Phys. Rev. B,* 1986, **33**, 8800- 8802.
26 J. P. Perdew, Y. Wang, *Phys. Rev. B* 1989, **40**, 3399.
27 J. P. Perdew*Phys. Rev. B* 1986, **33**, 8822–8824.
28 J. P. Perdew, *Phys. Rev. B* 1986, **34**, 7406.

29 M. D. Hanwell, D. E. Curtis, D. C. Lonie, T. Vandermeersch, E. Zurek, G. R. Hutchison, Avogadro: An Advanced Semantic Chemical Editor, Visualization, and Analysis Platform. *Journal of Cheminformatics* 2012, 4-17.
30 Spin contamination is small in this radical, e.g. $<\hat{S}2>=0.77$ at P86/IGLO-II.

Electronic Supplementary Material

Transmission of spin-polarization by π-orbitals: an approach to assessing its effect on NMR spin-spin coupling and EPR hyperfine structure

Olga L. Malkina,*[,a] Florian Lemken[a], James R. Asher[a,b], Jean-Cyrille Hierso[c], Michael Bűhl[d], Vladimir G. Malkin*[a]

[a] *Institute of Inorganic Chemistry, Slovak Academy of Sciences, Dúbravská cesta 9, SK-84536 Bratislava, Slovakia*

[b] *Faculty of Natural Sciences, Department of Inorganic Chemistry, Comenius University, Mlynská dolina CH2, SK-84215 Bratislava, Slovakia*

[c] *Institut de Chimie Moléculaire de l'Université de Bourgogne (ICMUB, UMR CNRS 6302), Université Bourgogne–Franche-Comté (UBFC), 9 avenue Alain Savary, 21078 Dijon Cedex, France*

[d] *EaStChem School of Chemistry, University of St Andrews, St Andrews, Fife KY16 9ST, UK*

Table S1. Calculated ^{n}J (C1- C_{n+1}) in 1,3,5,7,9-decapentaene in Hz calculated using the P86 exchange-correlation functional.

n	FC	PSO	DSO	SUM[a]
1	77.44	-8.60	0.14	68.98
2	1.86	0.16	-0.05	1.97
3	7.43	0.62	-0.08	7.97
4	-0.72	0.02	-0.04	-0.74
5	1.04	-0.11	-0.04	0.89
6	-0.70	0.02	-0.02	-0.70
7	0.73	0.05	-0.02	0.76
8	-0.54	0.01	-0.01	-0.54
9	0.52	0.01	-0.01	0.52

a) The calculation of the SD term is not implemented in the deMon program.

Table S2. Calculated ^{n}J(C1- C_{n+1}) in benzene in Hz calculated using the P86 exchange-correlation functional.

n	FC	PSO	DSO	SUM[a]
2	62.94	-6.61	0.21	56.54
3	-0.33	0.04	-0.02	-0.31
4	7.80	0.46	-0.01	8.25

a) The calculation of the SD term is not implemented in the deMon program.

Table S3. Calculated ^{n}J(C1- C_{n+1}) in naphthalene in Hz calculated using the P86 exchange-correlation functional.

n		FC	PSO	DSO	SUM[a]
1	C1-C2	67.97	-7.46	0.22	60.73
	C1-C9	61.28	-5.38	0.28	56.18
	C2-C3	59.07	-5.43	0.22	53.86
	C9-C10	55.82	-5.45	0.33	50.7
2	C1-C8	3.78	-0.05	0.01	3.74
	C1-C10	1.14	-0.03	0.03	1.14
	C2-C9	0.36	-0.02	0.02	0.36
	C1-C3	-0.03	0.08	-0.01	0.04
3	C3-C9	6.45	0.21	0.03	6.69
	C1-C4	5.33	0.34	0.01	5.68
	C1-C5	2.35	-0.21	-0.06	2.08
4	C2-C7	0.52	0.05	-0.06	0.51
	C1-C6	-0.50	0.01	-0.06	-0.55
5	C2-C6	0.46	0.01	-0.05	0.42

a) The calculation of the SD term is not implemented in the deMon program

Table S4. ^{n}J (C1- C_{n+1}) in 1,3,5,7,9-decapentaene in Hz calculated[a] using the BP86 and B3LYP exchange-correlation functionals.

n	V_{xc}	FC	SD	PSO	DSO	Total
1	BP86	70.88	3.01	-8.56	0.14	65.47
	B3LYP	83.76	4.69	-9.18	0.13	79.41
2	BP86	2.44	-1.85	0.17	-0.05	0.70
	B3LYP	-0.90	-4.00	0.17	-0.05	-4.78
3	BP86	6.92	2.64	0.65	-0.08	10.12
	B3LYP	9.77	4.53	0.66	-0.08	14.88
4	BP86	-0.37	-1.11	0.02	-0.04	-1.51
	B3LYP	-2.83	-2.84	0.02	-0.04	-5.69
5	BP86	0.68	1.79	-0.11	-0.04	2.32
	B3LYP	2.99	3.61	-0.11	-0.04	6.46
6	BP86	-0.48	-0.65	0.02	-0.02	-1.14
	B3LYP	-2.38	-1.89	0.02	-0.02	-4.28
7	BP86	0.45	1.47	0.05	-0.02	1.95
	B3LYP	2.26	3.06	0.05	-0.02	5.35
8	BP86	-0.39	-0.37	0.01	-0.01	-0.77
	B3LYP	-1.70	-1.06	0.01	-0.01	-2.77
9	BP86	0.30	1.18	0.00	-0.01	1.46
	B3LYP	1.56	2.39	0.01	-0.01	3.94

a) IGLO-II basis set (ref. 1), G03 package (ref. 21).

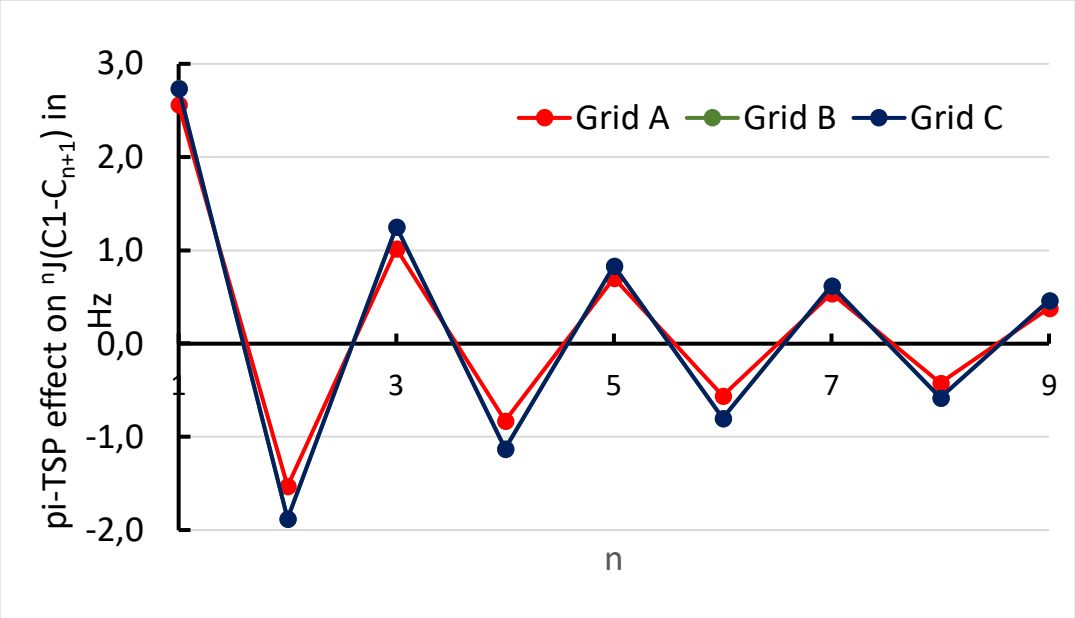

Figure S1. The π-TSP effect on ${}^{n}J^{FC}$(C1- C_{n+1}) in 1,3,5,7,9-decapentaene as a function of the number of bonds separating two carbons (in Hz) calculated using three different grids for numerical integration. Grid A: about 3000 points/atom during the main SCF procedure,then an extra SCF iteration with about 10500 points/atom; Grid B: about 10500 points/atom; Grid C: about 20000 points/atom.

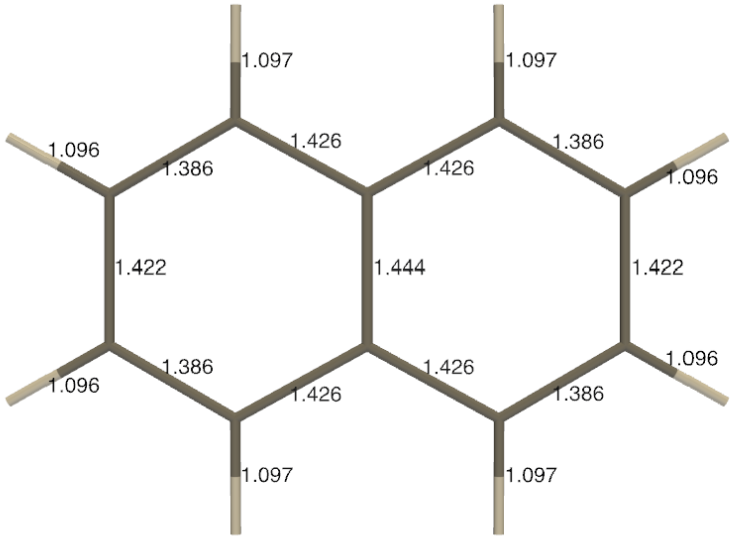

Figure S2. The bond lengths in the optimized structure of naphthalene.

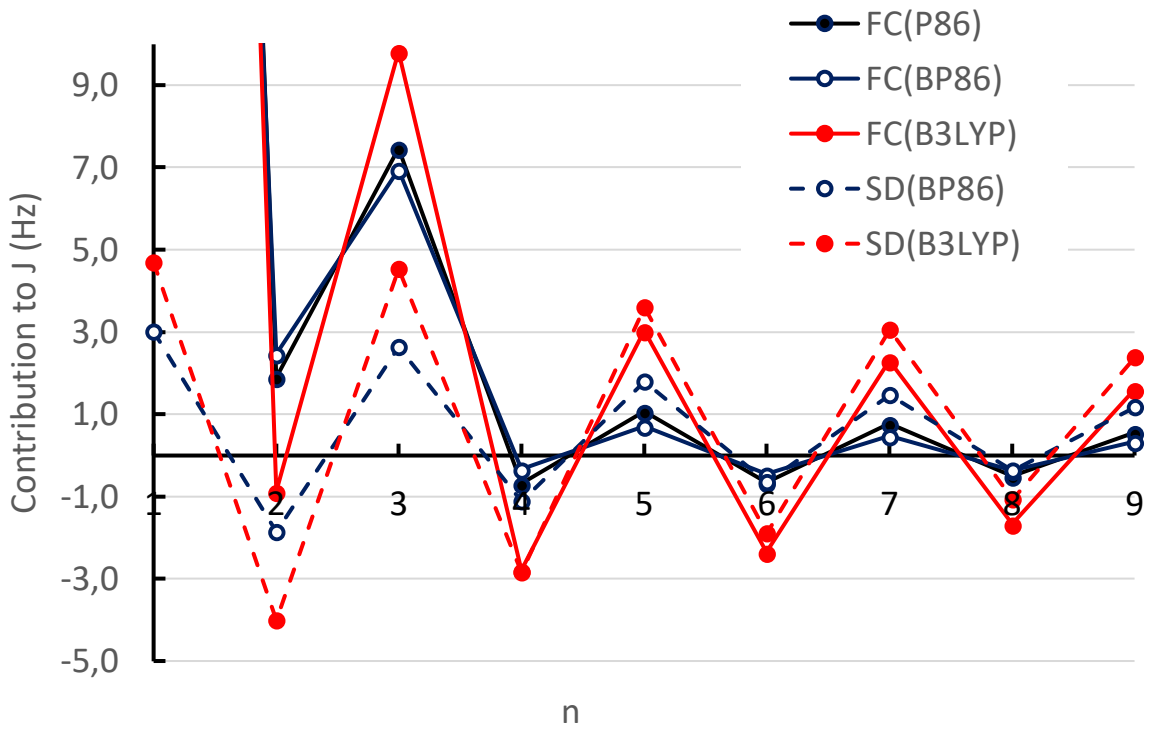

Figure S3. The FC and SD contributions to ^{n}J (C1- C_{n+1}) in 1,3,5,7,9-decapentaene calculated with different exchange-correlation functionals. The B3LYP and BP86 results were obtained using the G03 package (ref. 21).

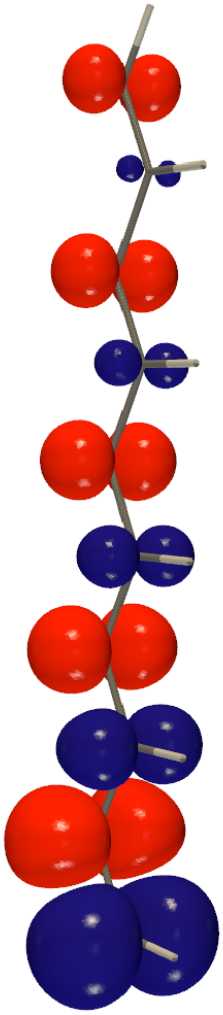

Figure S4. Spin-polarization of π-orbitals taken together in 1,3,5,7,9-decapentaene due to FC(C1). The isosurface value is 0.007 a.u.

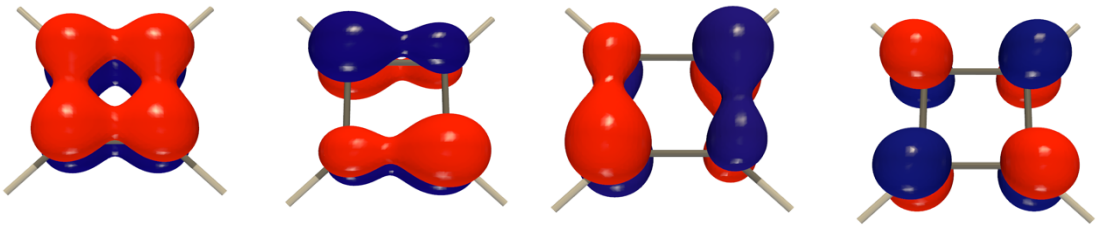

MO11 MO14 MO15 MO16

Figure S5. The occupied π-orbital (MO11) and the lowest vacant π-orbitals (MO14, MO15 and MO16) of a cyclobutadienyl dication. The isosurface value 0.1 a.u. .

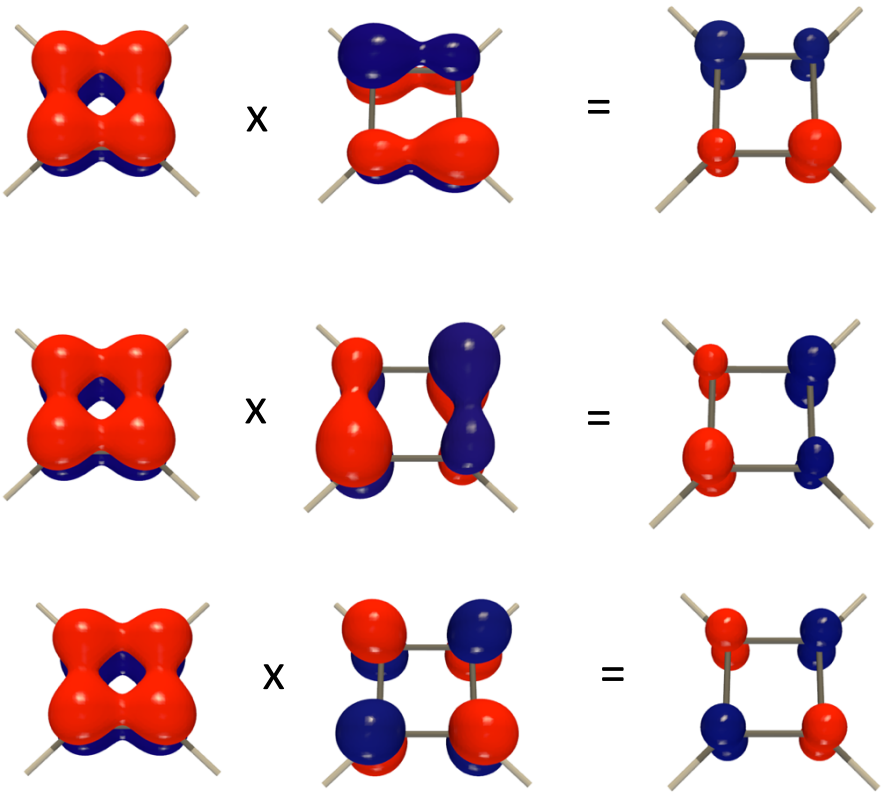

MO11 x MO14 + MO11 x MO15 + MO11 x MO16 =

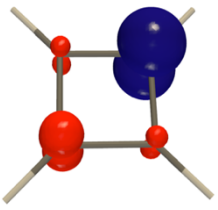

Figure S6. The contributions of the products of the occupied π-orbital with low-lying vacant π -orbitals to the spin-density induced by FC(C1) in a cyclobutadienyl dication. The isosurface value is 0.1 a.u. for MOs and 0.02 a.u. for their products.

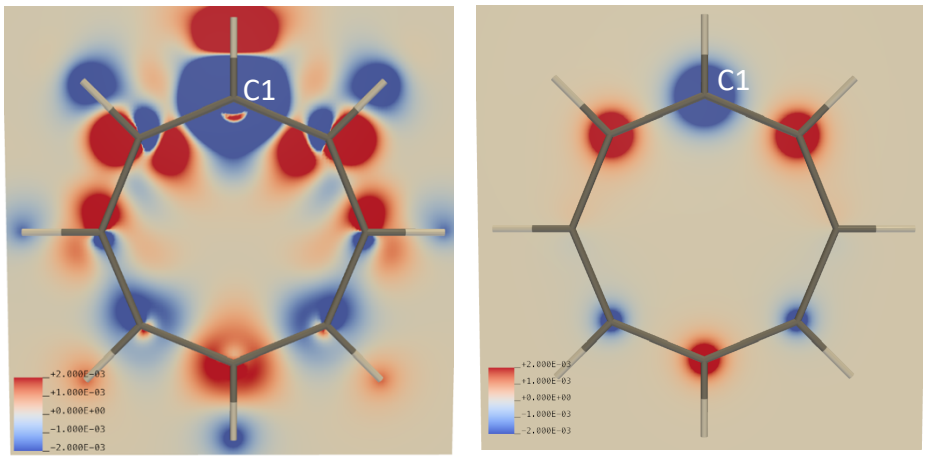

Figure S7. The π-TSP effect on the spin density in a cyclooctatetranyl dication induced by FC(C1) (left; color-coded according to the density values given in a.u.) in the dication plane and the total spin-polarization of the π-orbitals in the plane 0.5 Å below the molecular plane; right).

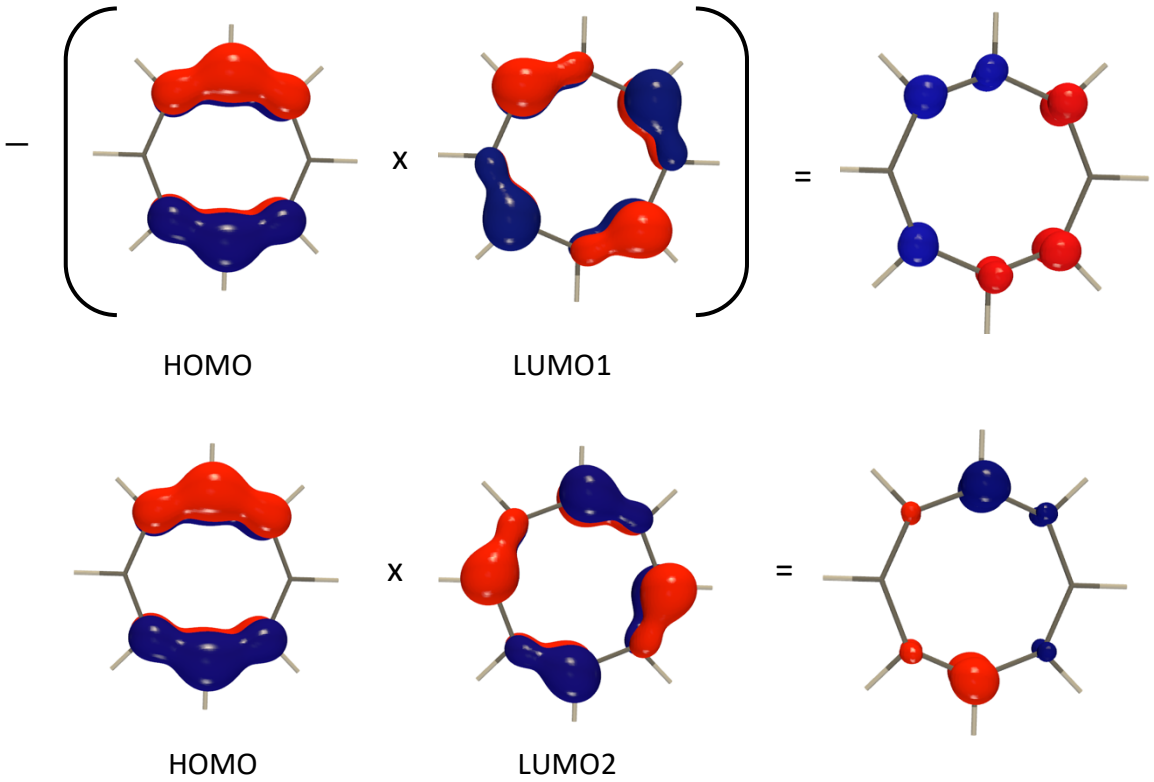

Figure S8. The products of the HOMO and LUMO orbitals for a cyclooctatetranyl dication. The first product is taken with a negative sign because the corresponding coefficient τ is negative (see Eqs. 2-4 in the main text). The isosurface value is 0.07 a.u. for MOs and 0.01 a.u for their products.

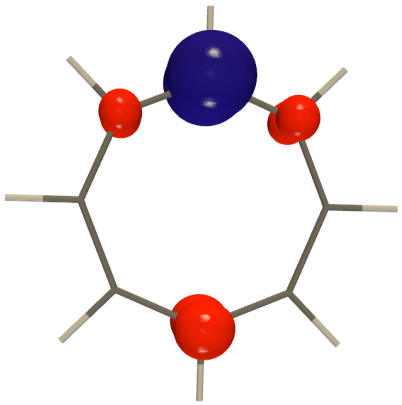

Figure S9. The overall contribution of the HOMO to the spin density induced by FC(C1) in a cyclooctatetranyl dication (compare with Figure S5, left). The isosurface value is 0.01.

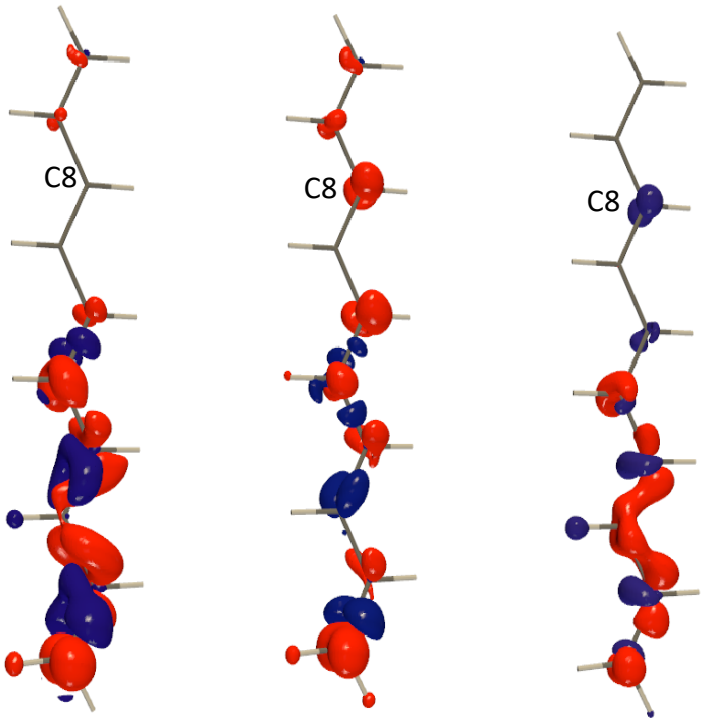

Figure S10. The CDD for ^{4}J(C1-C5) in 1,3,5,7,9-decapentaene: total (left), due the π-TSP effect (middle) and the CDD when the π-TSP effect is switched off (right). The isosurface value in all plots is 0.004 a.u.

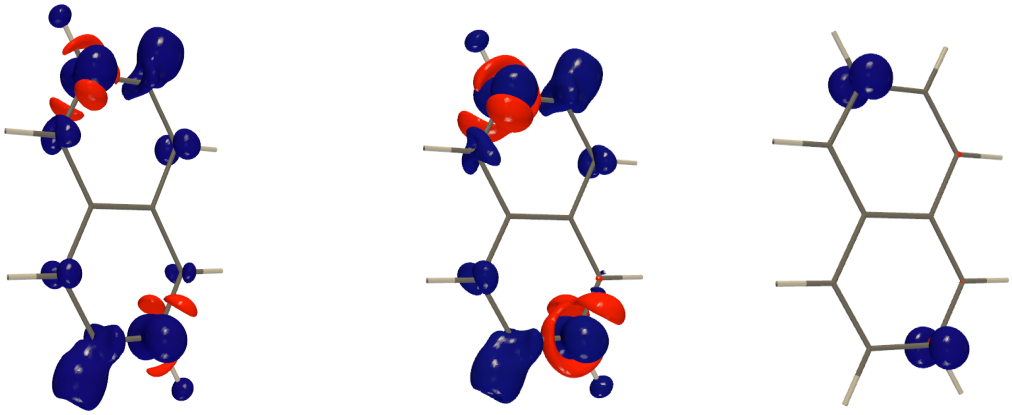

Figure S11. CDD for ^{5}J(C2-C6) in naphthalene: total (left), due the π-TSP effect (middle) and the CDD when the π-TSP effect is switched off (right). The isosurface value in all plots is 0.001 a.u.

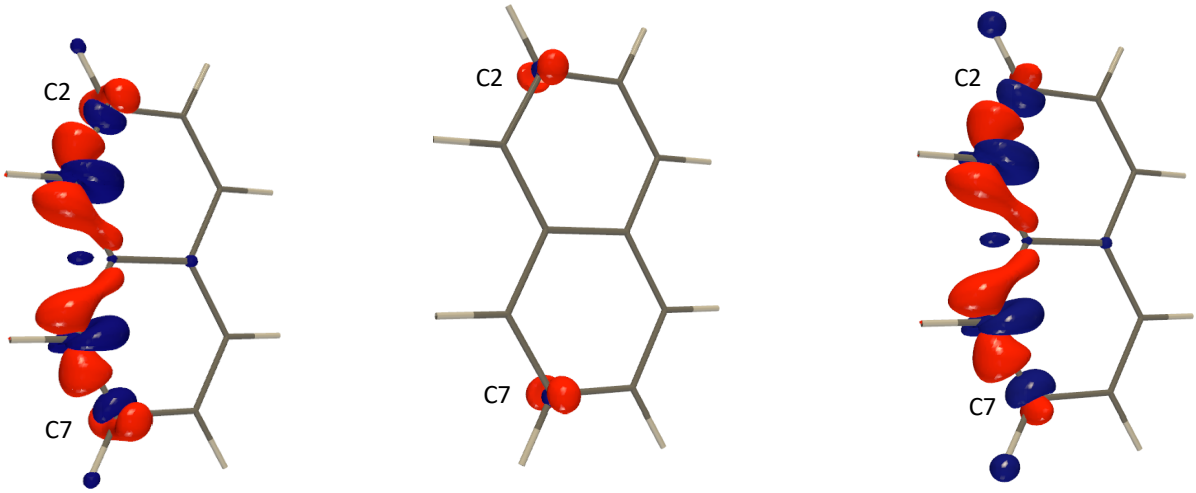

Figure S12. CDD for ^{4}J(C2-C7) in naphthalene: total (left), due the π-TSP effect (middle) and the CDD when the π-TSP effect is switched off (right). The isosurface value in all plots is 0.004 a.u.

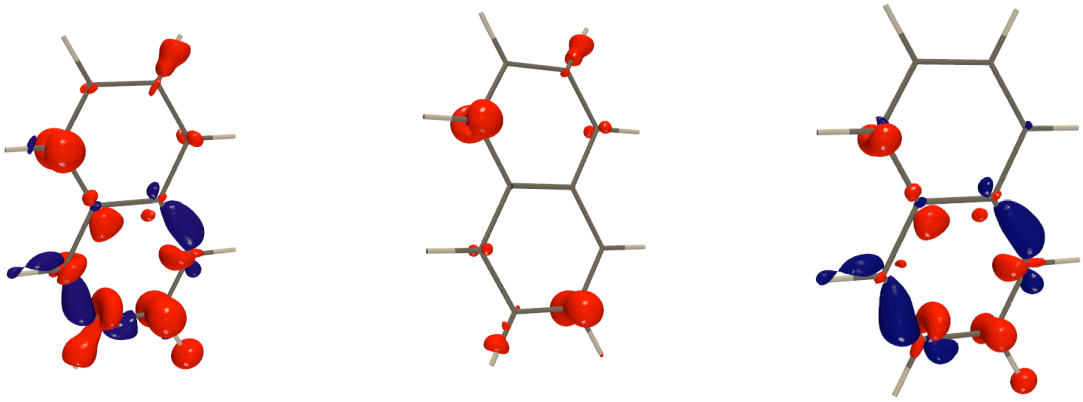

Figure S13. CDD for ^{4}J(C1-C6) in naphthalene: total (left) due the π-TSP effect (middle) and the CDD when the π-TSP effect is switched off (right). The isosurface value in all plots is 0.002 a.u.

Table S5. The π-TSP effect on ^{13}C HFCC in the 1,3,5,7,9-decapentaene-1-yl radical for the optimized structure. The values are given in MHz.

Carbon	π-TSP ON	π-TSP OFF	Difference
1	337.30	322.82	14.48
2	-3.31	2.39	-5.70
3	87.76	87.36	0.40
4	0.33	4.74	-4.41
5	5.73	2.65	3.07
6	-2.15	0.64	-2.79
7	2.72	0.01	2.71
8	-2.30	-1.05	-1.25
9	1.84	0.25	1.58
10	-1.73	-1.65	-0.08

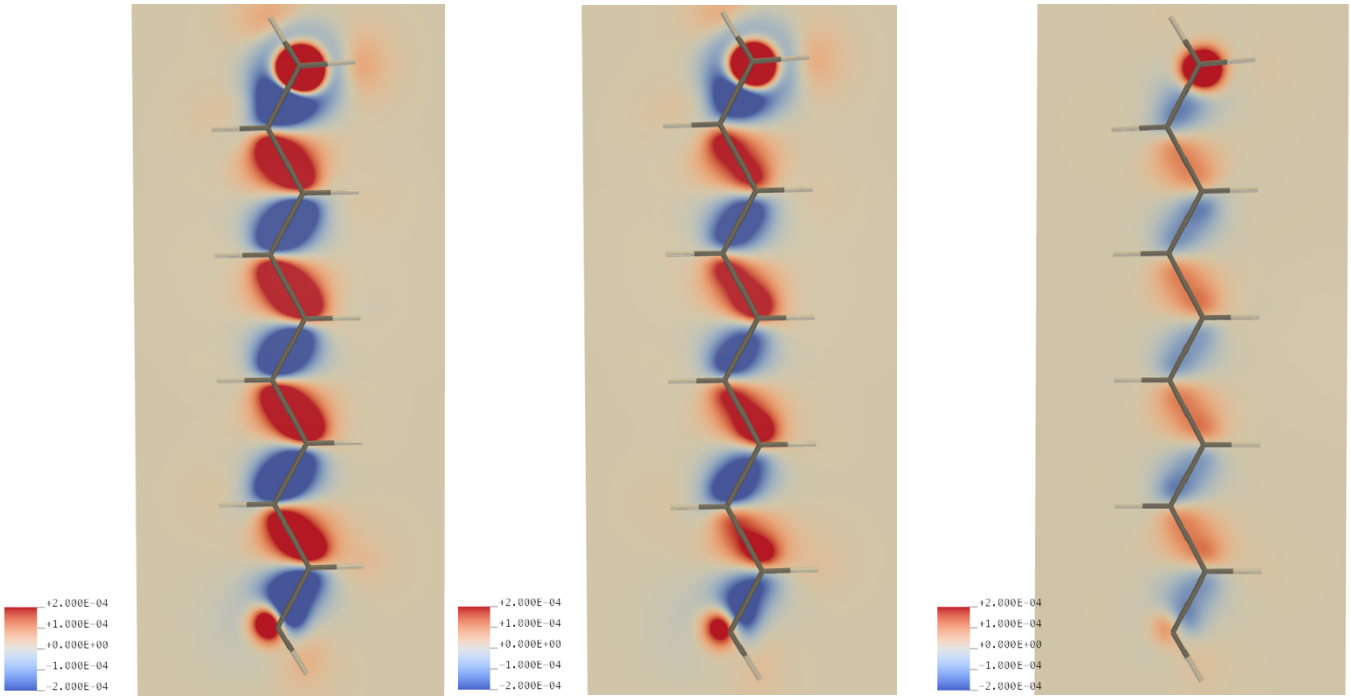

Figure S14. The C10 HFDD in the 1,3,5,7,9-decapentaen-1-yl radical (a); the π-TSP effect on the C10 HFDD (b) and the C10 HFDD when the π-TSP effect is switched off (c and d). The plots show HFDDs in the plane 0.5 Å below the radical plane.

Cartesian coordinates of the optimized structures used in this work (in Å):

1,3,5,7,9-decapentaene

C	5.57155652	0.22658449	0.00000000
C	4.36600585	-0.39674599	0.00000000
C	3.09207900	0.28462510	0.00000000
C	1.87752333	-0.35288057	0.00000000
C	0.60895764	0.31650229	0.00000000
C	-0.60666635	-0.32524946	0.00000000
C	-1.87524579	0.34410891	0.00000000
C	-3.08975700	-0.29350101	0.00000000
C	-4.36380817	0.38766895	0.00000000
C	-5.56925882	-0.23586894	0.00000000
H	6.51054405	-0.33548276	0.00000000
H	4.33296253	-1.49643498	0.00000000
H	3.11286760	1.38489525	0.00000000
H	1.86263989	-1.45364347	0.00000000
H	0.62183181	1.41703940	0.00000000
H	-0.61953786	-1.42578655	0.00000000
H	-1.86041124	1.44487033	0.00000000
H	-3.11035372	-1.39377864	0.00000000
H	5.64918963	1.32065942	0.00000000
H	-4.33100048	1.48735752	0.00000000

H	-5.64674361	-1.32995336	0.00000000
H	-6.50835102	0.32600995	0.00000000

Benzene

C	1.21636673	0.70226966	0.00000000
C	0.00000000	1.40453931	0.00000000
C	-1.21636673	0.70226966	0.00000000
C	-1.21636673	-0.70226966	0.00000000
C	0.00000000	-1.40453931	0.00000000
C	1.21636673	-0.70226966	0.00000000
H	2.16549152	1.25024712	0.00000000
H	0.00000000	2.50049422	0.00000000
H	-2.16549152	1.25024711	0.00000000
H	-2.16549152	-1.25024712	0.00000000
H	0.00000000	-2.50049422	0.00000000
H	2.16549152	-1.25024711	0.00000000

Naphthalene

C	-1.24872214	1.41037019	0.00000000
C	-2.44596401	0.71120114	0.00000000
C	-2.44596401	-0.71120114	0.00000000
C	-1.24872214	-1.41037019	0.00000000
C	1.24872214	-1.41037019	0.00000000
C	2.44596401	-0.71120114	0.00000000
C	2.44596401	0.71120114	0.00000000
C	1.24872214	1.41037019	0.00000000
C	0.00000000	0.72204322	0.00000000
C	0.00000000	-0.72204322	0.00000000
H	-1.24451964	2.50721371	0.00000000
H	-3.39819664	1.25308018	0.00000000
H	-3.39819664	-1.25308018	0.00000000
H	-1.24451964	-2.50721371	0.00000000
H	1.24451964	-2.50721371	0.00000000
H	3.39819664	-1.25308018	0.00000000
H	3.39819664	1.25308018	0.00000000
H	1.24451964	2.50721371	0.00000000

1,3,5,7,9-decapentaen-1-yl radical

C	-2.40149636	-5.01194437	0.00000000
C	-2.36081202	-3.67617444	0.00000000
C	-1.15104000	-2.86688171	0.00000000
C	-1.15759986	-1.49581841	0.00000000
C	0.02317277	-0.68074443	0.00000000
C	0.01494579	0.69367383	0.00000000
C	1.19470635	1.50971314	0.00000000

C	1.18921531	2.88132298	0.00000000
C	2.38146967	3.69733141	0.00000000
C	2.38341658	5.05445237	0.00000000
H	-3.31264099	-3.11772101	0.00000000
H	-0.18930342	-3.39833737	0.00000000
H	-2.12723114	-0.97493033	0.00000000
H	0.99313506	-1.20066202	0.00000000
H	-0.95523966	1.21331677	0.00000000
H	2.16430738	0.98846773	0.00000000
H	0.22257379	3.40725204	0.00000000
H	-1.68561535	-5.83685490	0.00000000
H	3.34204371	3.16095891	0.00000000
H	1.44789566	5.62698300	0.00000000
H	3.31468574	5.62919382	0.00000000

Cyclobutadienyl dication

C	0.72997582	0.72997582	0.00000000
C	-0.72997582	0.72997582	0.00000000
C	0.72997582	-0.72997582	0.00000000
C	-0.72997582	-0.72997582	0.00000000
H	1.51268973	1.51268973	0.00000000
H	-1.51268973	1.51268973	0.00000000
H	1.51268973	-1.51268973	0.00000000
H	-1.51268973	-1.51268973	0.00000000

Cyclooctatetranyl dication

C	1.85403202	0.00000045	0.00000000
C	1.31099830	-1.31099894	0.00000000
C	0.00000045	-1.85403202	0.00000000
C	-1.31099894	-1.31099830	0.00000000
C	-1.85403202	-0.00000045	0.00000000
C	-1.31099830	1.31099894	0.00000000
C	-0.00000045	1.85403202	0.00000000
C	1.31099894	1.31099830	0.00000000
H	2.95368374	0.00001701	0.00000000
H	2.08855777	-2.08858182	0.00000000
H	0.00001701	-2.95368374	0.00000000
H	-2.08858182	-2.08855777	0.00000000
H	-2.95368374	-0.00001701	0.00000000
H	-2.08855777	2.08858182	0.00000000
H	-0.00001701	2.95368374	0.00000000
H	2.08858182	2.08855777	0.00000000